THESIS

SPIN DYNAMICS IN SOLIDS

Submitted by

Charles E. Bronnimann

Department of Chemistry

In partial fulfillment of the requirements

for the Degree of Doctor of Philosophy

Colorado State University

Fort Collins, Colorado

Summer 1986

COLORADO STATE UNIVERSITY

Summer 1986

WE HEREBY RECOMMEND THAT THE THESIS PREPARED UNDER OUR SUPERVISION BY Charles E. Bronnimann ENTITLED SPIN DYNAMICS IN SOLIDS BE ACCEPTED AS FULFILLING IN PART REQUIREMENTS FOR THE DEGREE OF Doctor of Philosophy

Committee on Graduate Work

_____

_____

_____

_____

_____

_____
Adviser

_____
Department Head

ABSTRACT OF THESIS

The work described in this thesis falls into two largely unrelated categories. Part I of the thesis reports unusually fast ^{13}C spin diffusion in adamantane. A calculation of the ^{13}C spin-diffusion rate from first order perturbation theory is presented and compared to the experimental data. There is good agreement between calculation and experiment for relatively small mixing times. Motional averagng of ^{13}C-^{1}H dipolar coupling is found to be responsible for the unusually efficient ^{13}C spin-diffusion in adamantane. Further enhancement of ^{13}C spin-diffusion should be possible by carrying out mixing in the rotating frame. This is experimentally verified for adamantane.

Part II discussed ^{13}C NMR of methanol adsorbed on HY zeolite. Three species were distinguished on the basis of their different spin-lattice, spin-spin (spin diffusion) and chemical properties shift. These were: a species exhibiting liquid-like mobility, a species chemically adsorbed onto the wall of the large cage of the zeolite, and a species chemically adsorbed onto the wall of the small cage of the zeolite.

Charles E. Bronnimann
Chemistry Department
ColoradoState University
Fort Collins, CO 80523
Summer 1986

TABLE OF CONTENTS

PART 1

^{13}C SPIN DIFFUSION IN ADAMANTANE

1.1. Introduction.

A previous paper[1] described the detection of ^{13}C spin diffusion in solids by means of a two-dimensional (2-D) cross-polarization (CP) experiment employing magic angle spinning (MAS). This experiment, which is closely related to the liquid-state experiment developed by Jeener, Meier, Bachmann and Ernst[2], demonstrated ^{13}C spin-diffusion in natural-abundance in 1,4-dimethoxybenzene on a time scale on the order of the experimental mixing time of 90 sec. We report here results of a non-spinning 2-D experiment on solid adamantane demonstrating the occurrence of natural-abundance ^{13}C spin-diffusion on a time-scale that is an order of magnitude shorter than that of 1,4-dimethoxybenzene. It is seen that the unusual efficiency of ^{13}C spin-diffusion in this system is a result of motional averaging of ^{13}C-^{1}H dipolar coupling.

The pulse sequence that is used to study ^{13}C spin diffusion has been discussed in detail previously;[1] it is shown schematically in Figure 1. As discussed earlier, spin diffusion in the laboratory frame occurs during the mixing time, τ_m, when the z components of ^{13}C magnetizations of different carbon types, e.g., M_{CH} and M_{CH_2} in adamantane, become mixed by the appropriate mechanism(s).

Fig. 1. The pulse sequence used to detect exchange in the 2D CP experiment. Subscripts denote the relative phase of the rf pulses.

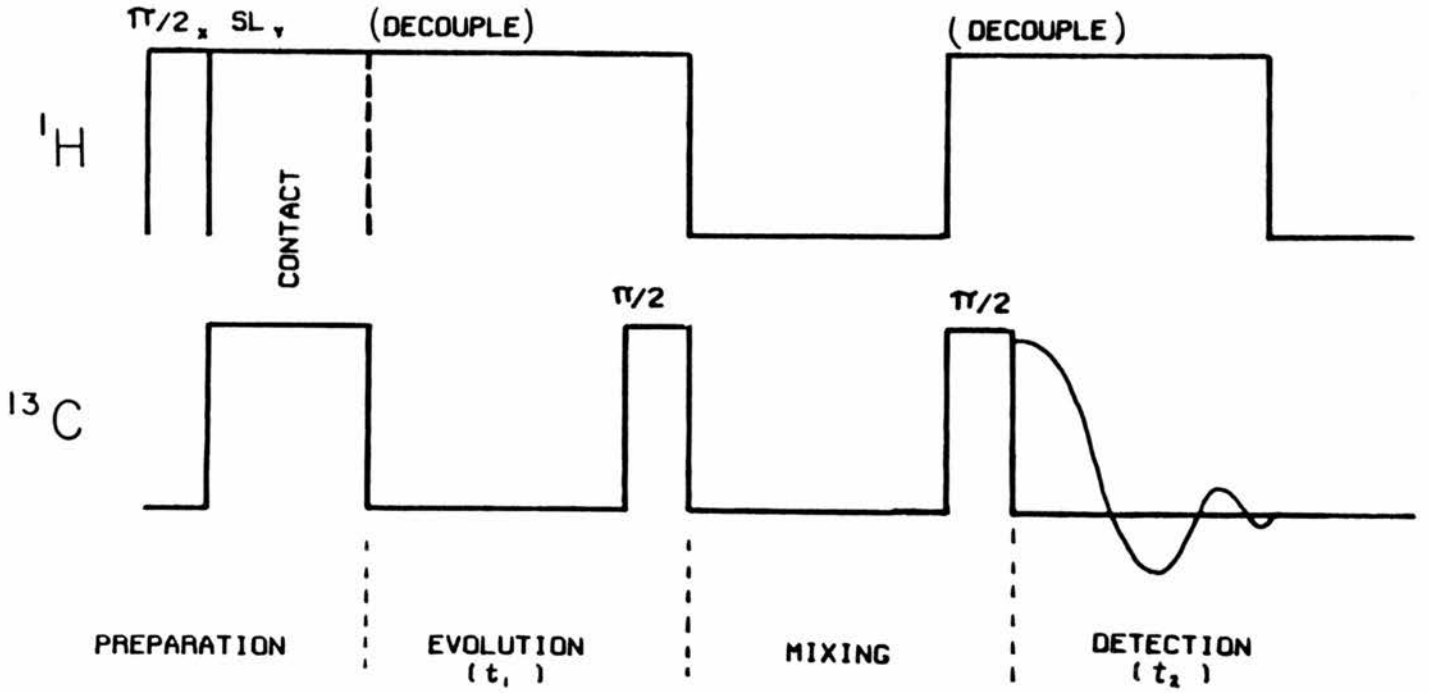
π/2 x SL y
(DECOUPLE)
(DECOUPLE)
^{1}H
CONTACT
π/2
π/2
^{13}C
PREPARATION
EVOLUTION
(t1)
MIXING
DETECTION
(t2)

1.2. Theoretical Formalism for 2-D Intensities.

Exchange during the mixing period is described for adamantane by the Bloch equations for the time derivatives of ^{13}C magnetization of the CH and CH_2 groups, $\dot{M}_{CH}$ and $\dot{M}_{CH_2}$, respectively.

$$\begin{pmatrix} \dot{M}_{CH} \\ \dot{M}_{CH_2} \end{pmatrix} = - \begin{pmatrix} (R_{1CH} + W_o) & -W_o \\ -W_o & (R_{1CH_2} + W_o) \end{pmatrix} \begin{pmatrix} M_{CH} - M_{CH}^{EQ} \\ M_{CH_2} - M_{CH_2}^{EQ} \end{pmatrix} \qquad (1)$$

In Equation (1) R_{1CH} and R_{1CH_2} represent spin-lattice relaxation rates, and M_{CH}^{EQ} and $M_{CH_2}^{EQ}$ represent equilibrium values of z magnetization. We have omitted all carbon-carbon transition probabilities, except that of the ^{13}C-^{13}C spin-spin flip-flop term, W_o, in the expectation that large static components of the dipolar interaction will cause this term to dominate. In the case of spin diffusion between carbons for which the ^{13}C resonances do not have appreciable spectral overlap, it is possible that single-quantum and double-quantum processes may occur at rates comparable to flip-flops.[3]

The evolution and detection periods, t_1 and t_2, respectively, are characterized by precession of the carbon magnetization under proton-decoupled conditions. We assume an isotropic chemical shift with Gaussian broadening due to ^{13}C-^{13}C dipolar coupling. If $W_o < 1/t_1, 1/t_2$ then spin diffusion is negligible during these periods and the Fourier transformed signal, $S(\omega_1, \omega_2)$, is a simple product of Gaussian functions centered at ω_{CH} and ω_{CH_2}. If both resonances experience the same dipolar broadening, then the intensities at the center of each resonance can be directly compared to determine the relative numbers of ^{13}C

spins contributing to the individual resonance line. Otherwise, the signals must be integrated, or if resolution does not allow integration, the peak intensities must be scaled according to the appropriate half-widths.

Solving Equation (1) and incorporating Gaussian decay during t_1 and t_2 results in the following 2-D lineshapes for the diagonal and cross-peaks:

$$S_{i,i}(\omega_1,\omega_2)\alpha \frac{1}{\Delta_i^2} e^{\frac{-(\omega_1-\omega_1)^2}{2\Delta_1^2}} e^{\frac{-(\omega_2-\omega_i)^2}{2\Delta_i^2}} \left\{\frac{M_i^{EQ} e^{a\tau_m}}{b}[b\cosh(b\tau_m) + c\sinh(b\tau_m)]\right\} \tag{2}$$

$$S_{i,j}(\omega_1,\omega_2)\alpha\frac{1}{\Delta_i\Delta_j} e^{\frac{-(\omega_1-\omega_i)^2}{2\Delta_i^2}} e^{\frac{-(\omega_2-\omega_i)^2}{2\Delta_j^2}} \left\{\frac{W_o}{b} e^{a\tau_m} M_i^{Eq} \sinh(b\tau_m)\right\} \tag{3}$$

$S_{i,j}(\omega_1, \omega_2)$ indicates the 2-D intensity in the vicinity of $\omega_1 = \omega_i$ and $\omega_2 = \omega_j$ and

$$b = \sqrt{W_o^2 + \tfrac{1}{4}(R_{1j} - R_{1i})^2}$$

$$a = -\tfrac{1}{2}(R_{1j} + R_{1i}) - W_o$$

$$c = \tfrac{1}{2}(R_{1j} - R_{1i})$$

Δ = half width at half height

In these equations we have assumed that the cross-polarization efficiencies are equal for both carbons, i.e., $M_{xi}(t_1 = 0) = KM_i^{EQ}$, a reasonable assumption for the conditions of the experiment. These equations,

apart from the choice of a Gaussian rather than a Lorentzian lineshape, are equivalent to those introduced previously for liquids.[2,4]

In addition to the cross peaks and diagonal peaks, peaks also occur at $(0, \omega_i)$ and $(0, \omega_j)$ in the 2-D spectra. These so-called "auto peaks" which arise because of spin-lattice relaxation during the mixing period, correspond to signals for which the evolution during t_1 and t_2 is uncorrelated. This situation can occur if τ_m/T_1 becomes appreciable. The auto peaks are given by:

$$S_i(0,\omega_2)\alpha\frac{1}{\Delta_i}e\left(\frac{-(\omega_2-\omega_i)^2}{2\Delta_i^2}\right)M_i^{EQ}[1-\frac{e^{-a\tau_m}}{b}]$$

$$[(a+R_{1i}+W_o)\sinh(b\tau_m)+b\cosh(b\tau_m)] \qquad (4)$$

Spin-temperature alternation attenuates these peaks, as their phase is independent of the cross-polarization phase.[1]

With a dilute spin system such as ^{13}C in natural abundance there will be a significant population which is only very weakly coupled to like spins and will not undergo spin-diffusion during τ_m. Contributions to the auto and diagonal peaks from such spins are given as follows:

$$S_{ii}(\omega_1,\omega_2)\ \alpha\ \frac{1}{\Delta_i}\left\{e^{\frac{-(\omega_1-\omega_i)^2}{2\Delta_i^2}\ \frac{-(\omega_2-\omega_i)^2}{2\Delta_i^2}}\right\}M_i^{EQ}e^{-R_{1i}\tau_m} \qquad (5)$$

$$S_i(0,\omega_2)\ \alpha\ \frac{1}{\Delta_i}\left\{e^{\frac{-(\omega_2-\omega_i)^2}{2\Delta_i^2}}\right\}M_i^{EQ}(1-e^{-R_{1i}\tau_m}) \qquad (6)$$

1.3. Experimental.

Chemicals were obtained from Aldrich Chemical company and used without further purification. Spectra were obtained on the same home-built spectrometer as described previously,[1] this time using a wide-bore Nalorac superconducting magnet at a ^{13}C frequency of 25.18 MHz. All 2-D exchange spectra of the present study were taken without magic-angle spinning. The pulse sequence used is as shown in Fig. 1, and discussed previously.[1] Phase cycling the ^{13}C $\frac{\pi}{2}$ pulse does not affect cross-peak and diagonal-peak intensities, but does attenuate the auto peaks. T_1 measurements were made while spinning at 2 KHz in order to quench ^{13}C spin-diffusion using a low-speed KEL-F bullet rotor.[5] The pulse sequence used in the T_1 measurements[6] is related to the standard T_1 experiment for solids,[7] with the exception that the ^{13}C $\frac{\pi}{2}$ pulse following cross-polarization is alternated 180° and the corresponding FID's added or subtracted in memory; this results in a Fourier transformed signal

$$S(t) = 2M_z(0)e^{-t/T_1} \qquad (7)$$

which decays to zero. A semilog plot of S(t) vs t is linear, with a slope of $-1/T_1$.

Lineshapes for undecoupled spectra were obtained for the two carbon resonances by using the sequence shown in Fig. 3. The ^{13}C transmitter frequency is placed at the frequency of the specific peak of interest (e.g., CH peak); then the system is cross-polarized and allowed to evolve for a time, $t = [4\delta]^{-1}$, where δ is the separation between the resonances in Hz. In this time the magnetization of the off-resonance spins evolves 90° out of phase with the rotating field,

after which a $\frac{\pi}{2}$ ^{13}C pulse shifted 180° in phase from the original ^{13}C cross-polarizing pulse tips it back up along the z axis. Then the FID of the on-resonance signal is acquired.

1.4. Results.

Experimental Data

A representative 2-D ^{13}C CP spectrum of solid adamantane is shown in Fig 2. Table 1 provides a summary of pertinent intensity ratios.

The lineshapes of the undecoupled ^{13}C signals resulting from the experiment shown in Figure 3 were reasonably well fit with a Lorentzian lineshape function with a half-width of 500 Hz; this is the shape expected for a dilute ^{13}C spin system coupled to an abundant proton reservoir.[8] The undecoupled spinning T_1's were measured to be T_{1CH} = 2.76 sec. and T_{1CH_2} = 1.76 sec.

1.5. Theoretical Model of ^{13}C Spin-Diffusion in Adamantane.

Generally the calculation of carbon spin-diffusion rates is complicated by the distribution of carbon-carbon dipolar couplings present in a solid. An exceptional situation occurs in adamantane, for which there is extensive motional averaging of these couplings. The adamantane molecule is very nearly spherical.[9] In fact its carbon atoms lie on a sphere, of radius, $r = 1.78$ Å. At room-temperature adamantane undergoes rapid isotropic rotation,[10] averaging to zero all intramolecular dipolar couplings. Whatever spin diffusion does occur must then be due to the substantially weaker intermolecular interactions, which are not completely removed by the rotation. The effect of rapid isotropic molecular rotation on intermolecular dipolar coupling is to average all intermolecular carbon-carbon vectors to a single value, as

Fig. 2. 2D CP exchange spectrum of adamantane obtained with a mixing time of 2s.

ω1
ω2

Table I. Experimental and calculated values of the ratios, X/D, for $\omega_2 = \omega_{CH}$ and $(X/D)_{\omega_2} = \omega_{CH_2}$.

	Experiment		Calculation	
τ_m	$\omega_2 = \omega_{CH_2}$	$\omega_2 = \omega_{CH}$	$\omega_2 = \omega_{CH_2}$	$\omega_2 = \omega_{CH}$
0.25	0.12	0.06	0.11	0.08
0.50	0.16	0.11	0.19	0.15
0.75	0.27	0.21	0.26	0.20
1.00	0.31	0.25	0.30	0.24
1.50	0.33	0.26	0.34	0.29
2.00	0.38	0.34	0.35	0.33
3.00	0.41	0.47	0.34	0.37
5.00	0.45	0.64	0.30	0.44
8.00	0.43	0.88	0.24	0.55

[a]Based on model restricted to nearest-neighbor coupling.

Fig. 3. (a) The pulse sequence used to obtain individual undecoupled lineshapes for the CH and CH_2 resonances of adamantane.

(b) Evolution of the on-resonance and off-resonance spins under the pulse sequence in (a). After a period, $\tau = 1/4\delta$, the off-resonance spins have evolved 90° out of phase with the rotating field, at which point they are pulsed back along the z-axis and the on-resonance signal is collected.

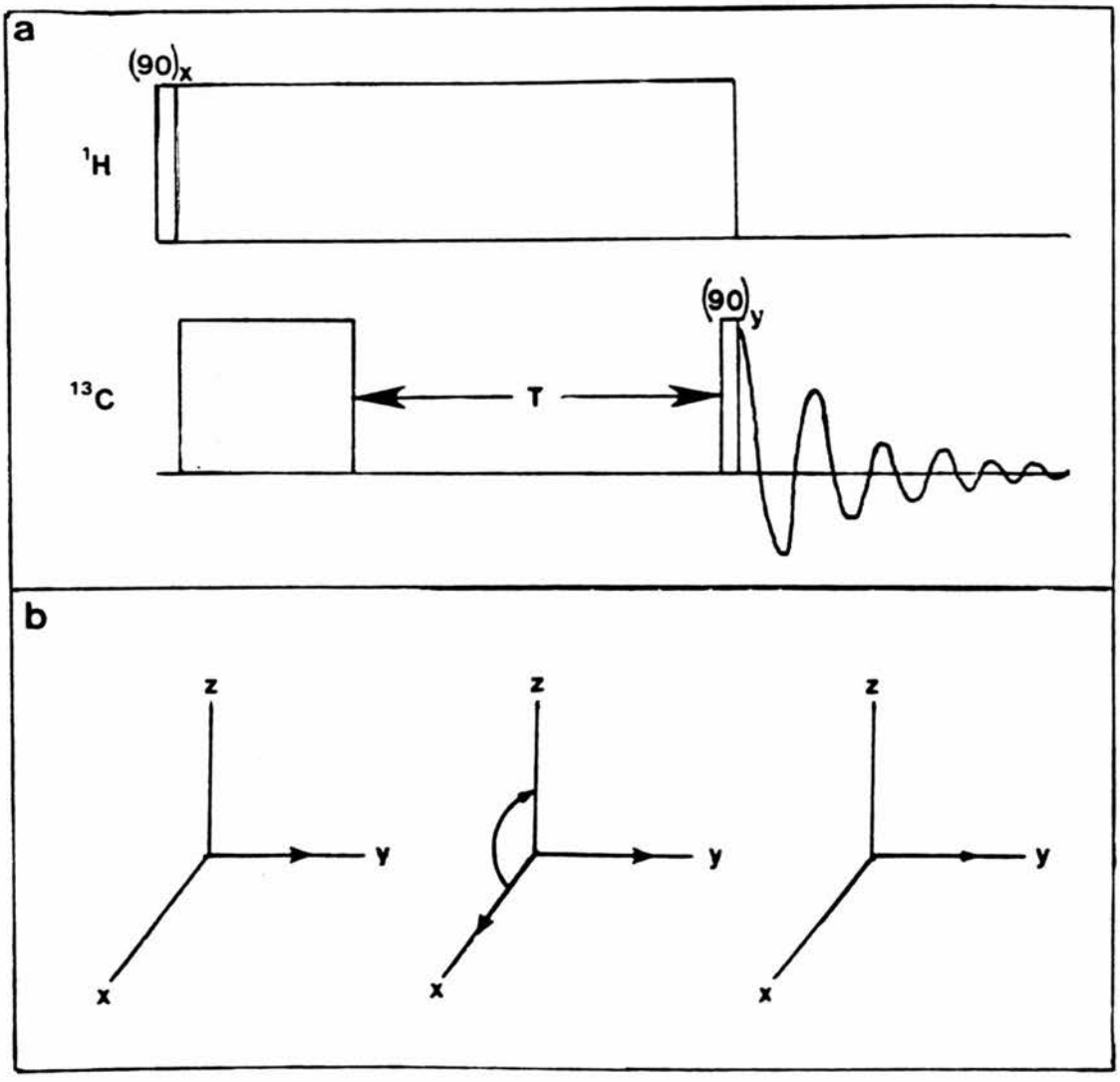
a
(90)x
1H
(90)y
13C
T
b
z
y
x
z
y
x
z
y
x

if the spins of a given molecule were lumped together at a central point and coupled to other "point" spins throughout the solid. Apart from lattice defects, each carbon spin sees the same average environment as any other.

X-ray data indicate that adamantane at room-temperature exists in a face-centered-cubic lattice[9]. In the immediate vicinity of a given adamantane molecule there are 12 neighbor molecules at a center-to-center distance of 6.60 Å, 6 at a distance of 9.34 Å and 16 at 11.4 Å. We expect that for relatively small values of τ_m, exchange occurs predominantly between nearest-neighbors at 6.60 Å, in which case a substantial fraction of ^{13}C spins which do not experience a nearest-neighbor ^{13}C-^{13}C interaction will not participate in spin exchange. Experimentally, this translates into a diagonal peak composed of exchanging and non-exchanging spins and cross-peak intensity due to the former. Rate constants obtained directly from such data reflect an average of the two situations.

An equation for calculating the transition probability, W_o, responsible for ^{13}C spin spin-diffusion in this system can be obtained from time-dependent perturbation theory.[11,12]

$$W_o = \frac{\pi}{2}\omega_{ij}^2 F_{ij}(0) \tag{8}$$

where ω_{ij} is given by

$$\omega_{ij} = \frac{1}{2}\frac{\gamma_c^2 h}{r_{ij}^3}(1 - 3\cos^2\theta_{ij}) \tag{9}$$

and $F_{ij}(0)$ is the probability that single-quantum spin transitions of carbons i and j occur at the same frequency, i.e., it is the density of energy-conserving flip-flop transitions.

$$F_{ij}(0) = \int_{-\infty}^{+\infty} d\omega f_i(\omega) f_j(\omega) \tag{10}$$

where $f_i(\omega)$ is the lineshape function of the undecoupled resonance of carbon (recall that the decoupler is off during τ_m, thus the principal broadening mechanism during mixing is ^{13}C-^{1}H dipole-dipole coupling). For a pair of Lorentzian lines

$$F_{ij}(0) = \frac{\Delta_i}{\pi} \frac{\Delta_i^2 - \Delta_j^2 + \delta^2}{(\Delta_i^2 - \Delta_j^2 + \delta^2)^2 + 4\Delta_j^2\delta^2} + \frac{\Delta_j}{\pi} \frac{\Delta_j^2 - \Delta_i^2 + \delta^2}{(\Delta_j^2 - \Delta_i^2 + \delta^2)^2 + 4\Delta_i^2\delta^2} \tag{11}$$

where Δ is the half width at half height and δ is the separation between the centers of the resonances. For the CH and CH_2 resonances of adamantane,

$$F_{CH_2CH}(0) = \frac{2\Delta}{\pi} \frac{1}{\delta^2 + 4\Delta^2} \tag{12}$$

which, at a given separation, δ, is maximized for $\Delta = \frac{1}{2}\delta$. Motional averaging of the C-H dipolar coupling in adamantane results in Δ = 500 Hz. This is approximately 2.2δ at 25 MHz for a value of $F_{CH_2CH}(0) = 4.81 \times 10^{-5}$; that is about 10 to 100 times that encountered in a typical organic solid.

In applying Equation (7) to adamantane, $\omega^2_{CHCH_2}$ is first averaged over the rotations of a pair of molecules with a fixed orientation of the center-to-center vector $\underset{\sim}{R}$ (where $|\underset{\sim}{R}| = 6.60$ Å) with respect to H_0. The resulting W_0 is then averaged over a powder distribution of orientations of $\underset{\sim}{R}$.

$$W_o = -\frac{1}{(4\pi)^5}\frac{\pi h^2\gamma_c^4}{8}\int_0^{\pi}\sin\theta d\theta\int_0^{2\pi}d\Phi\left[\int_0^{\pi}\sin\theta_1 d\theta_1\int_0^{2\pi}d\phi_1\int_0^{\pi}\sin\theta_2 d\theta_2\int_0^{2\pi}d\phi_2\right.$$

$$\left.\frac{(1-3\cos^2\theta_{12})}{r_{12}^3}\right]F(0)_{CHCH_2} \qquad (13)$$

where

$$r_{12} = \left\{R^2 + 2r^2[1-\sin\theta_1\sin\theta_2(\cos\phi_1\cos\phi_2 + \sin\phi_1\sin\phi_2) - \cos\theta_2\cos\theta_1]\right.$$
$$+ 2rR[\sin\Theta\cos\Phi(\sin\theta_2\cos\phi_2 - \sin\theta_1\cos\phi_1) + \sin\theta\sin\phi(\sin\theta_2\sin\phi_2$$
$$\left. - \sin\theta_1\sin\phi_1) + \cos\Theta(\cos\theta_2-\cos\theta_1)]\right\}^{1/2} \qquad (14)$$

and

$$\cos\theta_{12} = \frac{1}{r_{12}}[R\cos\Theta + r(\cos\theta_2 - \cos\theta_1)] \qquad (15)$$

Numerical integration of Equation (12) using Gaussian quadrature was carried out by means of a BASIC program on a microcoputer. The end result is a predicted transition probability of $W_o = 0.781\ sec^{-1}$ for spin-diffusion between ^{13}CH and $^{13}CH_2$ carbons of nearest-neighbor adamantane molecules.

Before the calculated W_o can be compared with the experimental results, the fraction of ^{13}C spins which actually experience a nearest-neighbor coupling must be determined, and the intensities scaled accordingly. Of the 120 carbon atoms (^{13}C and ^{13}C) in the nearest-neighbor shell of a specific carbon, 48 are CH and 72 are CH_2. The probability, P_{ij}, of i $^{13}CH_2$ and j ^{13}CH appearing among these 120 carbons is given as follows:

Fig. 4. Coordinate system for the integration in Eq. (12). ^{13}C spins on spheres 1 and 2, located by r_1 and r_2, with coordinates (r_1, θ_1, ϕ_1) and r_2, θ_2, ϕ_2) respectively, move freely over the surface of the spheres. The motion yields a nonzero value of $\langle(1-3\cos^2\theta_{12}\rangle$. After averaging over the motion of the spin, the orientation of the spheres, as represented by R, with coordinates (R_1 Ⓗ , Φ), is averaged over a powder distribution.

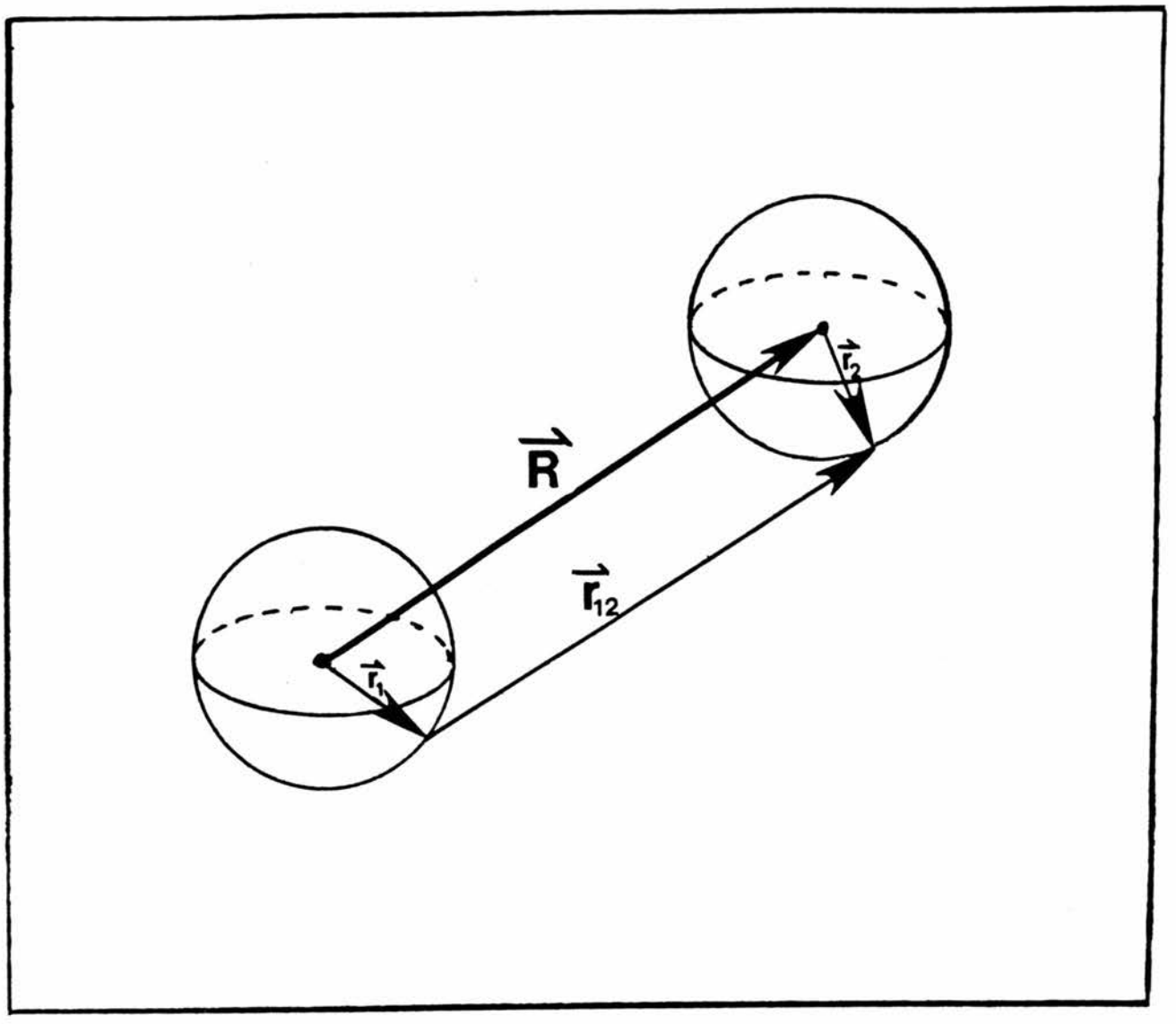
$\vec{R}$
$\vec{r}_{12}$
$\vec{r}_1$
$\vec{r}_2$

$$P_{ij} = \frac{(0.989)^{120-i-j}(0.011)^{i+j}72!48!}{i!j!(72-i)!(48-j)!} \qquad (16)$$

P_{ij} values for i and j running from 0 to 3 are listed in Table 2.

We then decompose the total spin system into a set of subsystems weighted according to the probability of i ^{13}CH and j $^{13}CH_2$ spins present in the nearest-neighbor shell. Intensities in the 2-D exchange spectrum are calculated by summing the contributions from all such subsystems. For example, for the ratio $S_{CHCH_2}(\omega_1, \omega_2)/S_{CH_2CH}(\omega_1, \omega_2)$ one has

$$\frac{S_{CH_2,CH}}{S_{CH,CH}} = \frac{\frac{W_o}{b} e^{a\tau_m} \sinh(b\tau_m) \sum_{j=0}^{2} \sum_{i=1}^{2} iP_{ij}}{e^{-R_{1CH}\tau_m} \sum_{j=0}^{2} P_{oj} + \frac{e}{b}^{a\tau_m} [b\cosh(b\tau_m) + c\sinh(b\tau_m)] \sum_{j=0}^{2} \sum_{i=1}^{2} P_{ij}} \qquad (17)$$

The cross-peak term in the numerator contains a sum of the probabilities that a spatially central $^{13}CH_2$ spin is coupled to 1 or 2 ^{13}CH resonances corresponding to the specific shell of 120 carbons under consideration. The individual probabilities P_{ij} are multiplied by i, the number of ^{13}CH spins, to account for the fact that S_{CH_2CH} is proportional to $M_{EQ}^{CH_2}$. The denominator contains contributions from $^{13}CH_2$ spins that are not coupled to ^{13}CH, contributions that are weighted according to the probabilities P_{oj}, and terms corresponding to $^{13}CH_2$ coupled to ^{13}CH that involve P_{1j} and P_{2j}. An analogous equation applies to the peaks for which $\omega_2 = \omega_{CH}$.

Figs. 5 and 6 show calculated ratios of cross-peak and diagonal-peak intensities (X/D) for values of τ_m ranging from 0.25 to 8 sec,

Table II. Probability, P_{ij}, of there being i $^{13}CH_2$ and j ^{13}CH in the nearest-neighbor shell of a given adamantane molecule. [a]

i	j	P_{ij}
0	0	0.265
1	0	0.212
0	1	0.142
1	1	0.113
2	0	0.084
0	2	0.037
2	1	0.0448
1	2	0.0296
3	0	0.0218
0	3	0.006

[a]Calculated from Equation 13.

plotted along with the corresponding ratios obtained from the experiment. Fig. 5 covers the case $\omega_2 = \omega_{CH_2}$ and Fig. 6 corresponds to $\omega_2 = \omega_{CH}$. In both figures there is a relatively steep rise in the experimental (X/D), which agrees with calculated values, but at longer τ_m the experiment and calculation diverge.

Figs. 7 through 12 are plots of X/D vs τ_m in which one of the parameters, W_o, R_{1CH}, R_{1CH_2}, is varied. As might be expected, these figures show that for $W_o > R_{1CH}, R_{1CH_2}$, the initial kinetics are determined largely by exchange, while the shape of the curves at longer τ_m depends on the relative values of R_{1CH} and R_{1CH_2}. When W_o is varied, one sees that for $W_o > R_{1CH}, R_{1CH_2}$ the behavior at longer τ_m is independent of W_o, while for $W_o < R_{1CH}, R_{1CH_2}$ exchange has a significant effect at longer τ_m.

1.5. Discussion.

As can be seen from the comparison of the experimental and calculated intensity ratios in Figs. 5 and 6, the simple model developed in the last section reasonably describes spin-diffusion for small values of τ_m. For larger τ_m values, although the fit is quite poor, the model correctly predicts general trends for both CH and CH_2. The quality of the fit for each species (CH or CH_2) begins to deteriorate when τ_m approaches T_1 for its partner in exchange; i.e., the fit for $\omega_2 = \omega_{CH_2}$ deteriorates when $\tau_m \approx T_{1CH}$.

The poor fit at larger τ_m is doubtless due to spin diffusion occurring beyond the nearest-neighbor shell at a center-to-center distance of 6.60 Å. This can occur either directly via longer-range couplings, or indirectly through higher-order processes involving more than two spins. For the former one expects W_o for exchange with the

Fig. 5. Plot of the ratio of cross-peak to diagonal-peak intensity (X/D) at $\omega_2 = \omega_{CH_2}$ as a function of the mixing time τ_m, in seconds. The filled circles represent experimental values and the solid line represents the prediction obtained from a simple exchange model using values of W_0, T_{1CH} and T_{1CH_2} given in the text.

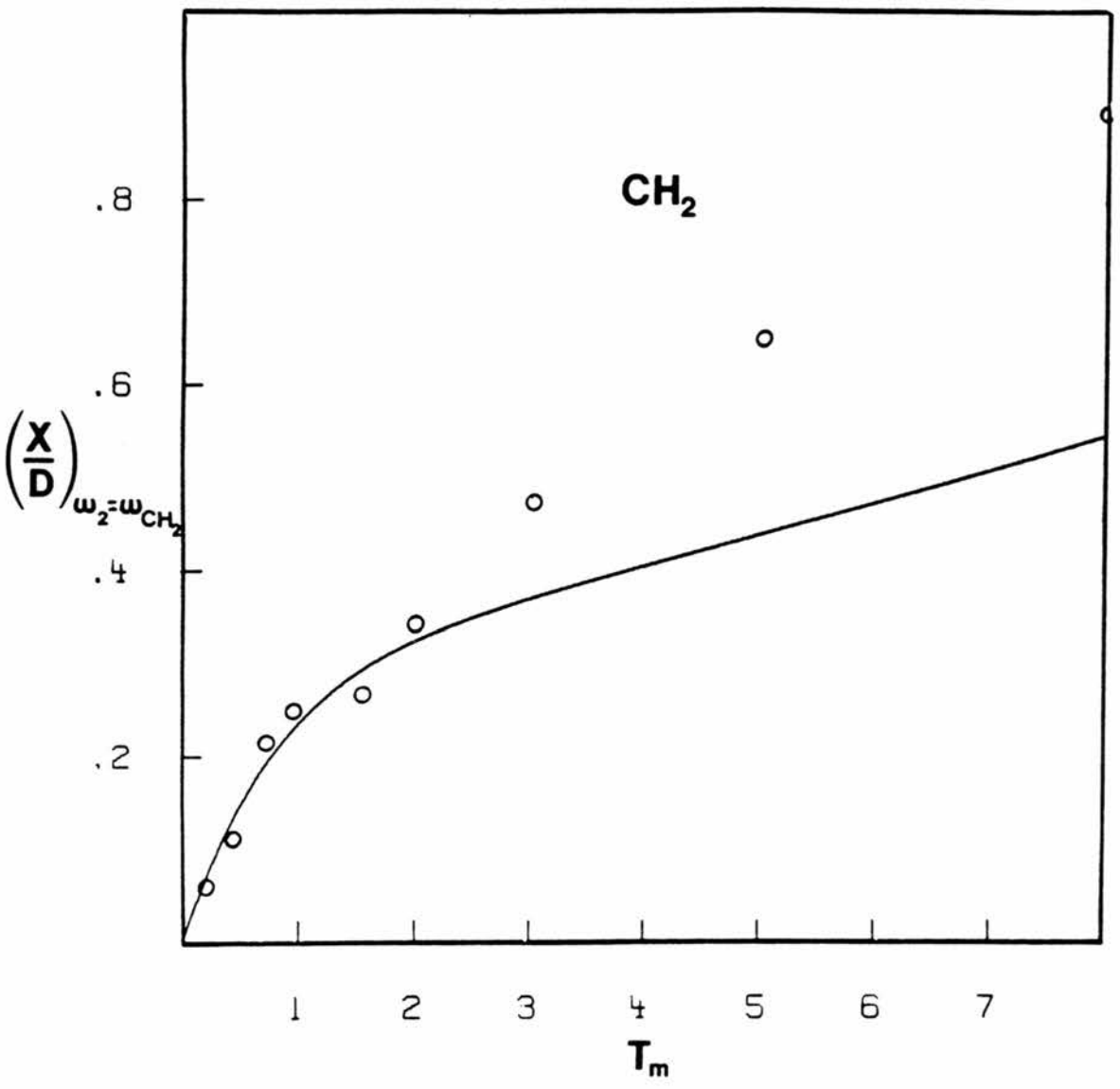
CH2
.8
.6
.4
.2
(X/D)ω2=ωCH2
1
2
3
4
5
6
7
Tm

Fig. 6. Plot of (X/D) at $\omega_2 = \omega_{CH}$ vs. the mixing time in seconds. The filled circles represent experimental values. The solid line is obtained from a simple exchange model using the value of W_o, T_{1CH} and T_{1CH_2} given in the text.

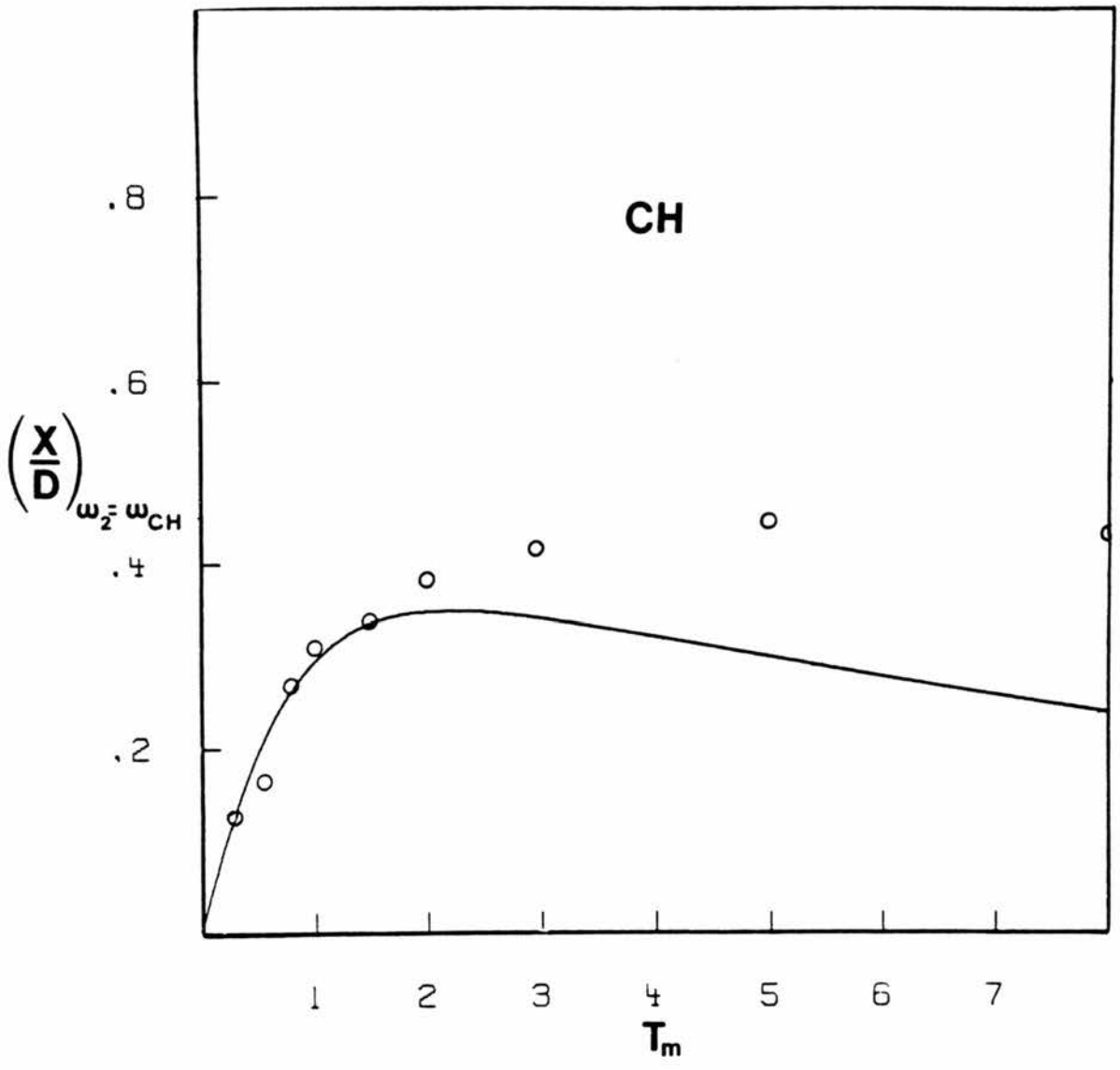
CH
.8
.6
.4
.2
$\left(\frac{X}{D}\right)_{\omega_2 = \omega_{CH}}$
1
2
3
4
5
6
7
T_m

Fig. 7. Plots of (X/D) at $\omega_2 = \omega_{CH}$ for several values of the flip-flop transition probability, $^{CH}W_o$, using values of T_{1CH} and T_{1CH_2} values given in the text.

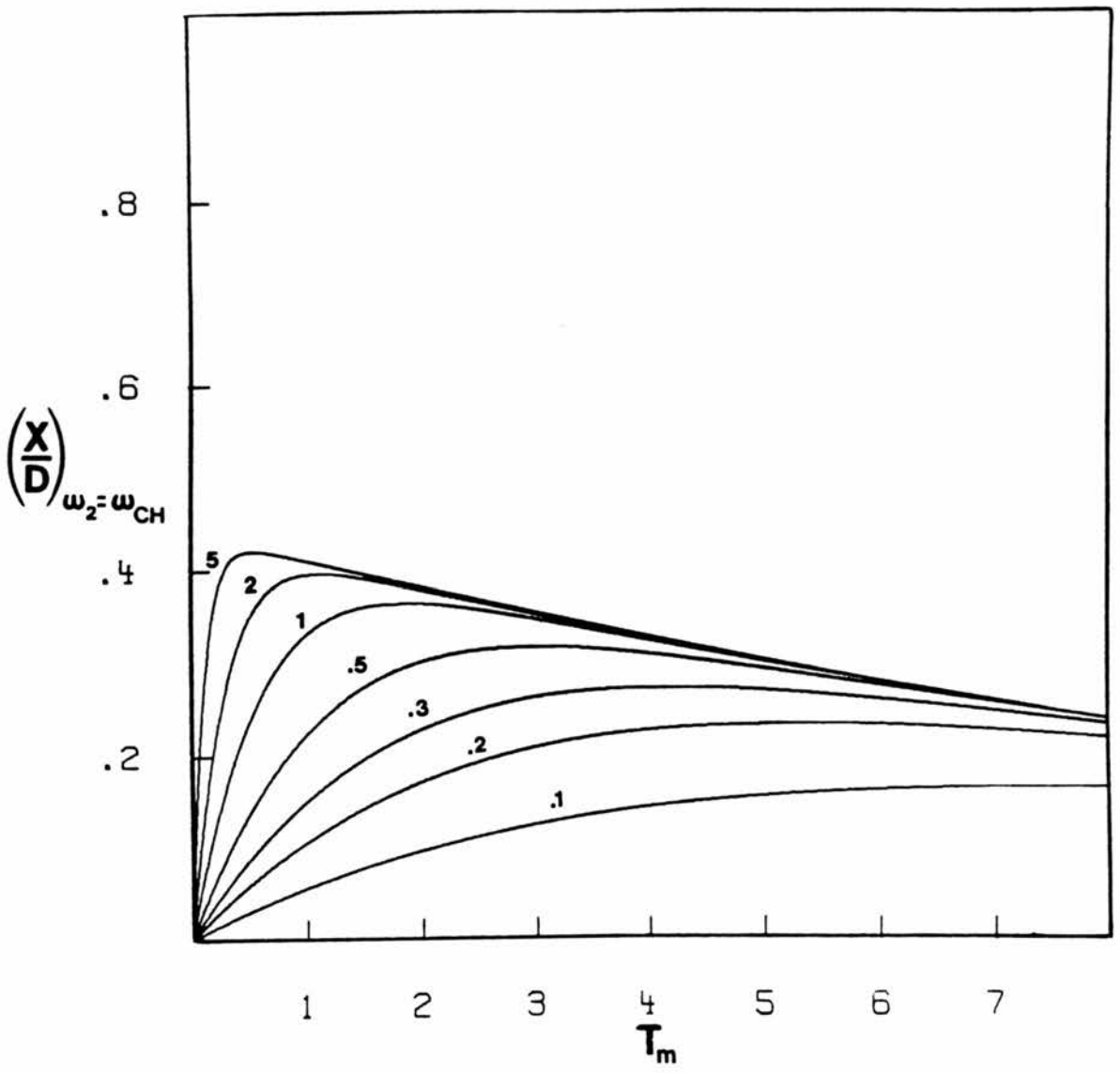
.8
.6
$\left(\frac{X}{D}\right)_{\omega_2=\omega_{CH}}$
.4
.2
5
2
1
.5
.3
.2
.1
1
2
3
4
5
6
7
T_m

Fig. 8. Plots of (X/D) at $\omega_2 = \omega_{CH_2}$ vs τ_m for several values of the transition probability W_o using T_{1CH} and T_{1CH_2} values given in the text.

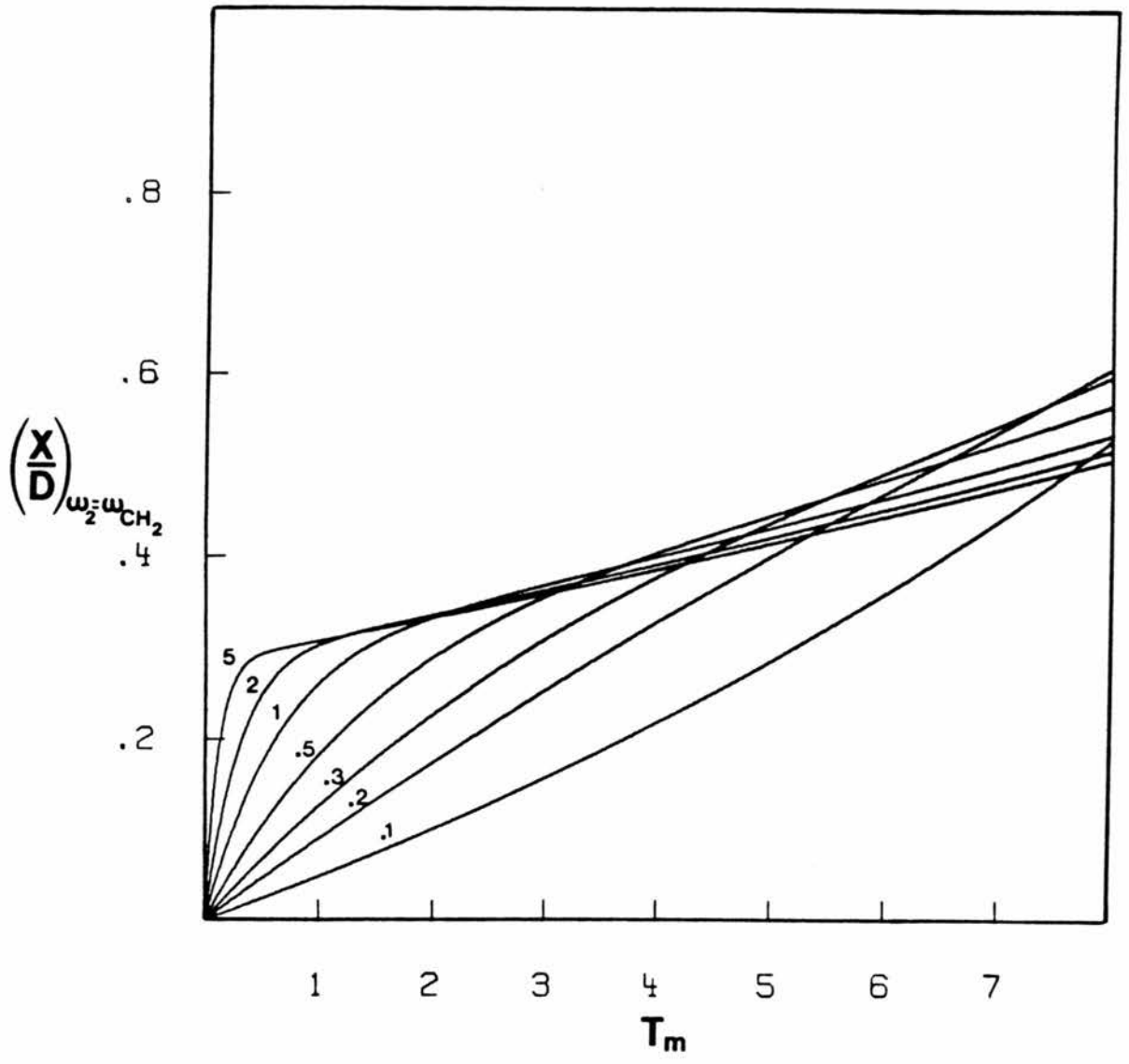
.8
.6
$\left(\frac{X}{D}\right)_{\omega_2=\omega_{CH_2}}$
.4
.2
5
2
1
.5
.3
.2
.1
1
2
3
4
5
6
7
T_m

Fig. 9. Plots of (X/D) at $\omega_2 = \omega_{CH}$ vs τ_m for several values of T_{1CH}, using W_o and T_{1CH_2} values given on the text.

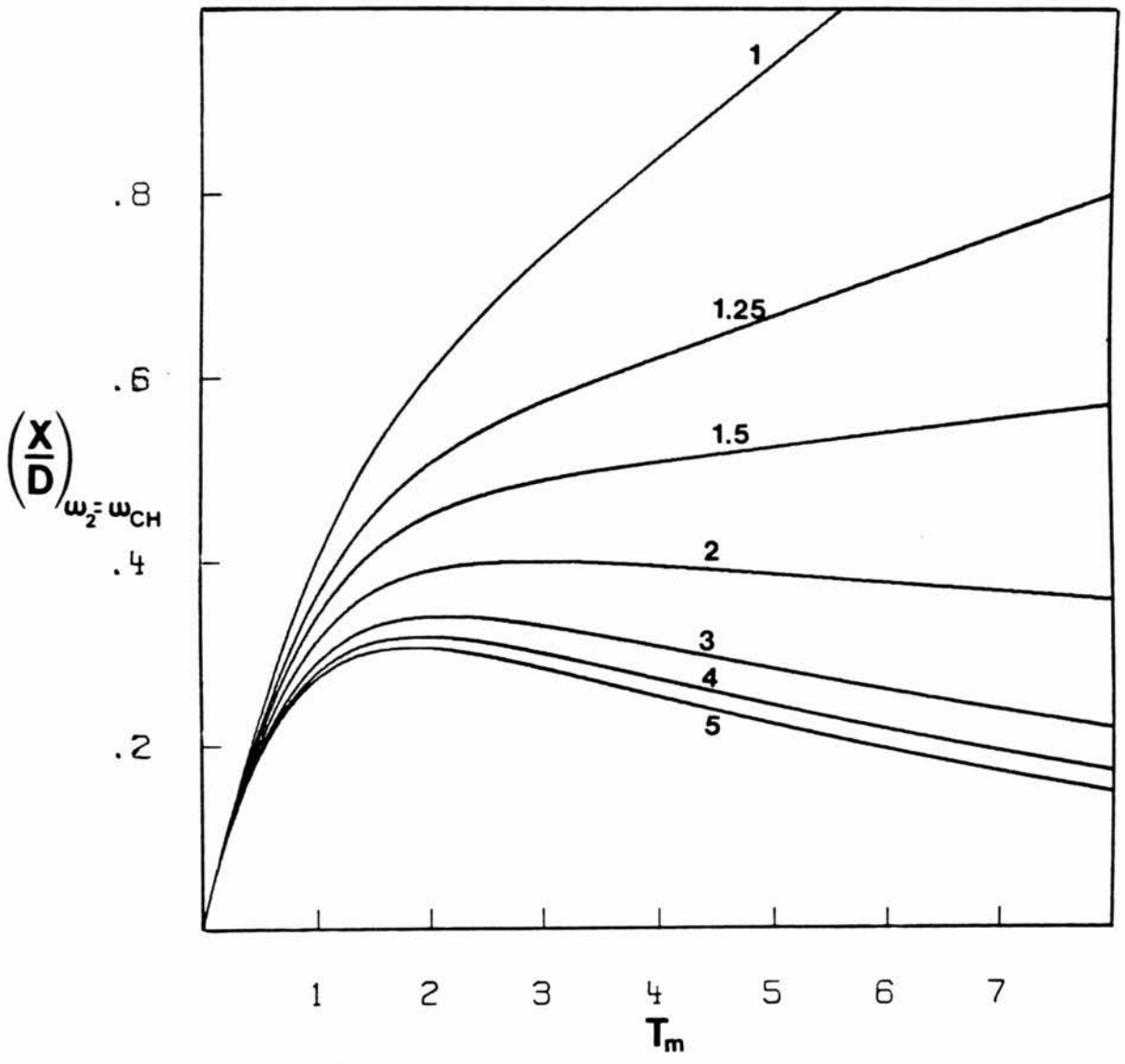
1
1.25
1.5
2
3
4
5
.8
.6
.4
.2
$\left(\frac{X}{D}\right)_{\omega_2 = \omega_{CH}}$
1
2
3
4
5
6
7
T_m

Fig. 10. Plot of (X/D) at $\omega_2 = \omega_{CH_2}$ vs τ_m for several values of T_{1CH} using W_o and T_{1CH_2} values given in the text.

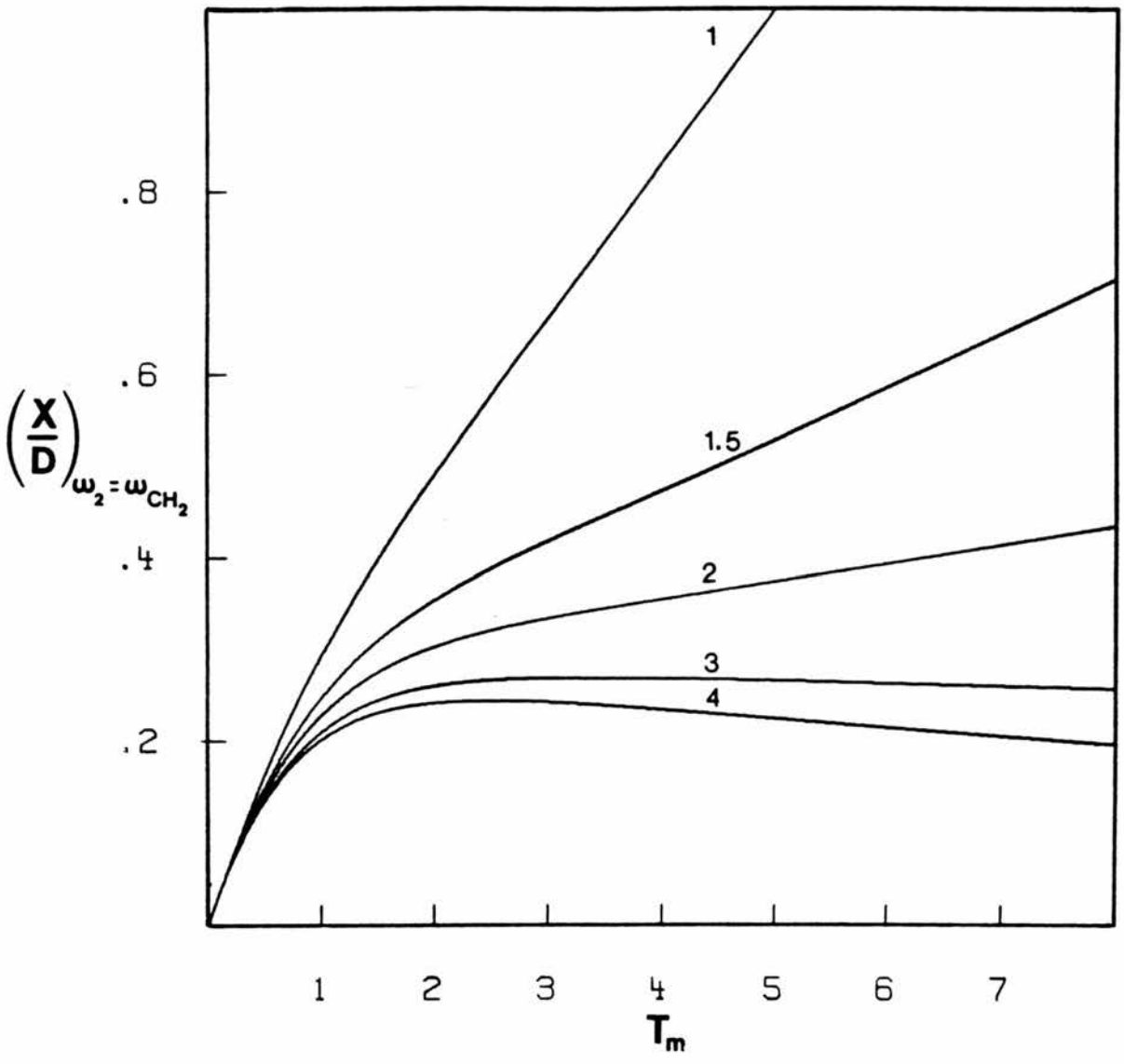
1
1.5
2
3
4
.8
.6
.4
.2
$\left(\frac{X}{D}\right)_{\omega_2 = \omega_{CH_2}}$
1
2
3
4
5
6
7
T_m

Fig. 11. Plot of (X/D) at $\omega_2 = \omega_{CH}$ vs τ_m for several values of T_{1CH_2} using W_o and T_{1CH} values given in the text.

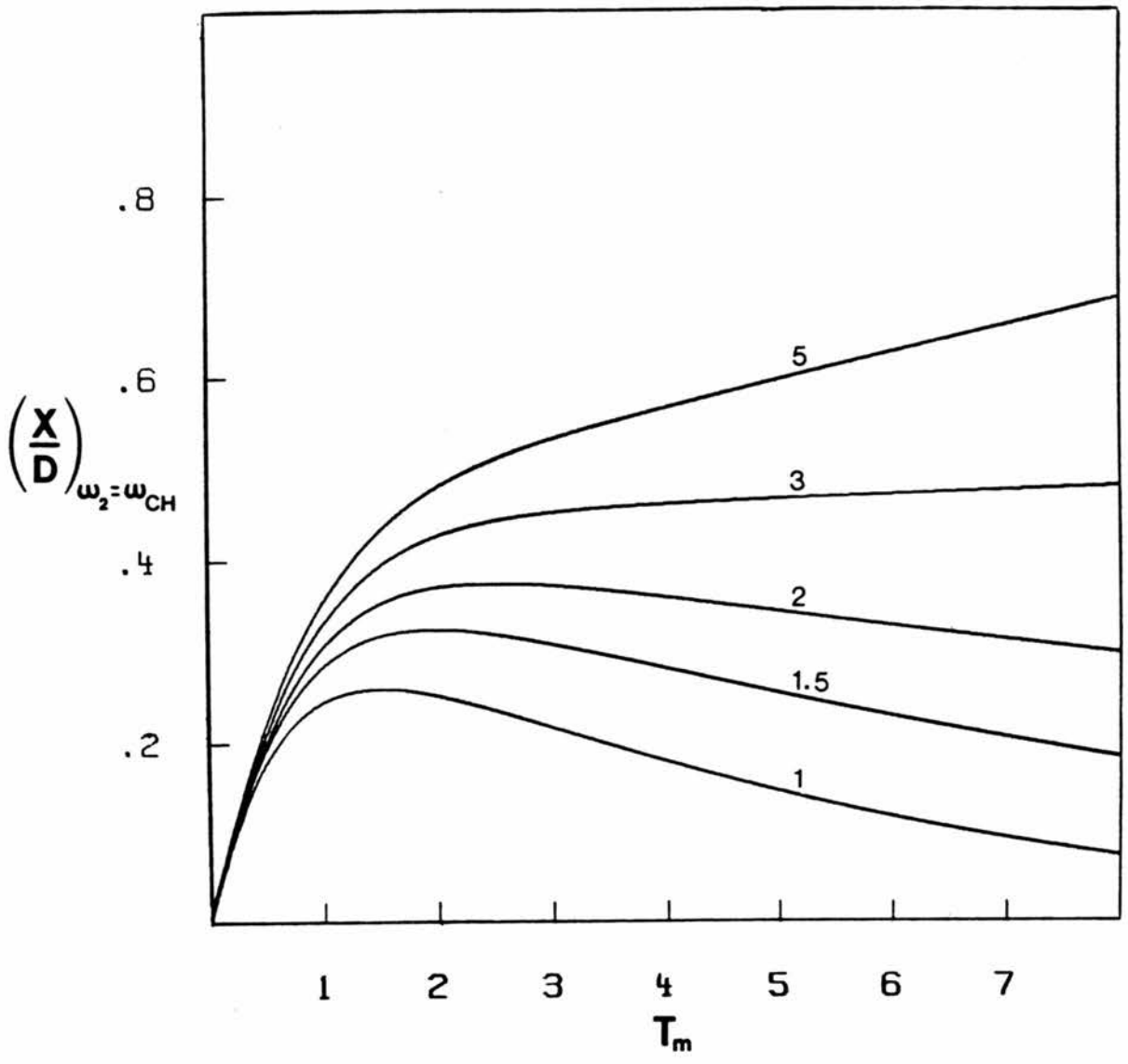
.8
.6
.4
.2
$\left(\frac{X}{D}\right)_{\omega_2=\omega_{CH}}$
5
3
2
1.5
1
1
2
3
4
5
6
7
T_m

Fig. 12. Plot of (X/D) at $\omega_2 = \omega_{CH_2}$ vs τ_m for several values of T_{1CH_2} using W_o and T_{1CH} values given in the text.

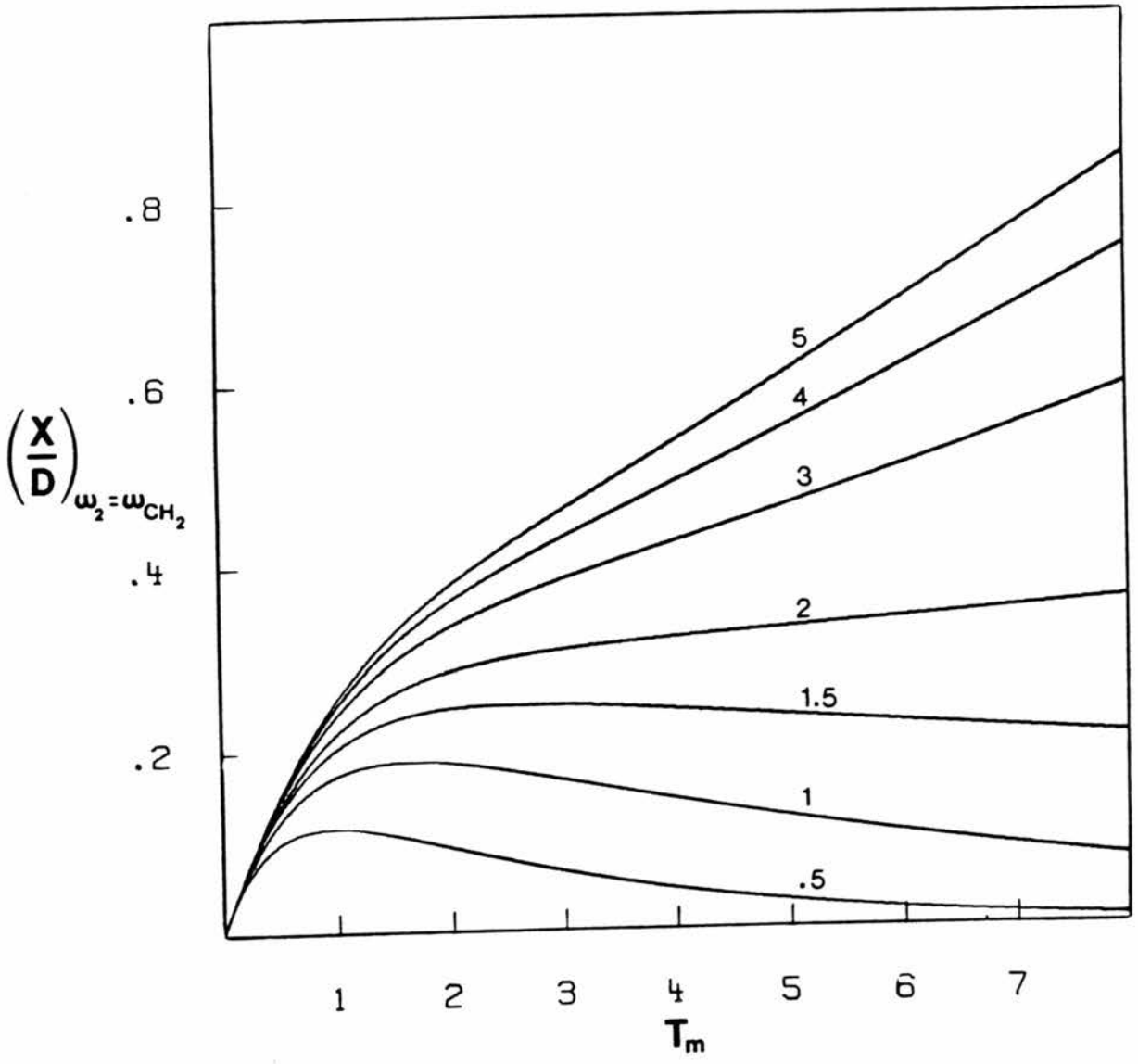
.8
.6
.4
.2
$\left(\frac{X}{D}\right)_{\omega_2=\omega_{CH_2}}$
5
4
3
2
1.5
1
.5
1
2
3
4
5
6
7
T_m

second shell to be roughly $(6.6/9.3)^6 W_o \approx 0.13 W_o$; an example of the latter is a central CH exchanging with a distant CH_2 via a CH that is a neighbor of both. One of the aims of this work was to determine whether this type of change in spin-diffusion behavior could be observed with increasing τ_m, indicating the progressive involvement of wider spheres of influence as τ_m is increased.

That the quality of the experimental fit to the behavior predicted by the equations deteriorates for $\tau_m \approx T_1$ is in part a coincidence due to the particular values of W_o and R_1 encountered in adamantane. In this case $W_o > R_{1CH}, R_{1CH}$ and the initial kinetics are largely determined by spin-diffusion up to a mixing time of about $1/W_o$, at which point ^{13}C spin-lattice relaxation begins to exert a noticeable influence. There is a "directionality" to the cross-peaks in the sense that $S_{CH,CH_2}(\omega_1, \omega_2)$ corresponds to CH_2 intensity in the ω_2 domain that derives from CH magnetization during t_1, with an analogous interpretation for $S_{CH_2,CH}(\omega_1,\omega_2)$. We have chosen the ratios $S_{CH,CH_2}(\omega_1,\omega_2)/S_{CH_2,CH_2}(\omega_1,\omega_2)$ and $S_{CH_2,CH}(\omega_1,\omega_2)/S_{CH,CH}(\omega_1,\omega_2)$ in the data analysis and long-time behavior must be interpreted with this distinction in mind. Fig. 6 shows that the ratio $S_{CH_2,CH}(\omega_1,\omega_2)/S_{CH,CH}(\omega_1,\omega_2)$ bends over at $\tau_m \approx T_{1CH_2}$. The CH_2 spins have by this time undergone significant ^{13}C spin-lattice relaxation, thus damping the effect of $CH_2 \rightarrow CH$ exchange during τ_m. The equations predict a gradual decay in X/D because the cross-peak intensity, which depends on CH_2 relaxation, dies off more quickly than diagonal-peak intensity is transferred to auto peak intensity. The experimental curve, however, shows a continual gradual rise to $\tau_m \approx 8$ sec before

beginning to fold over. This is due to spin-diffusion with more isolated spins for which $W_0 < R_{1CH}, R_{1CH_2}$, in which case spin-diffusion will continue to increase the X/D value well past a mixing time equal to T_{1CH_2}.

A similar argument applies to $S_{CH,CH_2}(\omega_1,\omega_2)/S_{CH_2CH}(\omega_1,\omega_2)$. Here the X/D ratio continues to increase for longer mixing times because of slower relaxation of the cross-peak source as compared to the diagonal-peak source. Again, the effects of slower spin diffusion with more isolated spins is to produce larger cross-peaks than predicted at longer times.

1.6. Summary.

The two-dimensional exchange experiment has been applied to the problem of ^{13}C spin diffusion in solids, demonstrating that it can occur at appreciable rates. The observation of significant ^{13}C spin diffusion points to a need for considering this phenomenon in the planning and interpretation of solid-state ^{13}C NMR experiments. The role of the protons in determining these rates has been demonstrated. Over relatively short times, it is possible to interpret spin-diffusion data in terms of short-range interactions. However, the extraction of geometric information from such data will generally be difficult due to the diversity of carbon-carbon dipolar couplings in an organic solid.

The main point of interest here is that ^{13}C spin-diffusion can in fact occur at significant rates if the ^{13}C-^{1}H coupling is of the right size to allow effective spectral overlap. In the case of adamantane, molecular motion reduces the undecoupled ^{13}C linewidth sufficiently to provide this overlap. This suggests the possibility of experimentally

controlling spin-diffusion rates by altering the ^{13}C-^{1}H dipolar coupling. Adamantane is sufficiently weakly coupled that magic-angle spinning or the application of low-power ^{1}H decoupling during τ_m is enough to quench ^{13}C spin-diffusion over the time-scale of this study. Alternatively, ^{13}C mixing can occur while the ^{13}C magnetization is spin-locked in the rotating frame, compressing the chemical shift scale by a factor of 10^3 to 10^4 and decoupling carbon from the protons.[13] Spectral overlap may still occur as a result of homogeneous broadening such as that resulting from the reduced (by 1/2) ^{13}C-^{13}C dipole coupling and result in relatively rapid spin-diffusion. Such an experiment was carried out with adamantane, producing appreciable cross-peaks for τ_m as small as 10 ms. This experiment does not rely on such fortuitous overlap as occurs in adamantane and potentially has a wider range of application than the experiment discussed here. However, neither the execution nor the interpretation of a rotating-frame experiment is straightforward. We are presently undertaking a more detailed study of this alternate experiment with a view toward inducing spin-diffusion in less mobile systems and using it as a probe of structural heterogeneity.

REFERENCES

1. N.M. Szeverenyi, M.J. Sullivan and G.E. Maciel, J. Magn. Reson., 47, 462 (1982).
2. J. Jeener, B.H. Meier, P. Bachmann and R.R. Ernst, J. Chem. Phys., 71, 4546 (1979).
3. J. Virlet and D. Ghesquieres, Chem. Phys. Lett., 73, 323 (1980).
4. S. Macura and R.R. Ernst, Mol. Phys., 41, 95 (1980).
5. V.J. Bartuska and G.E. Maciel, Anal. Chem., 54, 2194 (1982).
6. D. Torchia, J. Magn. Reson., 30, 613 (1978).
7. M.J. Sullivan and G.E. Maciel, Anal. Chem., 54, 2194 (1982).
8. A. Abragam, "The Principles of Nuclear Magnetism" Oxford University, London, 1961, p. 123.
9. W. Nowacki, Helv. Chim. Acta., 28, 1233 (1945).
10. D.W. McCall and D.C. Douglass, J. Chem. Phys., 33, 77 (1960).
11. D.L. VanderHart and A.N. Garroway, J. Chem. Phys., 71, 2773 (1979).
12. Reference 8, p. 137.
13. C.S. Yannoni, Acc. Chem. Res., 15, 108 (1982).

PART 2

ZEOLITES

1.1 Introduction

Part II discusses the applications of solid-state ^{13}C NMR techniques to the study of a simple zeolite adsorbtion system. The system of methanol adsorbed onto Hydrogen Y zeolite was studied using a variety of solid-state NMR techniques. Species of differing mobility and dipolar couplings were observed and assigned. The nature of ^{13}C-^{1}H dipolar coupling within the methyl group was found to be an important parameter in this study.

1.2 Structure and Composition.

The zeolites are "framework" aluminosilicates consisting of AlO_4 and SiO_4 tetrahedra linked together by the sharing of all oxygens to form a regular, infinite three-dimensional network of pores and cavities.[1] Their composition is given by the general formula

$$M^{n+}(AlO_2)_x(SiO_2)_y \cdot zH_2O \qquad (1)$$

where M^{n+} is a cation of charge n, typically from Group I or II, balancing the negative charge of the tetrahedral aluminum. These cations along with adsorbed water occupy the pores and cavities, forming a highly ionic "intracrystalline fluid".

It is the regularity of the zeolite framework and the consequent uniform pore size which distinguishes zeolites from other adsorbents, such as activated charcoal, silica gel, or glass, which display relatively broad distributions of pore sizes. The boundary between adsorption and rejection is usually sharp with zeolites, making them quite attractive as "molecular sieves". In a fully hydrated zeolite, the cations residing in the pores and cavities are usually quite mobile and are readily exchanged with other cations without significantly perturbing the framework structure.

Dehydration of some ion-exchanged zeolites initiates a chemical transformation of the zeolite into a highly active species capable of catalysing a variety of reactions in species that are subsequently

adsorbed into the zeolite. The activated zeolite generally acts as a Bronsted or Lewis acid and thus can be grouped with the other surface acids in terms of its chemical proclivities. As a class, the zeolites display catalytic activity that can be 10 to 100 times that of other solid acids.[2]

This fact alone has generated substantial interest in zeolite catalysts, but it is the wide range of cations that can be introduced into the zeolite, allowing for the "fine tuning" of catalytic behavior, and the steric control exerted by the framework on reactants and products that primarily distinguish the zeolites from the other solid acids.

1.3 Activation

As stated above, the zeolite may be activated by first exchanging a Group I or II cation with some other cation and then heating. Other methods may be used,[3] but will not be discussed here. A brief description of the activation of polyvalent-cation-exchanged (PCE) and alkylammonium-cation-exchanged (ACE) zeolites, two of the more common types, is given here in demonstration of the general features of the activation process. A more detailed discussion of materials used in this work is deferred to a later section.

1.3.1 Activation of polyvalent-cation-exchanged zeolites

The details of the mechanism for the activation of PCE zeolites are controversial[4] and will probably remain so for some time. The results of activation are strongly influenced by both the nature of the zeolite, e.g., the method of synthesis or the degree of ion exchange,

and the activation method, e.g., rate of heating and time spent at a given temperature, whether the activation was carried out under vacuum, in an inert atmosphere or in air. Nonetheless, it is generally believed that, as the zeolite is brought to progressively higher temperatures, the polyvalent cation undergoes hydrolysis, resulting in the generation of acidic moieties in the zeolite framework that are commonly referred to as structural hydroxyl groups. These structural hydroxyl groups are commonly denoted in the literature as shown in the structure below

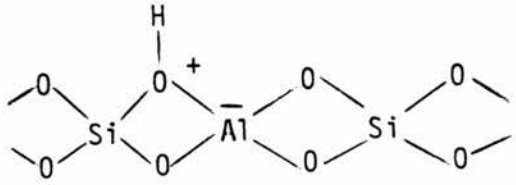

(2)

in which a proton is attached to an oxygen atom that is attached to an aluminum atom with a formal charge of -1 and a silicon atom with a formal charge of zero. An infrared spectrum of an activated zeolite will typically contain several bands in the OH stretching region corresponding to these groups. The number of structural hydroxyl groups generated by the activation is greater for more highly charged cations.

The activation of a trivalent cation exchanged zeolite is sketched below.[5] In the wet zeolite, the cation is present as a mobile hydrated species:

$$M(H_2O)_n^{3+} \qquad (3)$$

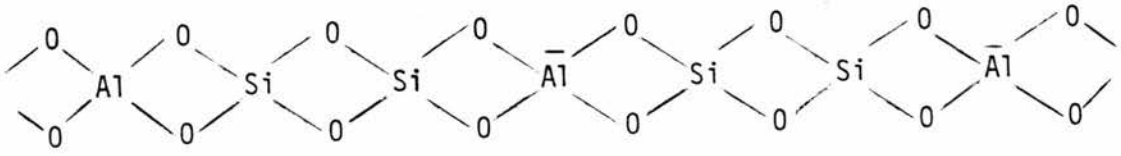

(I)

Activation at lower temperatures (300-400°C) removes intracrystalline water. As the dehydration nears completion, residual water molecules dissociate in the electrostatic field of the metal cation, resulting in the formation of structural hydroxyl groups. Several mechanisms have been proposed:

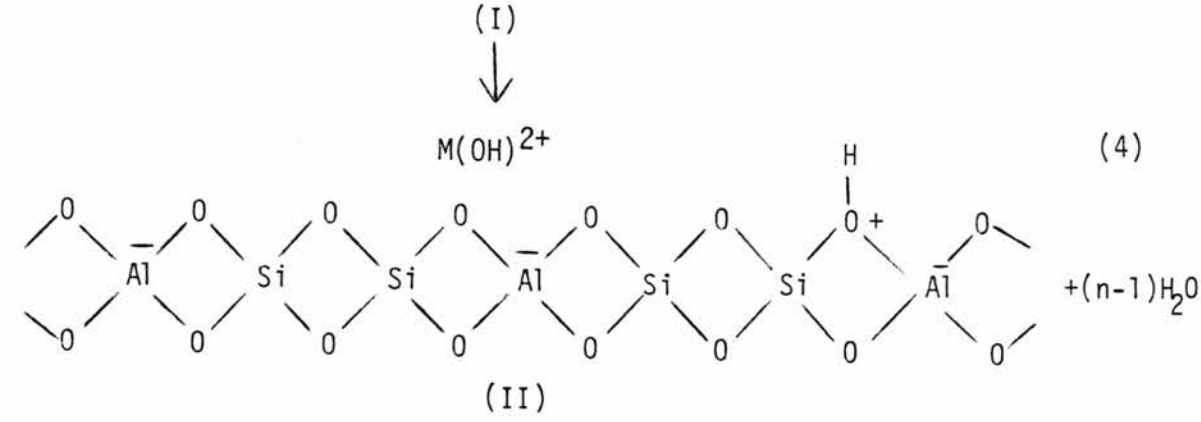

(4)

(II)

or

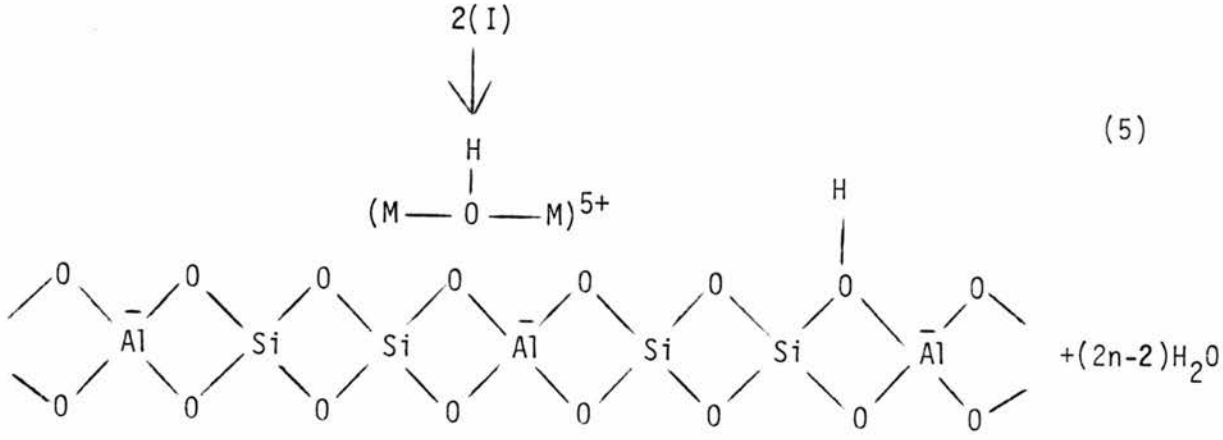

(5)

(III)

or

(I)

$\downarrow$

$M(OH)_2^{+}$ (6)

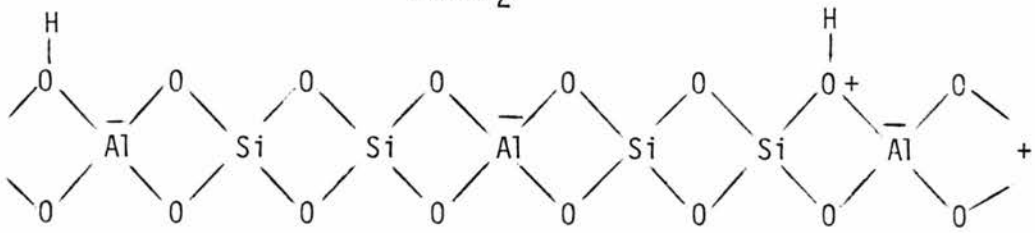

$+ \quad (n-2)H_2O$

Continued heating in the range 400 - 600°C removes the structural hydroxyl groups

(II), (IV)

$\downarrow$

M^{3+} (7)

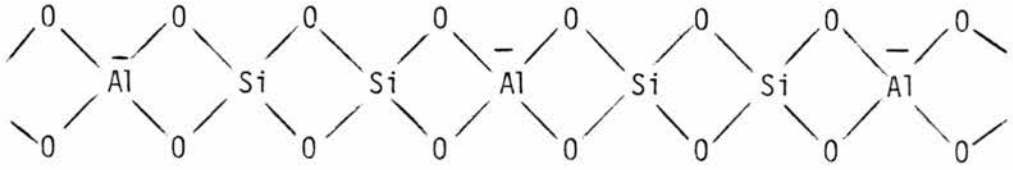

(V)

$+ H_2O$ (II) or $+ 2H_2O$ (IV)

or

(III)

$\downarrow$

$(M—O—M)^{4+}$ (8)

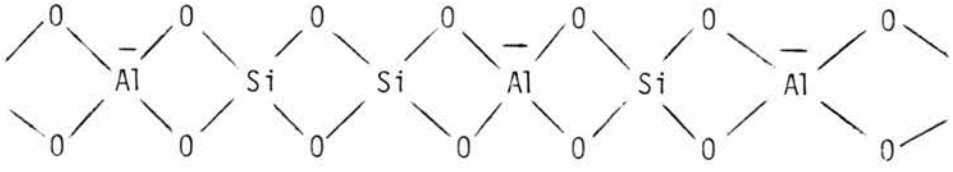

$+ H_2O$

(VI)

In the above mechanisms the dehydroxylation of (II) and (IV) is predicted to restore the original framework structure. Dehydroxylation of (III) generates a silicium ion, tricoordinate aluminum and a defect in the framework structure associated with the loss of an oxygen atom.

1.3.2. Alkylammonium-Cation-Exchanged (Ace) Zeolites

The activaton of ACE zeolites is achieved through the thermal decomposition of the alkylammonium cation into the corresponding amine and a proton which attaches to a framework oxygen. The most commonly used cation is the ammonium cation, which is used in the discussion below. Ideally, the alkylammonium cations are replaced by structural hydroxyl groups, and the activated zeolite should contain no exchangeable metal cations. Hence, activation by decomposition of the alkylammonium cation is sometimes referred to as decationization. Further heating results in the loss of framework water, which necessarily generates defects.

Heating the ammonium-exchanged zeolite at roughly 300 - 400°C results in the evolution of gaseous ammonia and the generation of structural hydroxyl groups:

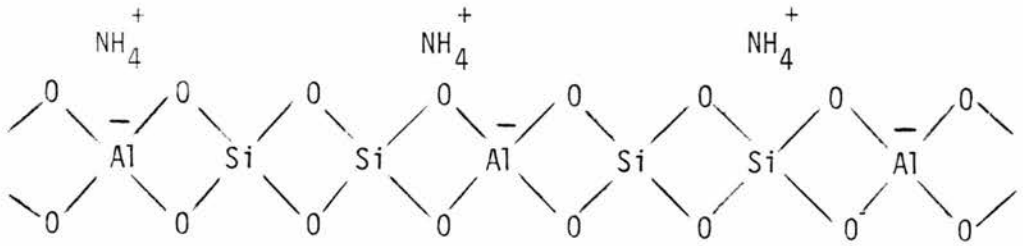

(9)

(VII)

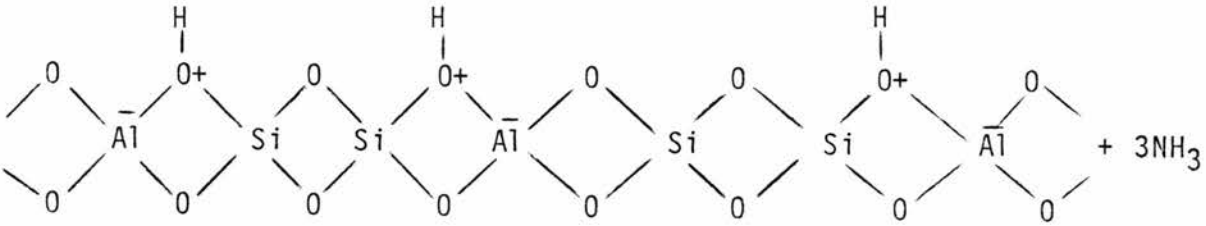

(VIII) (10)

Heating above 400°C results in dehydroxylation:

(VIII)

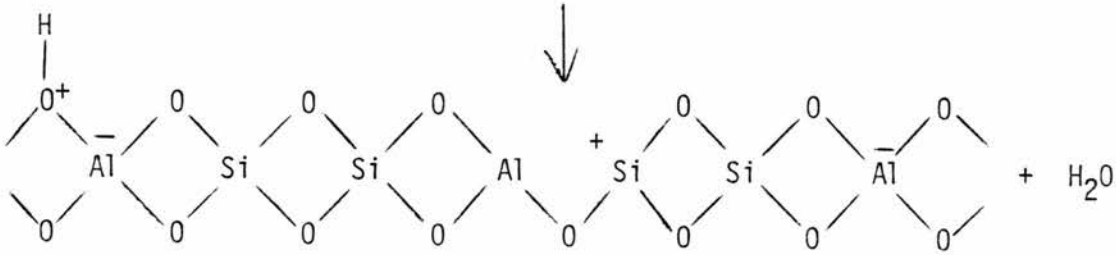

(IX) (11)

1.3.3. Catalytic Properties of Activated Zeolites.

The literature on zeolite chemistry is quickly reaching encyclopedic volume.[6,7,8] Whereas the principal uses of zeolites were once largely limited to separations and catalytic cracking, they are now being applied to areas as diverse as bulk chemical synthesis, pollution control, water softening and beverage carbonation. As the uses of zeolites multiply, so do the number of synthetic zeolites available to

the chemist. This section presents a brief selection of the more common reaction types that are catalysed by the zeolites. The discussion below is limited to reactions in which the zeolite catalyst behaves as an acid. There is a substantial range of non-acidic zeolite behavior,[9] but its discussion is beyond the scope of this work.

The reactions catalysed by the acidic zeolites are analogous to those occurring in acidic solutions and are thought to occur via carbonium-ion intermediates.[10] Some common types of reactions are listed below.

1. Double Bond Migrations
   e.g., 1-butene $\longrightarrow$ 2-butene
2. Condensation Reactions
   e.g., ethylene $\longrightarrow$ isobutene
3. Alkylation
   e.g., isobutane + ethylene $\longrightarrow$ 2,3, dimethylbutane
4. Elimination
   e.g., ethyl alcohol $\longrightarrow$ ethylene
5. Polymerization
   e.g., methyl, ethyl alcohol $\longrightarrow$ gasoline
6. Cracking
   e.g., hexane $\rightarrow$ ethylene + ethane

The unique feature of zeolite catalysts is their ability to determine the direction and extent of reaction through steric interactions in what has become known as "shape selective catalysis". Access to and departure from active sites in the interior of the zeolite is diffusion controlled. This property of "mass transport selectivity" can produce dramatic results. For example, in a mixture of n-butyl alcohol and isobutyl alcohol over a 5 Å zeolite, only the n-butyl alcohol is dehydrated, whereas if the same mixture is reacted over a wider pore zeolite, CaX both alcohols are dehydrated. The now famous reaction of methyl and ethyl

alcohols over ZSM-5 zeolite to form gasoline is also due to shape selectivity for relatively short chain-length (C_4-C_{10}) hydrocarbons in ZSM-5.[11] A second mechanism, "spatioselectivity", selects for differences in the size and structure of reaction intermediates, leading to different products.[12] In high temperature reactions with several possible pathways the geometry of the active site can influence the direction of the reaction.

1.4. The Faujasite Zeolites.

The zeolite used in this study is HY, or Hydrogen Y, which is derived from NaY (Sodium Y), a synthetic faujasite, by ammonium exchange and calcination (heating). The selection of HY was motivated by its relative stability, ease of preparation, catalytic activity, and the presence of a large body of data with which to integrate the results of a solid-state NMR investigation. The faujasites in general and HY in particular are discussed below.

The mineral Faujasite and its synthetic analogues, X and Y, are among the most extensively studied zeolites. They have a relatively simple framework structure, consisting of an infinite array of truncated cubooctahedra (also known as sodalite units or beta cages) that are linked tetrahedrally through the 6-membered rings (Fig. 1). The linked beta cages form a network of "supercages" some 12 Å in diameter which are linked together by a three-dimensional system of intersecting pores roughly 8 Å in diameter (Fig. 2). The faujasite framework is stable to temperatures on the order of 800°C, with some exceptions to be mentioned later, so that activation is readily achieved. The pore diameter of 8 Å is quite large for a zeolite; more typical values range from 2.5 to 5 Å. One has a wider range of acceptable adsorbates and

Fig. 1. The beta cage structure of faujasite zeolites. Silicon or aluminum atoms are located at the vertices of the structure. Oxygen atoms lie between the vertices at the locations labelled 1-4.

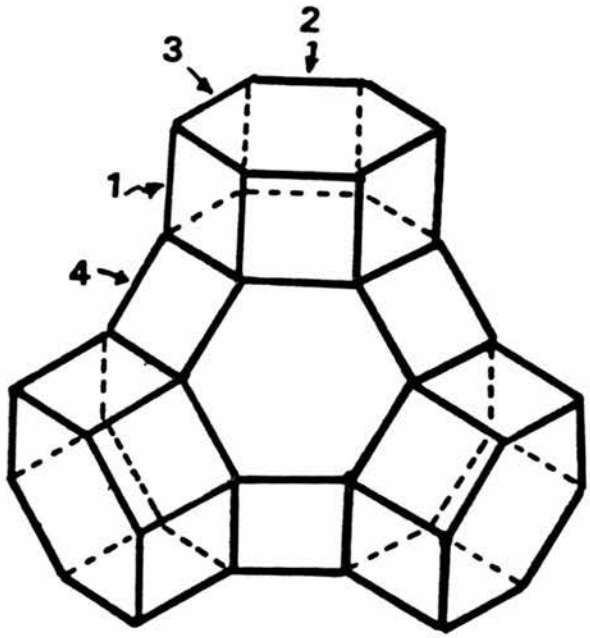
2
3
1
4

Fig. 2. Beta cages linked through the 6-rings to form the faujasite structure.

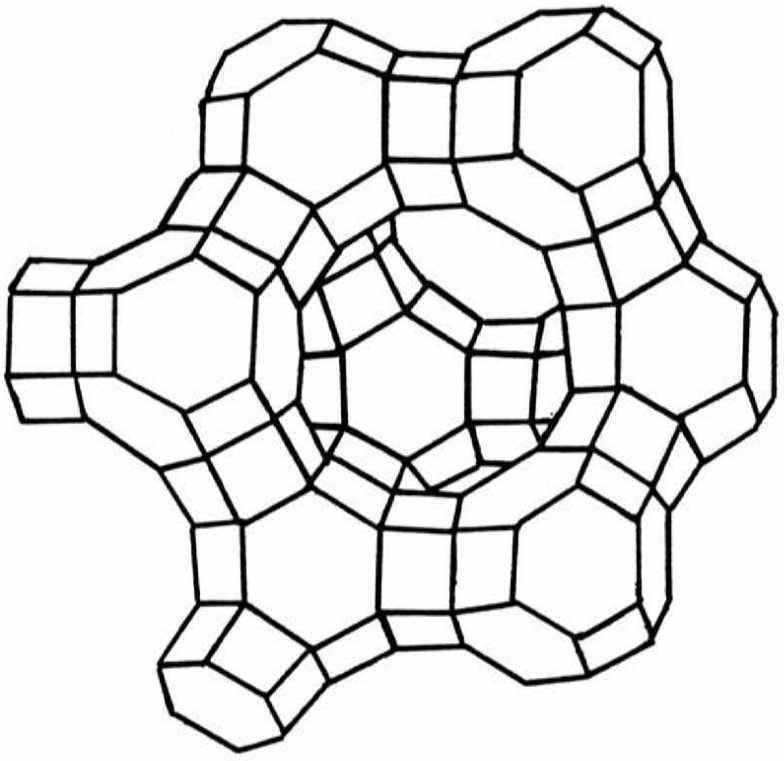

thus a wider range of catalytic behavior with the faujasites than with the majority of zeolites. Finally, the faujasites have the largest internal volume of the zeolites; roughly 50% of the volume of the dehydrated faujasite is void volume.

The naturally occurring mineral faujasite is rare and of rather ill defined composition and is thus not very well suited for model studies. Both X and Y are commercially available with a variety of counterions. X and Y differ mainly in the amount of aluminum present in the framework, which is usually expressed in terms of the ratio of the number of silicon atoms to the number of aluminum atoms, R.

$$R = N_{Si}/N_{Al} \qquad (12)$$

For zeolite X, $1 < R < 1.5$; and for Y, $1.5 < R < 3$. Generally Y zeolites display greater chemical and thermal stability than X zeolites[13] and the activated species are more acidic,[14] with the result that the Y zeolites are more frequently used, the major exception being the extensive use of various X zeolites as dessicants.

1.4.1. Activation of Zeolite Y.

Activation of zeolite Y can be achieved in many ways,[15] the two most common methods being those discussed earlier. Activation by decomposition of the ammonium exchanged species, or decationization, was selected here since it should ideally result in a cation-free zeolite, thereby avoiding the potential complication of cation-adsorbate interactions. In fact, the decationization of NH_4Y is more complex than indicated in the simple scheme above and can produce a variety of products, including cationic forms.

It is generally agreed that the activation of NH_4Y by thermal decomposition of the ammonium ion proceeds in four more-or-less overlapping steps: dehydration, deammoniation, dehydroxylation and dealumination. At temperatures in the range of 100 - 200°C and atmospheric pressure the bulk of the adsorbed water is removed. Somewhere in this temperature range, depending on the details of the activation technique, decomposition of the ammonium ion begins. Decomposition of the ammonium cation is largely complete at around 400°C. In the 300 - 400°C range dehydroxylation begins; this is the formation of water from the hydroxyl groups and lattice oxygen (see Eqn. 10), and is essentially complete at 600 - 700°C. In more-or-less the same temperature range as dehydroxylation occurs, aluminum(III) may be hydrolyzed by residual water and extracted from the framework in the form of a cationic or neutral hydroxide. The extent of this "dealumination" process depends on the amount of water available to perform the hydrolysis. If the activation takes place in a sealed vessel (self-steaming) or in the presence of water vapor, extensive dealumination occurs and the framework composition and structure is modified.

As stated above, the decomposition of the ammonium cation is accompanied by the generation of structural hydroxyl groups, which in the past have been conveniently monitored with infrared spectroscopy.[16] The activaton of NH_4Y always produces three distinct bands in the hydroxyl stretch region:[17] 3740 cm^{-1}, 3650 cm^{-1}, and 3540 cm^{-1}. Other bands have been observed under particular activation conditions,[18] but these do not correlate with catalytic activity and are attributed to defect sites generated in the activation. Of the three characteristic bands, the one at 3740 cm^{-1} is not catalytically important and has been

attributed to either amorphous silicon impurities or to hydroxyl groups existing at crystallite boundaries. The remaining two bands are attributed to structural hydroxyl groups. The 3640 cm^{-1} or high frequency (HF) band is broad and assymetric and is perturbed by the adsorption of non-polar gases onto the zeolite. The 3540 cm^{-1} or low frequency (LF) band is narrow and remains unperturbed upon the adsorption of non-polar gases. This behavior is motivation for the assignment of the HF band as originating from structural hydroxyl groups projecting into the supercage, and the LF band as originating from structural hydroxyl groups projecting into the beta cage. Evidence confirming this assignment, mainly from X-ray diffraction[19] and wideline proton NMR[20] is available. In further support of this assignment, it has been shown that the adsorption of the sterically hindered base, pyridine, onto HY destroys the HF band but leaves the LF band intact. However, the adsorption of the stronger base, piperidine, attenuates both bands. It has been argued that in the presence of such a strong base the beta-cage protons migrate to positions where they are available for interaction[21]. Measurements of proton mobility tend to support this assertion.[22]

Decomposition of the ammonium cation can begin at temperatures as low as 100°C. Maximum intensity of the structural hydroxyl bands is attained at 300 - 400°C and remains roughly constant up to 500 - 600°C, at which point significant dehydroxylation occurs. Catalytic activity tends to decrease with increasing dehydroxylation,[23] substantiating the claim that the structural hydroxyl grops are the catalyticaly active centers.

According to the simple model presented earlier in this chapter, complete dehydroxylation of the zeolite should produce a species with

no residual cations and therefore no ion-exchange capacity, since the ionic charge is predicted to reside entirely within the framework. However, a residual ion exchange capacity of up to 50% of that of the original unactivated zeolite has been observed for NH_4Y,[24] indicating the formation of an exchangeable species during the activation. The exchangeable species is thought to be a cationic hydroxide of aluminum that is removed from the lattice during the activation. In a related observation it was discoverd that activating NH_4Y in the presence of water vapor results in the formation of a species with enhanced thermal stability.[25] The activation was again observed to involve the removal of aluminum from the lattice as a cationic hydroxide.

It is believed that formation of the cationic aluminum species is achieved by the hydrolysis of framework aluminum by residual water (see below). The extent of the hydrolysis depends strongly on the amount of water available. If the activation is done in vaccuo or in an inert atmosphere, a relatively unstable species is formed. Activation in a closed container (self-steaming) or in the presence of excess water yield "ultrastable" Y. It has been proposed that the effect of the excess water is to heal framework defects caused by dealumination by transporting silicon to the defect site.

When the activation is carried out with the rapid removal of water from the system, the resulting zeolite is very reactive towards water and decomposes at roughly 800°C. A mechanism consistent with the observed stoichiometry of dealumination is presented below.[26] Dehydration proceeds smoothly until the water:ammonium ratio nears 1:1, when further deammoniation occurs simultaneously with hydrolysis of the framework.

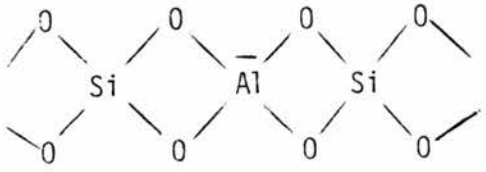

$+ NH_4^+ + H_2O$ (13)

(X)

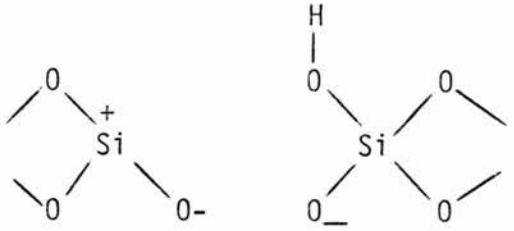

$+ Al(OH)_2^+ + NH_3$ (14)

(XI)

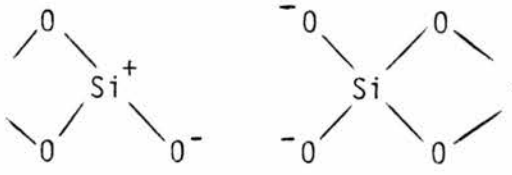

$+Al(OH)^{2+} + H_2O + NH_3$ (15)

(XII)

The mechanism in the presence of excess water is believed to be somewhat different:[27]

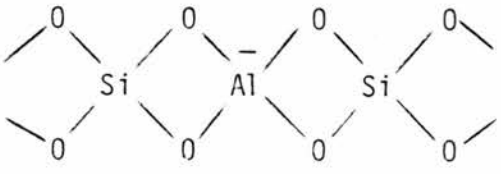

$+ NH_4^+ + 3H_2O$ (16)

(X)

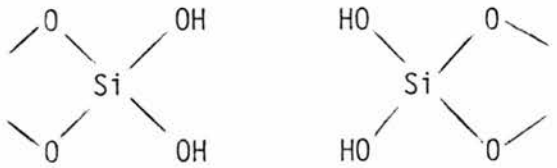

$$+ Al(OH)_3 + NH_3 \qquad (17)$$

(XIII)

Aluminum hydroxide then reacts with remaining acidic protons in the framework (e.g., structural hydroxyl protons).

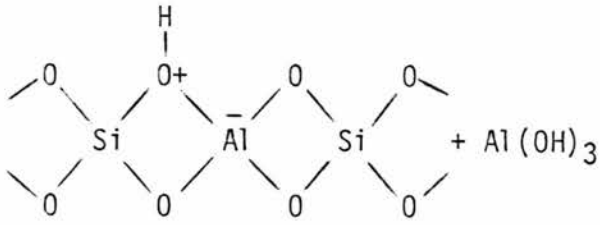

$$+ Al(OH)_3 \qquad (18)$$

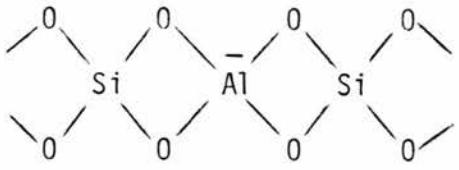

$$+ Al(OH)_2^+ + H_2O \qquad (19)$$

At higher temperatures, silicon that originates from either amorphous silica impurities in the zeolite or from regions in which the framework has decomposed is transported to the defect site and the framework structure is regenerated.

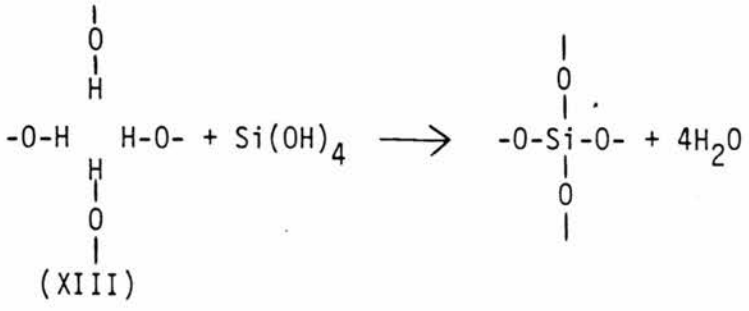

(20)

In the present study a sample bed of 4-6 cm depth was activated under vacuum. Such "normal bed" activation produces results intermediate between the ultrastable product of self-steaming and the unstable product of "thin-bed" activation in which a 2-3 mm thick bed is activated under vacuum.[28] Samples were activated in three stages. First a sample would be evacuated at room-temperature to remove loosely held water, then the temperature was brought to 200°C, where further dehydration occurs with minimum decationization. After 12 hr. at 200°C the temperature was slowly brought to the final value.

CHAPTER 2

NMR AND ZEOLITES

There have been several liquid-state NMR studies of materials adsorbed onto zeolites. Most of these share the limitation of the restriction of liquid-state NMR techniques to the observation of molecules undergoing rapid random motion. Although ^{23}Na and wideline ^{1}H studies have yielded significant results,[29,30] the majority of the NMR studies have been restricted to the observation of materials adsorbed on unactivated zeolites, or on activated zeolites at elevated temperatures or at relatively high loading levels;[31] in such cases the environments are those in which the bulk of the adsorbed material can be expected to be mobile enough to average anisotropic spin interactions.

^{13}C and ^{1}H NMR studies in the past have focussed mainly on the motion of the adsorbate, either *via* standard relaxation studies or through field gradient techniques.[32,33] This focus is in part due to an inability to detect significant perturbations of the chemical shift of these nuclei under the constraint of liquid-like conditions, e.g., high-loading levels, high temperature, unactivated zeolite, all of which are likely to induce rapid chemical exchange in the system. If one of these restrictions is relaxed, mobility is reduced and spectral resolution decays. It should be mentioned that wideline ^{1}H NMR has been used to observe species undergoing anisotropic motion in zeolites.[34] Moment analysis of the wideline proton signal can give information about the arrangement and motion of molecules within the zeolite,

indirectly yielding information about their interaction with the active sites. Relaxation studies have the potential of giving information about interactions with active sites, particularly proton relaxation, but proton relaxation in commercially available zeolites has often been found to be dominated by interaction with paramagnetic impurities in the framework.[35] This is not a fundamental limitation, since one may synthesize the zeolite from ultrapure starting materials. This option has not often been exercised. ^{13}C relaxation may be less sensitive to paramagnetic impurities,[36] since the carbon nucleus cannot be expected to approach the paramagnetic center as closely as protons. The carbon nucleus is sterically shielded from the active sites in the same manner, and one expects intramolecular (e.g., dipolar) relaxation to play an important role.

There have been a number of solid-state NMR studies of the zeolite framework itself.[37] The majority of these have used the standard 90° preparation pulse and magic-angle spinning (FTMAS or Bloch decay) to observe framework ^{29}Si and ^{27}Al resonances. The silicon studies have been particularly useful in studying the silicon-aluminum ordering of the framework, since the ^{29}Si chemical shift is sensitive to the number of aluminum neighbors. In a more practical sense the ^{29}Si spectrum provides a reliable nondestructive means of determining the silicon-to-aluminum ratio.

On the other hand there has been surprisingly little work done with solid-state NMR of adsorbed species. This is in spite of the well-established utility of CP/MAS in the study of similar systems.[38] Magic-angle spinning has been used with proton observation to assess the acidity of activated faujasites through perturbations in the

chemical shift,[39] and ^{2}H powder patterns of para-xylene adsorbed onto ZSM-5 have been interpreted in terms of anisotropic rotation.[40]

The advent of solid state ^{15}N methods should certainly prove useful in this regard, as has already been demonstrated for silica-alumina surfaces.[41] The use of ^{31}P as a probe nucleus is also quite promising.[42] ^{31}P is particularly attractive because of its 100% natural abundance and large gyromagnetic ratio, which provide quite good sensitivity in the NMR experiment. Apart from the chemical shift, there is a variety of interactions that can potentially prove useful in the study of chemisorbed species: the chemical shift anisotropy (CSA) and its modulation by molecular motion, dipolar coupling and spin diffusion, and the dynamics of the cross-polarization process.

The following sections describe a ^{13}C NMR study of a simple zeolite/absorbate system. Both solid-state and liquid-state techniques were used in that study.

CHAPTER 3

EXPERIMENTAL

3.1. Materials.

Alcohols were obtained from J.T. Baker Chemical Co. and Fisher Scientific Co.. Triethyl amine was obtained from the Malinckrodt Chemical Works. Gaseous methyl amine was obtained from the Matheson Co. and methanol enriched to 90% ^{13}C was obtained from Merck, Sharp and Dohme Canada, Limited. NH_4Y zeolite was obtained from the Strem Chemical Co. All liquids, other than enriched methanol, were distilled and stored over dried 3A molecular sieve. Methyl amine was used without further purification.

3.2. Sample preparation.

Zeolite samples were activated by heating under vacuum. The unactivated zeolite was placed in a quartz vacuum tube fitted with a vacuum stopcock. The quartz tube was then placed in a tube furnace, evacuated and brought to the desired temperature. The sample was kept at elevated temperature until the pressure stabilized at approximately 1 micron. After returning the sample to room temperature, the stopcock was closed and the sample stored in a dry box until needed. When needed for an experiment, the sample was transferred to a vacuum flask tared under 1 atm N_2. The flask was then reweighed. The flask was designed in conjunction with Roy Wier, the glassblower in the Department of Chemistry. It is shown schematically in Fig. 3. It

Fig. 3. Top: Schematic representation of vacuum bulb used in preparation of loaded zaolite samples.

Bottom: Arrangement used in transfer of a liquid to a zeolite.

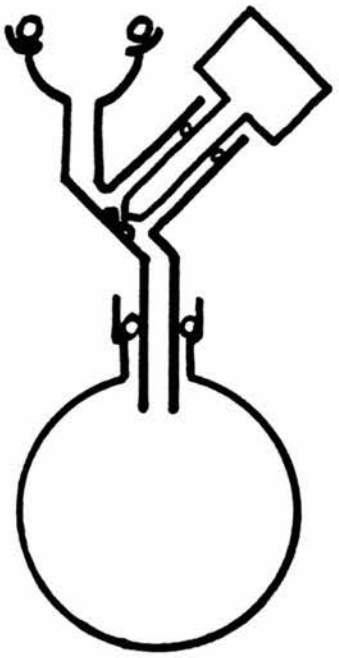

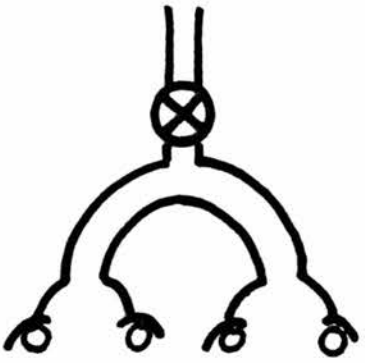

programming capability thanks to the "Spin Temperature Alternation box" built by Dr. Dale McKay.

^{13}C chemical shifts were measured relative to a value of 16.9 ppm for the methyl resonance of hexamethylbenzene measured via external reference to TMS.

No specific modification of the instruments was necessary. In fact the spectra were relatively easy to obtain. At natural abundance levels of ^{13}C, recording 2,000-40,000 scans at a 1 to 2 s repetition rate was generally sufficient for CPMAS spectra. For relaxation studies and two-dimensional experiments, samples were enriched to roughly 10% ^{13}C, after which 10-100 scans were adequate to record a single spectrum. For this level of ^{13}C enrichment the probability of there being more than one labelled molecule per cage is small.

The only "technical innovation" to result from this work is a design for a convenient water-tight spinner. The traditional method for handling water-sensitive materials has been to spin using dry nitrogen drive gas. Experience with unloaded activated HY has shown that during a long run (overnight), the zeolite will rehydrate. In several bench tests, weight gains of 15-30% were observed in an unloaded zeolite sample spun with nitrogen. A reasonable approach that does not involve major redesigning of the spinning system appears to be some sort of gasket or seal. The gasket matrial should not have NMR signals that interfere with those from a sample. It was found that Dow Silicone Rubber Sealant works well for this purpose. A cylindrical plug of the rubber is placed in the bottom of the insert (Fig. 4) with a 2-3 mm segment left protruding from the insert. The plug diameter is equal to the i.d. of the spinner body, so the protruding part forms a

Fig. 4. Schematic of a water-tight spinning system (Windmill spinner design shown). A silicone rubber plug with a diameter equal to the i.d. of the rotor is inserted into the Teflon insert, forming a gasket.

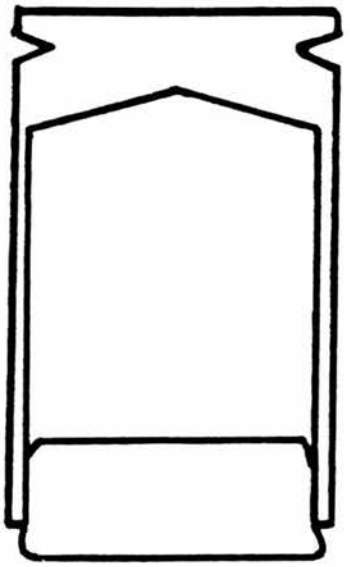

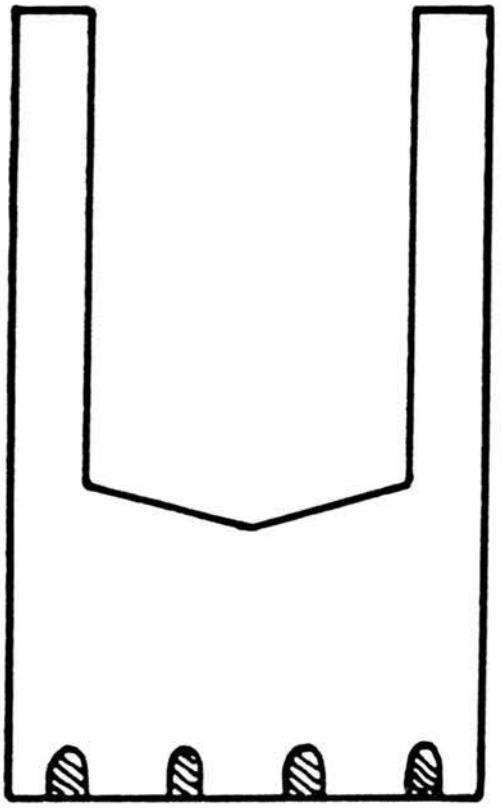

seal when the insert is placed in the spinner. With this arrangement an unloaded activated zeolite sample can be spun using air as a drive gas for 24 hours with no appreciable weight gain (< 1 mg with 300 mg of sample). The same sample when opened to the air after spinning will take up water on the order of 1 mg/min.

The sealant gives a very narrow ^{13}C signal at 1.14 ppm. Undecoupled, the carbon signal is a baseline-resolved quartet, which can be acquired for 100-200 msec and used as a (inconvenient) shimming standard. The sealant signal appears in both the CPMAS and FTMAS spectra. The ^{29}Si signal of the sealant at -20 ppm can be seen in the FTMAS experiment but has so far not been observed in the CP/MAS experiment. A significant disadvantage of this system is that one must sacrifice 10-20% of the sample volume to accommodate the plug. Thin plugs do not work; they evidently distort under the large forces encountered by spinning, and push the insert up. Thicker plugs seem to be fixed in place by centrifugal force, which provides a second sealing mechanism.

Dr. James Frye of the Regional NMR Facility at CSU has developed a sealing system using a thin Teflon insert that work quite well and is useful for most of the types of ^{13}C NMR measurement of this study. However, for some ^{13}C Bloch-decay experiments, the Teflon resonance falls in the middle of the ^{13}C spectrum.

Cross-polarization spectra were obtained using the pulse sequence in Fig. 5.[43] The phase of the proton 90° pulse was shifted 180° on alternate scans in order to remove baseline artifacts from the spectrum.[44] ^{13}C rotating-frame spin-lattice relaxation times were measured using the sequence shown in Fig. 6.[45] Laboratory-frame spin-lattice relaxation times were measured using the pulse-sequence discussed in

Fig. 5. The cross-polarization pulse sequence. ^{1}H polarization is rotated into the x-y plance by a 90° pulse. The ^{1}H rf field is then shifted 90° in phase, creating a spin lock of the ^{1}H spins. Simultaneous with the ^{1}H spin lock, a ^{13}C rf field is applied. The transfer of polarization from ^{1}H to ^{13}C is optimized under the Hartmann-Hahn condition, $(\gamma_H H_{1H}) = (\gamma_C H_{1C})$.

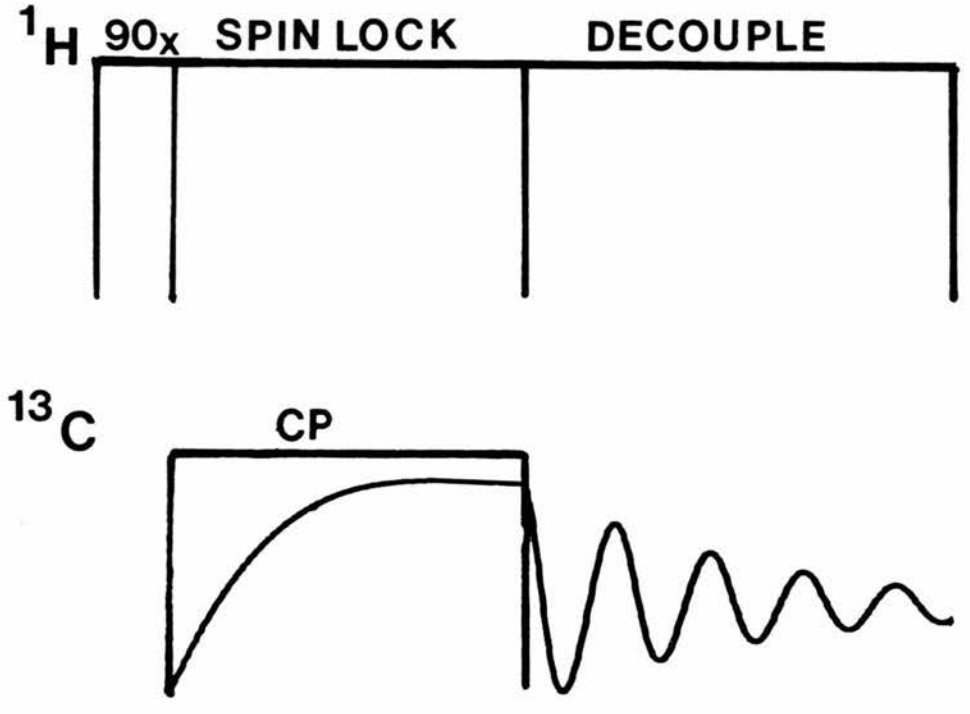
^{1}H
90x
SPIN LOCK
DECOUPLE
^{13}C
CP

Fig. 6. Pulse sequence for measuring $T_{1\rho}$. After preparation by cross-polarization, ^{13}C magnetization is lest to evolve in the ^{13}C spin-locking field for a variable time, t.

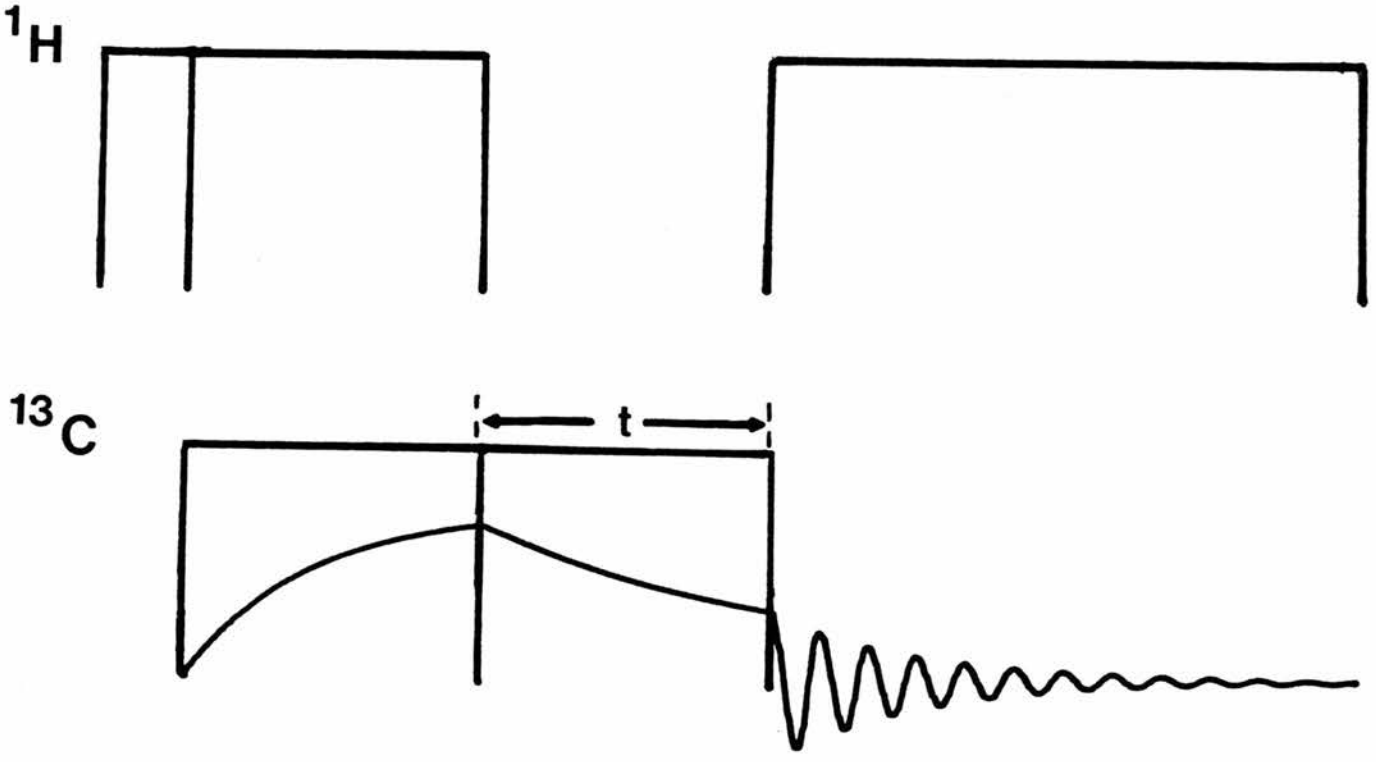
^{1}H
^{13}C
t

Fig. 7. Pulse sequence to measure the 90° pulse length of the ^{13}C r.f. field. ^{13}C magnetization is rotated back toward H_o immediately after preparation by cross-polarization.

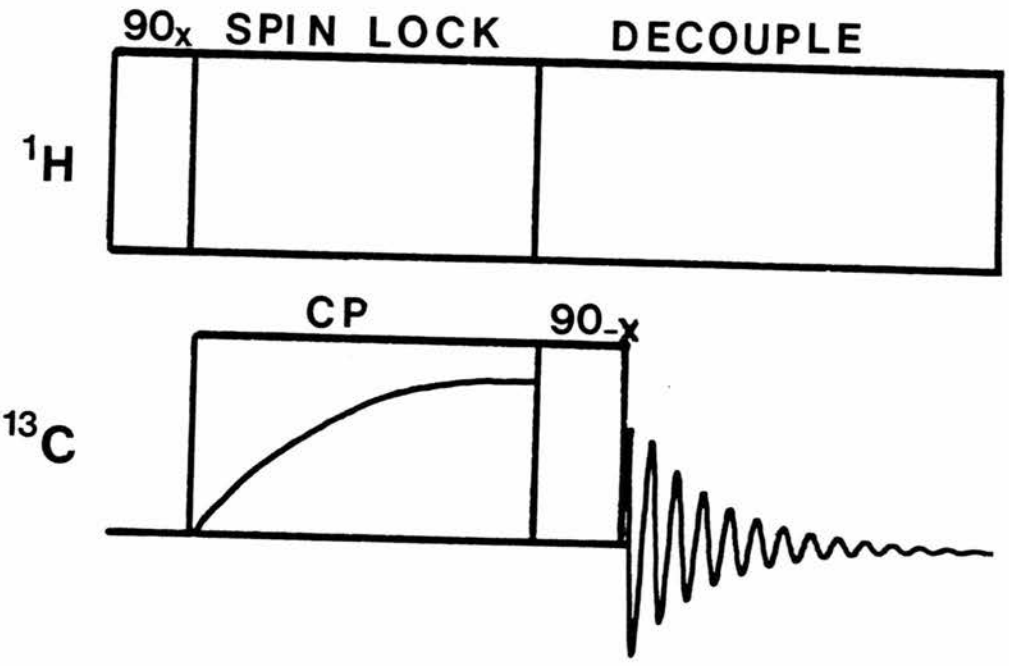
90x SPIN LOCK
DECOUPLE
1H
CP
90-x
13C

Chapter I.[47] The ^{13}C 90° pulse length in the CPMAS experiment was measured using the sequence shown in Fig. 7. In this experiment the carbon magnetization that is generated by cross-polarizaton is immediately pulsed towards H_0 by a short pulse shifted 90° in phase from the carbon spin-lock pulse and the FID recorded. A 90° pulse is characterized by a null in the magnetization, a 180° pulse by inversion of the magnetization, etc.

CHAPTER 4

CHOICE OF ADSORBATE

The first materials investigated were a pair of simple alkyl amines. The amines are relatively strong bases and thus ought to have a fairly strong interaction with the structural hydroxyl groups of HY. Methyl amine and triethyl amine were chosen for study. They are structurally simple and have significantly different basicities. Methyl amine has a K_b of 4.5×10^{-4} and triethyl amine has a K_b of 5.6. Fig. 8 shows the CPMAS spectrum of a sample consisting of 16% methyl amine by weight adsorbed onto NH_4Y activated at 450°C (HY(450)/16% CH_3NH_2). In this case, as in those discussed below, it is significant that a cross-polarization spectrum can be obtained at all, as this indicates the existence of a static component of the C-H dipolar coupling. This in turn suggests that the molecular motion of the adsorbate is restricted. In any event, the methyl resonance of methyl amine in this sample occurs at 25.8 ppm relative to TMS, as opposed to a liquid state value of 28.3 ppm.

The CPMAS spectrum of a sample of 17% methyl amine by weight on NH_4Y activated at only 150°C (HY(150)/17% CH_3NH_2) is shown in Fig. 9. As discussed above, activation of the zeolite at 150°C should not be adequate to maximize the number of structural hydroxyl groups in the zeolite. Only relatively weak acid sites should be present in this

Fig. 8. ^{13}C CPMAS spectrum of 16% methylamine by weight adsorbed onto HY(450).

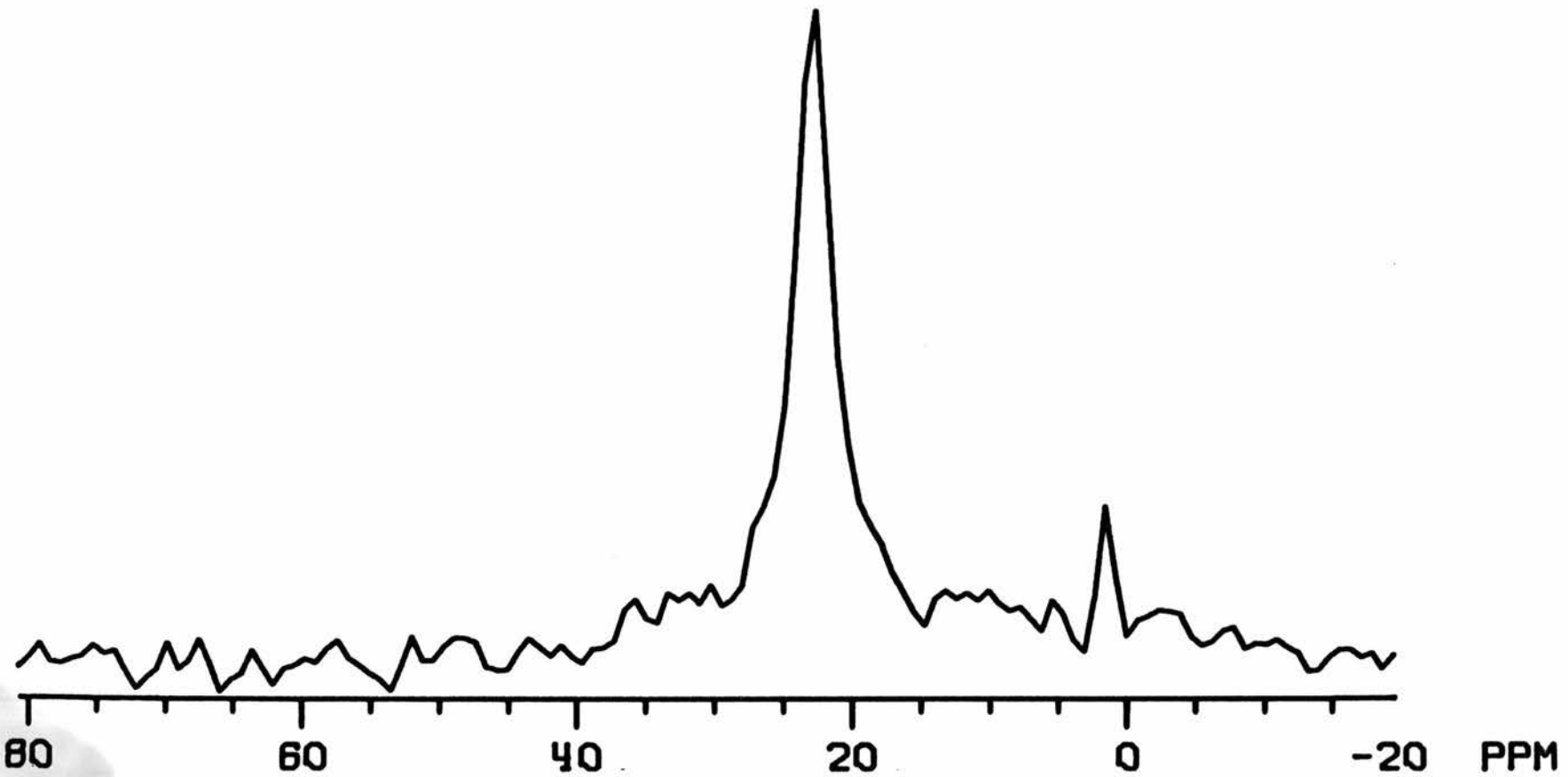
80
60
40
20
0
-20
PPM

Fig. 9. ^{13}C CPMAS spectrum of 17% methylamine by weight adsorbed onto HY(150).

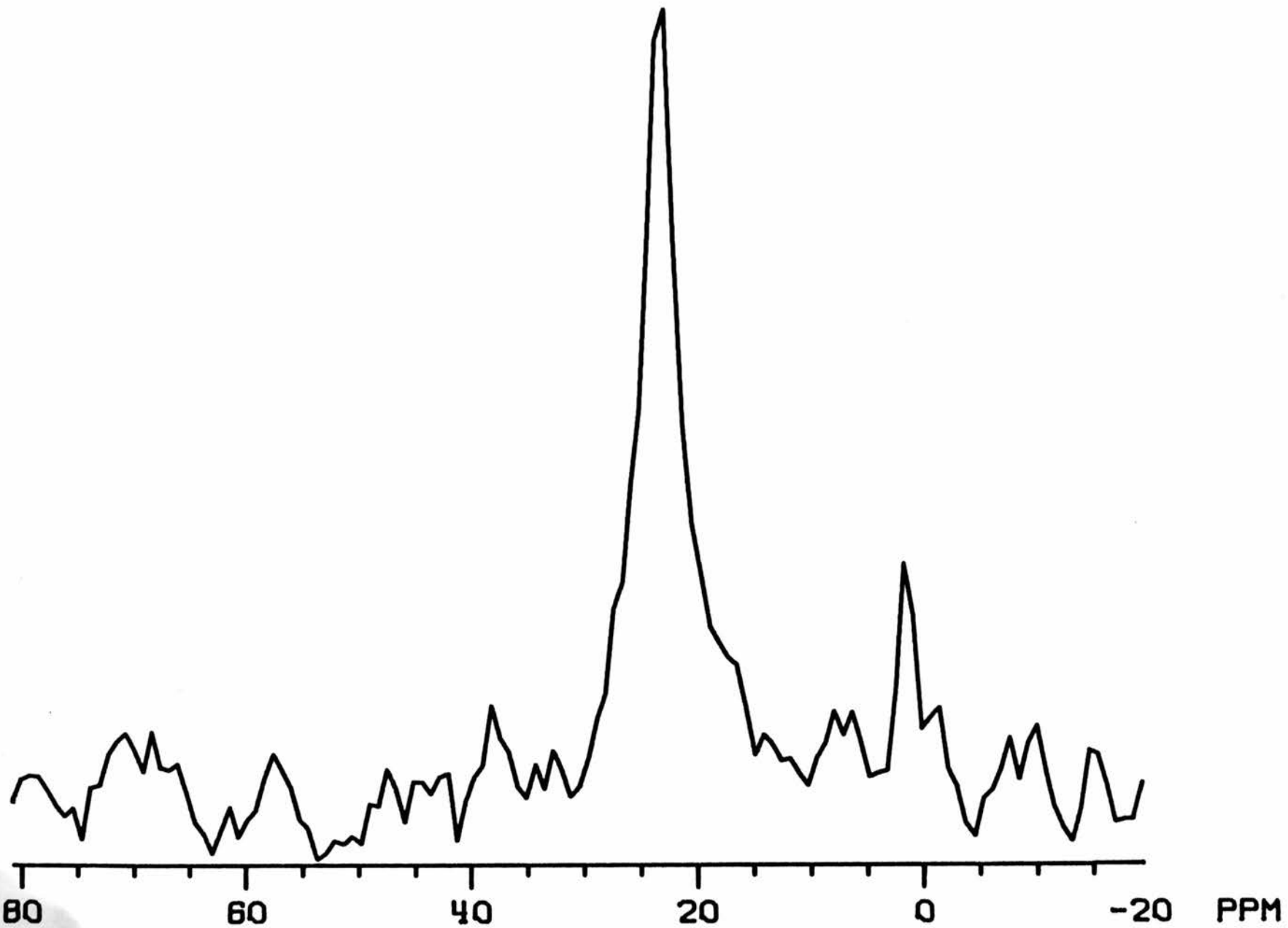
80
60
40
20
0
-20
PPM

sample.[48] The chemical shift of the methyl group does not indicate any difference between methyl amine in the two samples. HY(150)/17% CH_3NH_2 also contains a single line at 25.8 ppm.

The two samples do exhibit different behavior in the variable contact time experiment. In this experiment, for which the pulse sequence is given in Fig. 10, the ^{13}C spins are kept in contact with the ^{1}H spins for a variable time, t, after which the free induction decay is recorded. For smaller t, up to 1-5 ms for a typical organic solid, the ^{13}C magnetization will increase as a result of the transfer of polarization from the ^{1}H spins. The buildup of ^{13}C magnetizaton is governed by the time constant T_{CH}. At longer times the ^{13}C magnetization decays as spin-lattice relaxation processes drain the coupled ^{13}C-^{1}H system. This decay is generally governed by the relaxation of the larger proton system, which is characterized by the time constant $T_{1\rho_H}$. As a rule of thumb T_{CH} will increase and $T_{1\rho_H}$ will decrease with increased mobility of a spin system. Qualitatively, this is because the transfer of polarization from ^{1}H to ^{13}C under the condition of Hartmann-Hahn matching is a resonant process that will be hindered by modulation of the ^{13}C-^{1}H dipolar coupling resulting from molecular motion. On the other hand, $T_{1\rho_H}$ relaxation depends on fluctuations in the dipolar coupling to induce transitions along the spin-locking field. Fig. 11 presents the results of variable contact time experiments carried out on the two methyl amine samples. When fit to the usual phenomenological equation,[49]

$$M(t) = K(e^{-t/T_{1\rho H}} - e^{-t/T_{CH}}) \qquad (21)$$

Fig. 10. Pulse sequence for the variable contact time experiment. The transfer of polarization from ^{1}H to ^{13}C proceeds for a variable time, t.

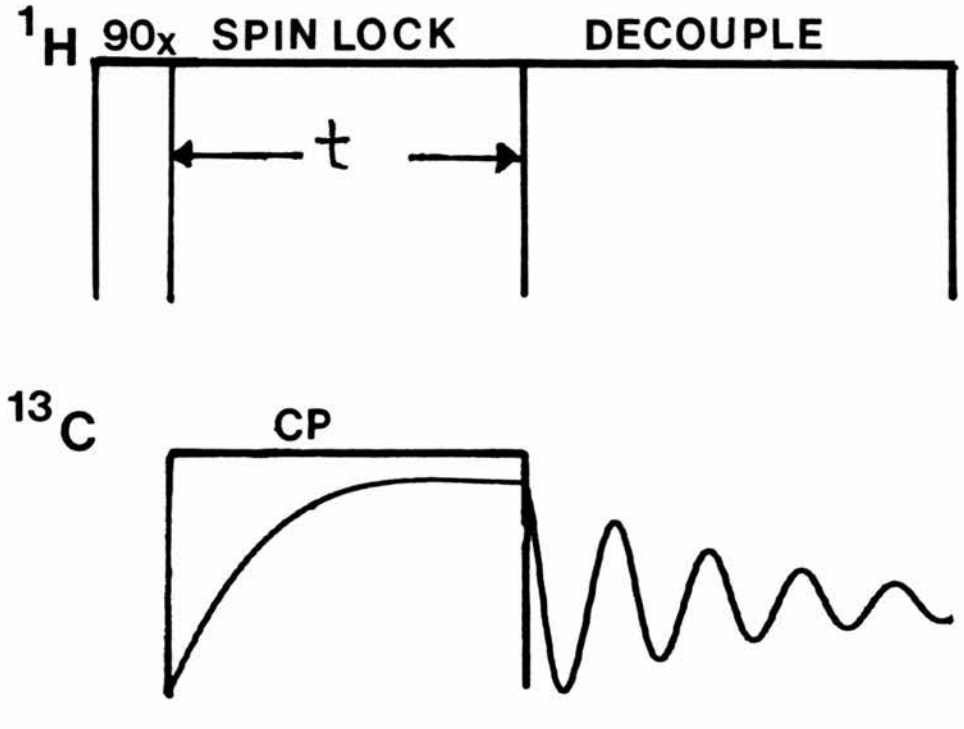
^{1}H
90x
SPIN LOCK
DECOUPLE
t
^{13}C
CP

Fig. 11. Comparison of the variable contact time results for methylamine adsorbed on HY(450) and HY(150). Data are plotted as ^{13}C signal strength as a function of contact time. Filled circles represent data on 17% methyl amine by weight on HY(150). Open circles represent data on 16% methyl amine by weight on HY(450).

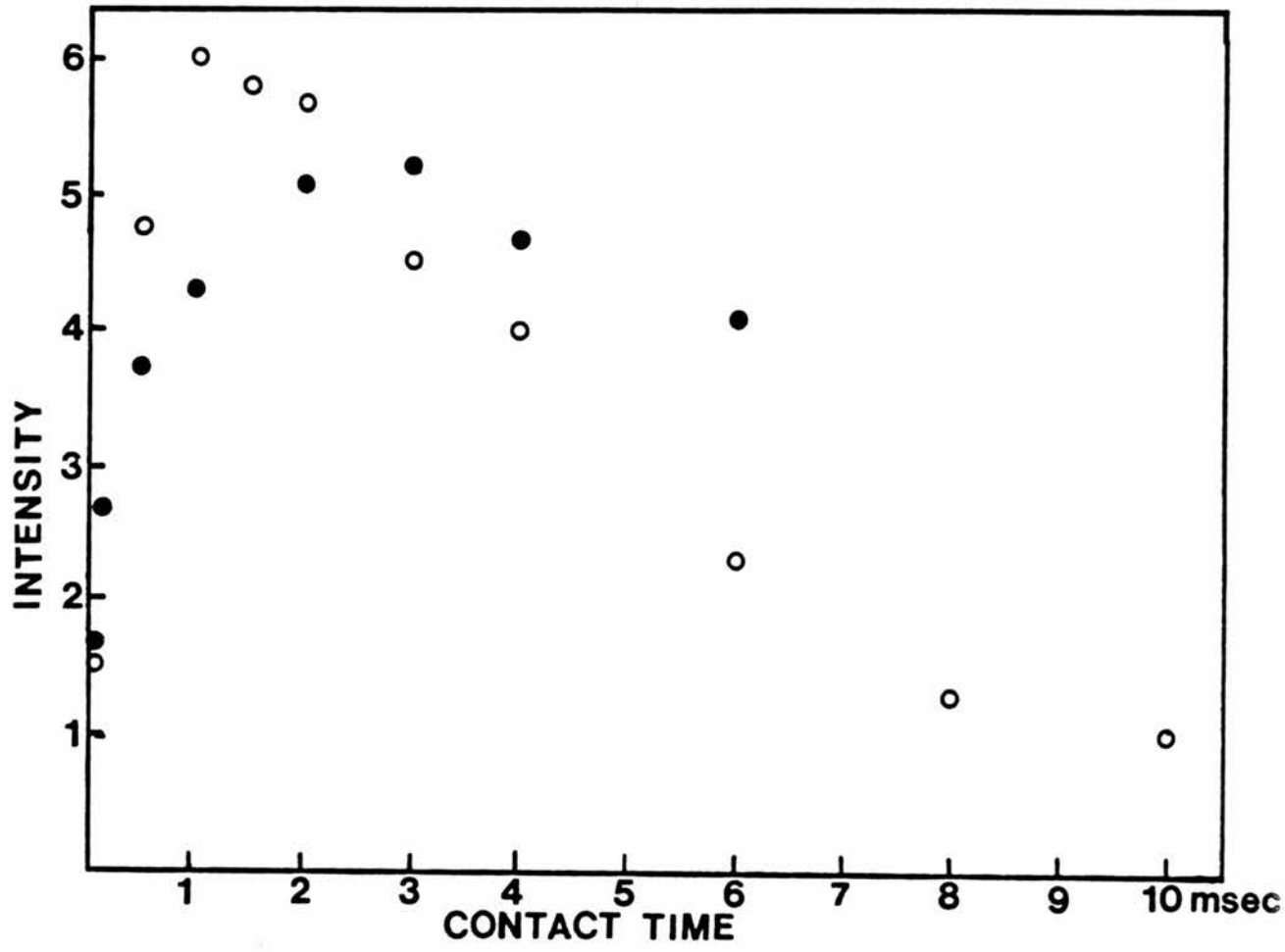
INTENSITY
6
5
4
3
2
1
1
2
3
4
5
6
7
8
9
10 msec
CONTACT TIME

it is found that the ^{13}C spins of methyl amine adsorbed onto HY(450) have both a smaller T_{CH} (520 us vs. 1.6 ms) and a longer $T_{1\rho}$ (4.5 ms vs. 6.2 ms) than when adsorbed onto HY(150). The trend in these values indicates a reduction in the mobility of methyl amine adsorbed into HY(450) relative to its mobility in HY(150). As mentioned above, activation at 450°C should result in both a larger number of structural hydroxyl groups and in greater overall acidity of the zeolite. Thus it appears that the mobility of methyl amine adsorbed into HY zeolite can be correlated with the number and acidity of the structural hydroxyl groups in the zeolite.

Fig. 12 shows the CPMAS spectrum of triethyl amine adsorbed onto HY(450). Here there is a more substantial perturbation of the chemical shifts from values in the liquid state. The methylene carbon is at 58.2 ppm and the methyl carbon is at 10.1 ppm as compared to the corresponding values of 46.8 ppm and 13.2 ppm in the liquid state. The results of a variable contact time performed on this sample are given in Fig. 13. The methyl carbon is slower to cross polarize than is the methylene carbon, probably as a result of internal rotation of the methyl group, which partially averages the CH_3 dipole-dipole interactions. The intensities of both resonances decay with a single time constant, which reflects the fact that proton spin diffusion occurs rapidly enough to average any local differences in $T_{1\rho_H}$ relaxation rates.

Quite a few materials were found to react upon adsorbtion into an activated zeolite. Thiophene adsorbed onto HY(400), Fig. 14, shows a new peak at 145 ppm and what appears to be at least two peaks in the area around 46 ppm in addition to the usual thiophene resonance at 127

ppm. It isn't clear whether the expected 125-ppm thiophene resonance is absent or contained within the line at 127 ppm. Both acetone and acetaldehyde adsorbed onto HY(400) very exothermically and resulted in color changes of the material. A CPMAS spectrum of the acetaldehyde system is given in Fig. 15 without explanation. After a while, the author learned to identify these violent reactions by the production of large amounts of heat and colored product and did not carry the investigation to the NMR stage. Certain alkenes, however, were novel with respect to the amounts of heat produced.

Small alcohols were found to yield cross-polarization spectra readily. The spectrum of a sample of 30% methyl alcohol by weight on HY(400) in Fig. 16 contains a single peak at 50.1 ppm (vs. a liquid shift of 49.7 ppm). The ^{13}C linewidth of 150 Hz in this spectrum is fairly large in comparison with the ^{13}C CPMAS linewidth of a typical crystalline solid (nominally 20-50 Hz for a 150-200 MHz spectrometer). Such broadening could result from a distribution of chemical shifts for the adsorbed methanol, as might occur if there is a distribution of interactions between methanol and the acid sites of the zeolite. It is often possible to detect such an inhomogeneous broadening mechanism in a variable contact time experiment. One might be able to observe variations in the growth and decay of the carbon magnetization in different parts of the line as each component of the line evolves according to its particular C-H dynamics. A stacked plot of the data from a variable contact time experiment is presented in Fig. 17. From this it appears that, within the limits of the signal-to-noise ratio, the methanol resonance polarizes and decays homogeneously.

Fig. 12. ^{13}C CPMAS spectrum of 12% triethylamine by weight adsorbed on HY(400).

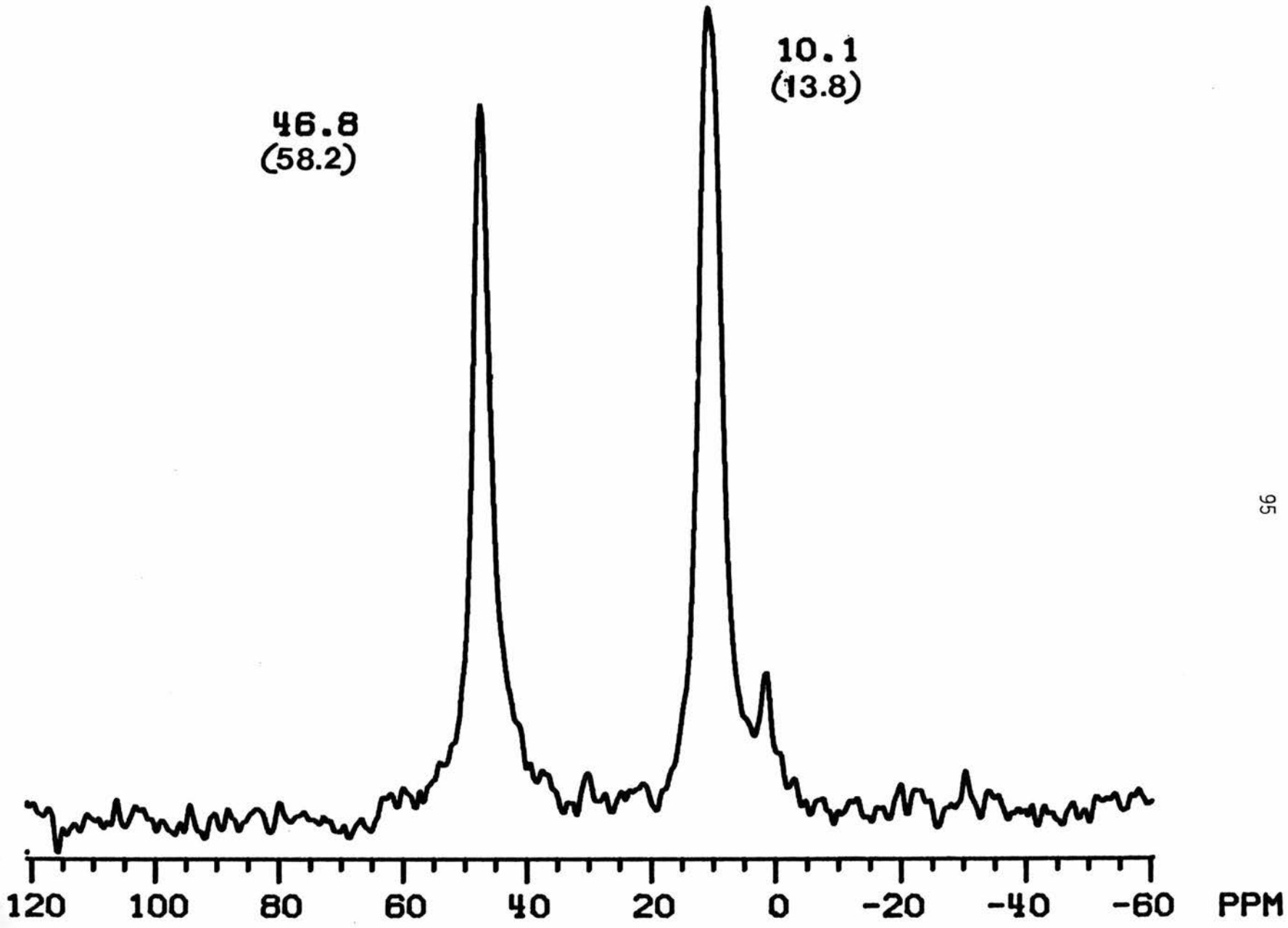
46.8
(58.2)
10.1
(13.8)
120
100
80
60
40
20
0
-20
-40
-60
PPM

Fig. 13. Plot of the results of a variable contact time experiment for 12% C triethylamine by weight adsorbed onto HY(400). Filled circles represent the CH_2 carbon. Open circles represent the CH_3 carbon.

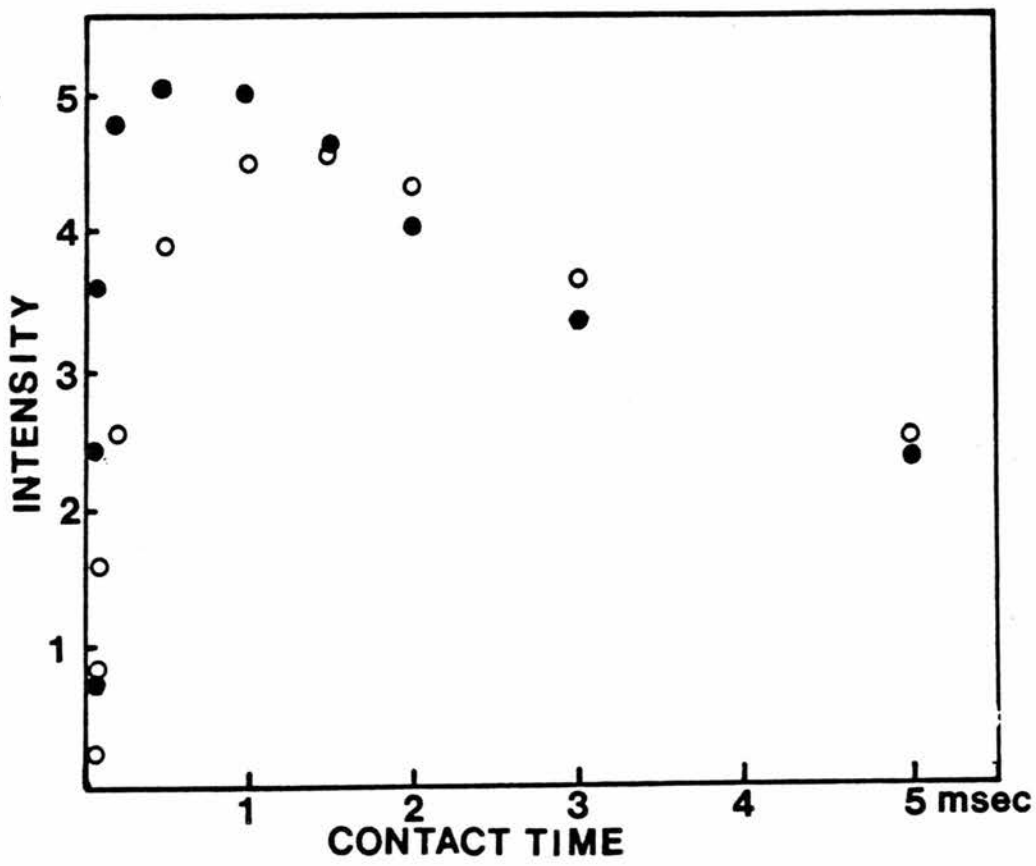
INTENSITY
5
4
3
2
1
1
2
3
4
5 msec
CONTACT TIME

Fig. 14. ^{13}C CPMAS spectrum of 10% thiophene by weight adsorbed onto HY(400). Numbers by the structure indicate liquid-state ^{13}C chemical shifts.

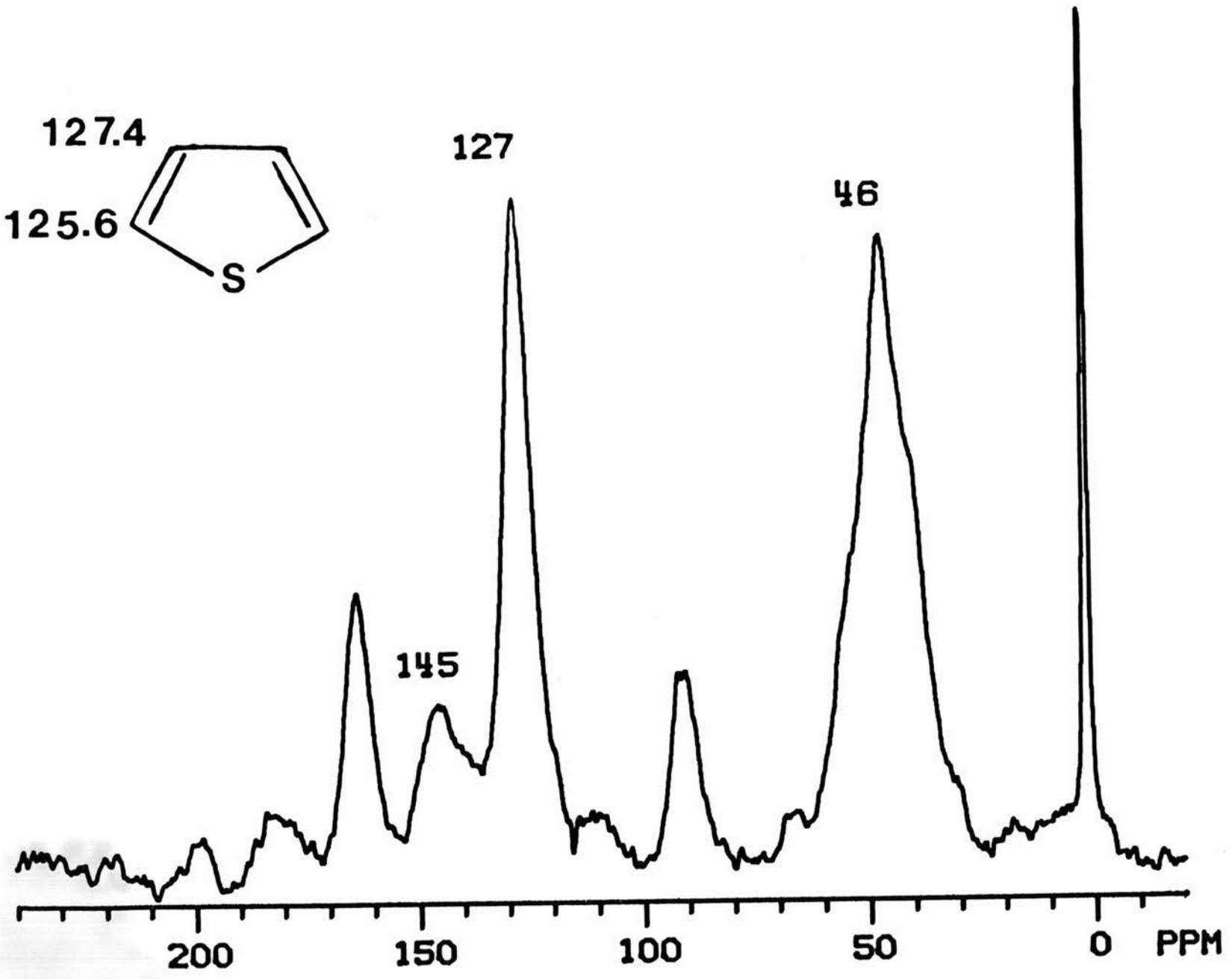
127.4
125.6
S
127
46
145
200
150
100
50
0
PPM

Fig. 15. ^{13}C CPMAS spectrum of 15% acetaldehyde by weight on HY(400).

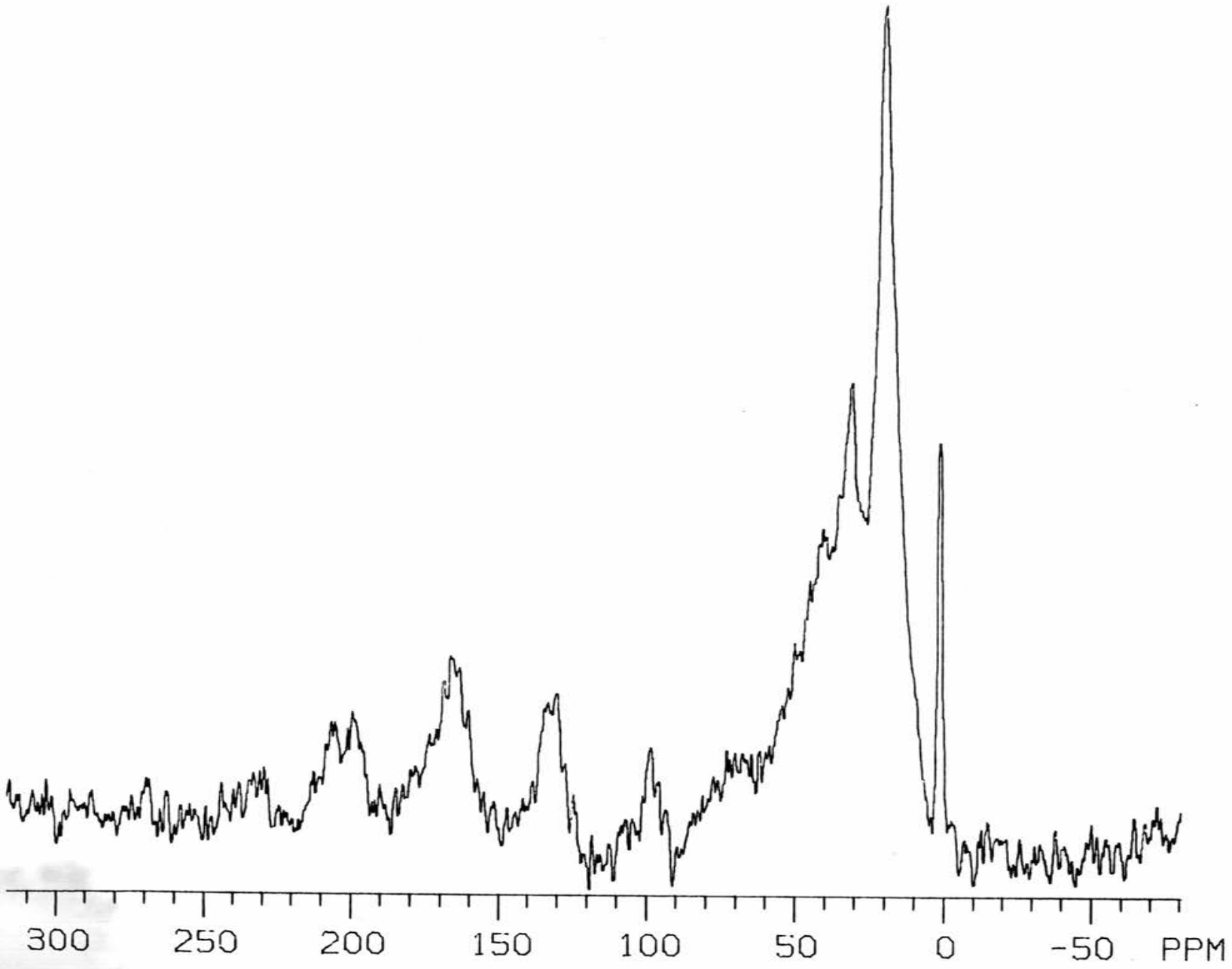
300
250
200
150
100
50
0
-50
PPM

Fig. 16. ^{13}C CPMAS spectrum of 30% methyl alcohol by weight adsorbed on HY(400).

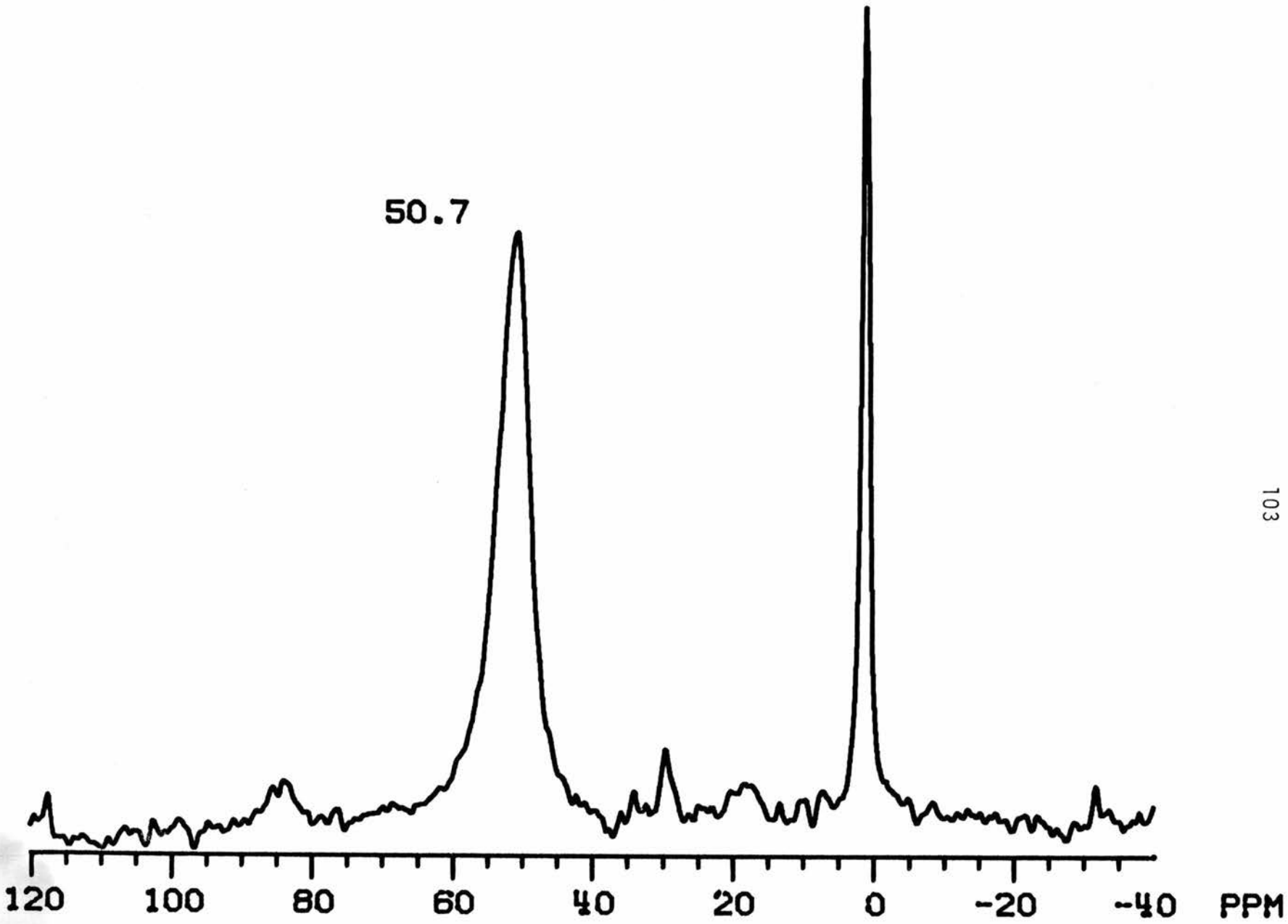
50.7
120
100
80
60
40
20
0
-20
-40
PPM

Fig. 17. Stacked plot of the $^{13}C\ CH_3$ magnetization of a sample of 30% by weight methyl alcohol on HY(400) as a function of the contact time.

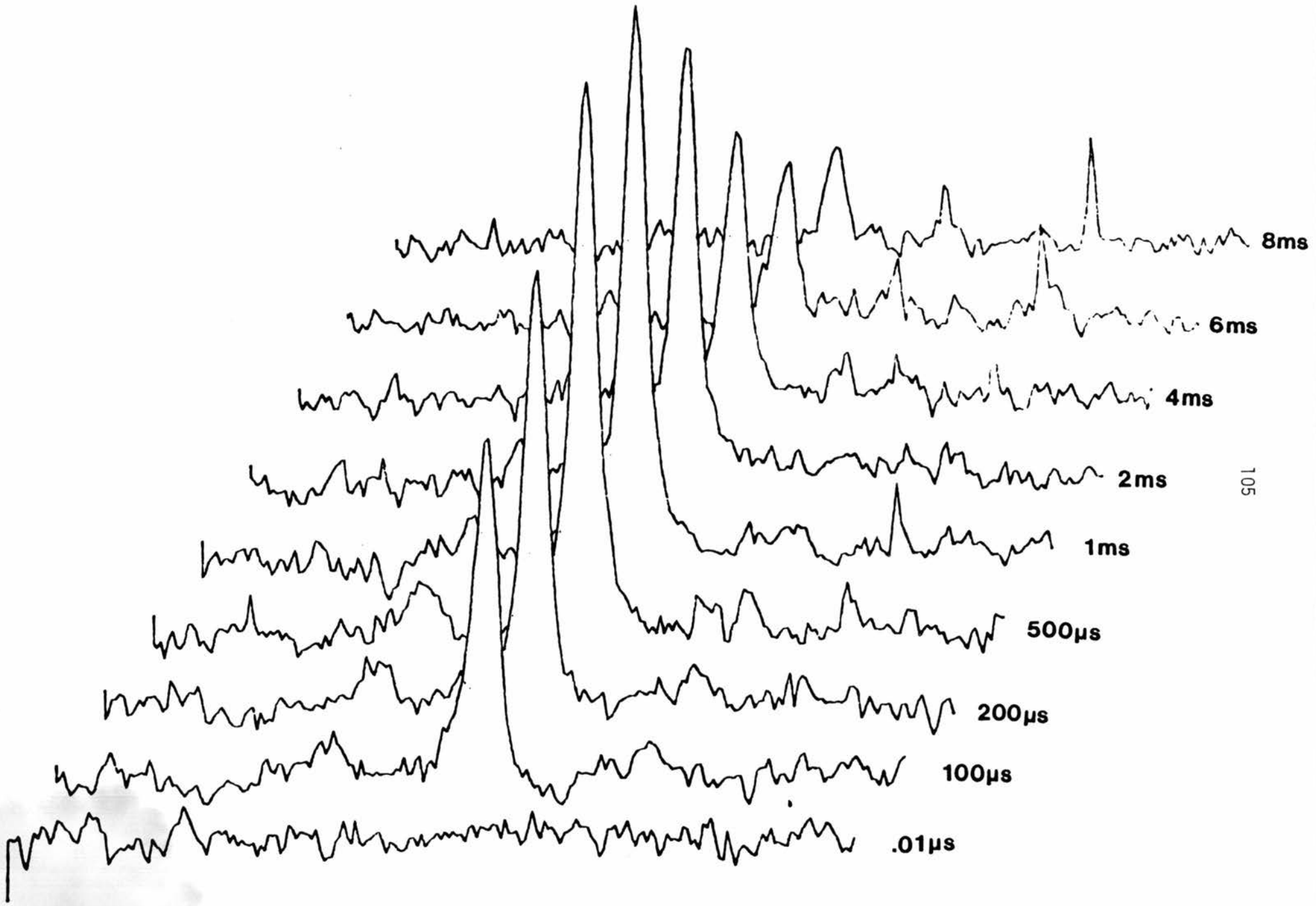
8ms
6ms
4ms
2ms
1ms
500µs
200µs
100µs
.01µs

The results of a ^{13}C rotating-frame relaxation experiment performed on HY(400)/30% MeOH are given in Fig. 18. A least squares fit of the data to a single exponential decay yields a value of 12 msec for $T_{1\rho_C}$.

Fig. 19 presents the CPMAS spectrum of 2-propanol on HY(400). The ^{13}C chemical shifts are not greatly different from those observed in solution. The methyl groups are at 24.1 ppm compared to 25.4 ppm in the liquid. The carbinol ^{13}C resonates at 67.3 ppm compared to 63.7 ppm in the liquid. The resonance of the carbinol ^{13}C is significantly broader than the methyl resonances. The results of a variable contact time experiment performed on this sample are given in Fig. 20. A least-squares fit to Eqn. 13 yields T_{CH} values of 280 μs for the carbinol ^{13}C and 60 μs for the methyl ^{13}C. The respective $T_{1\rho_H}$ values obtained from this analysis are 960 μs and 2 ms. Note that in this case it does not appear that ^{1}H spin diffusion is rapid enough to average rotating frame relaxation rates.

The results of a ^{13}C rotating-frame relaxation experiment on 2-propanol are presented in Figs. 21 and 22. ^{13}C relaxation is substantially more rapid for the carbinol ^{13}C than for the methyl ^{13}C. $T_{1\rho_C}$ is measured at 878 μs for the carbinol ^{13}C as compared with a value of 5.35 ms for the methyl ^{13}C.

The ^{13}C CPMAS spectrum of t-butyl alcohol, a tertiary alcohol, is given in Fig. 23. The carbinol resonance is not visible in this spectrum, nor could it be seen at any value of the contact time between 100 μs and 10 ms. The methyl resonance appears to be a superposition of a broad resonance and a sharp resonance, such as might occur if there were two or more chemical environments for the methyl carbons.

Fig. 18. Results of a rotating frame ^{13}C relaxation experiment on 30% by weight methyl alcohol on HY(400).

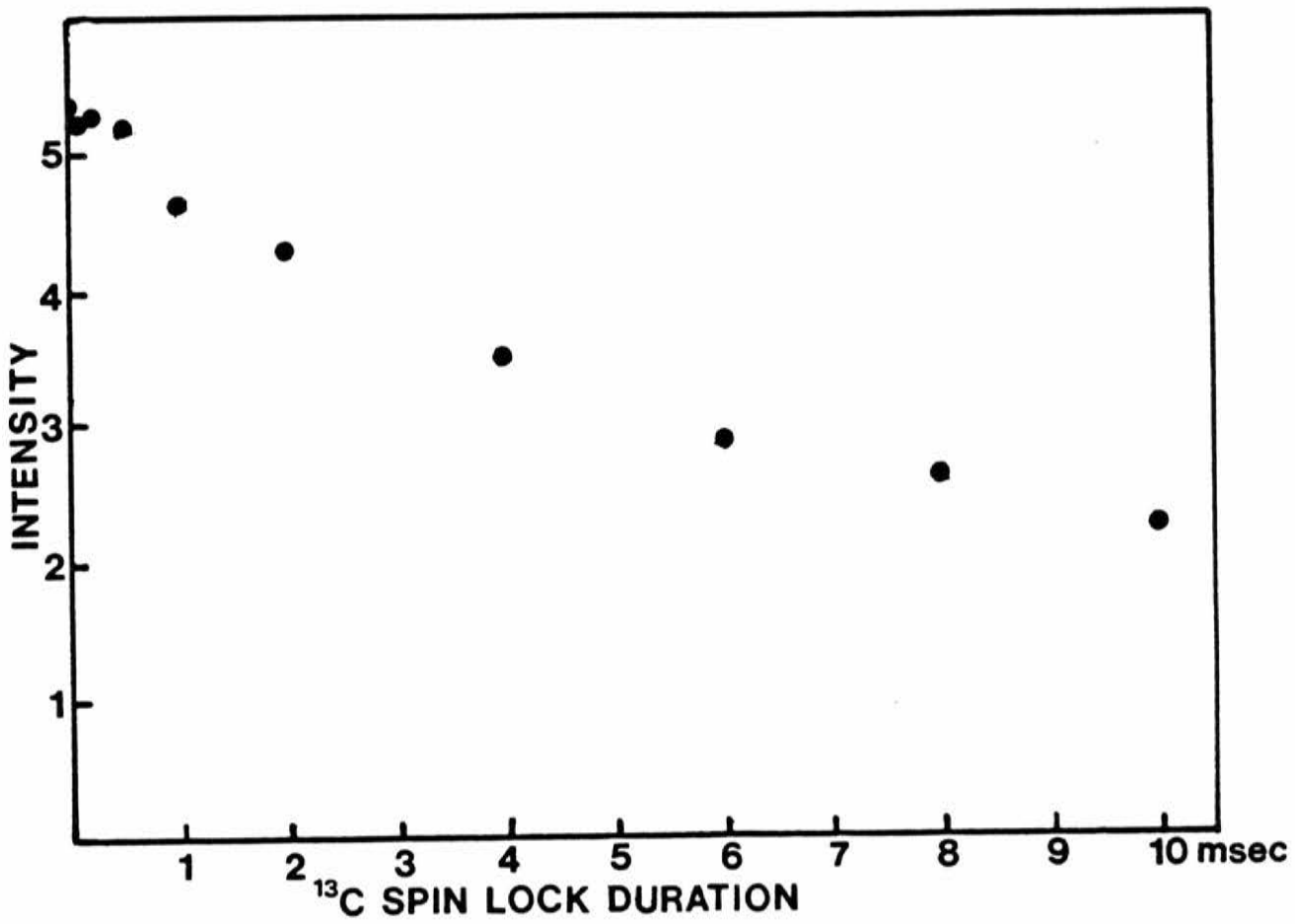
INTENSITY
5
4
3
2
1
1
2
3
4
5
6
7
8
9
10 msec
13C SPIN LOCK DURATION

Fig. 19. ^{13}C CPMAS spectrum of 15% 2-propanol on HY(400).

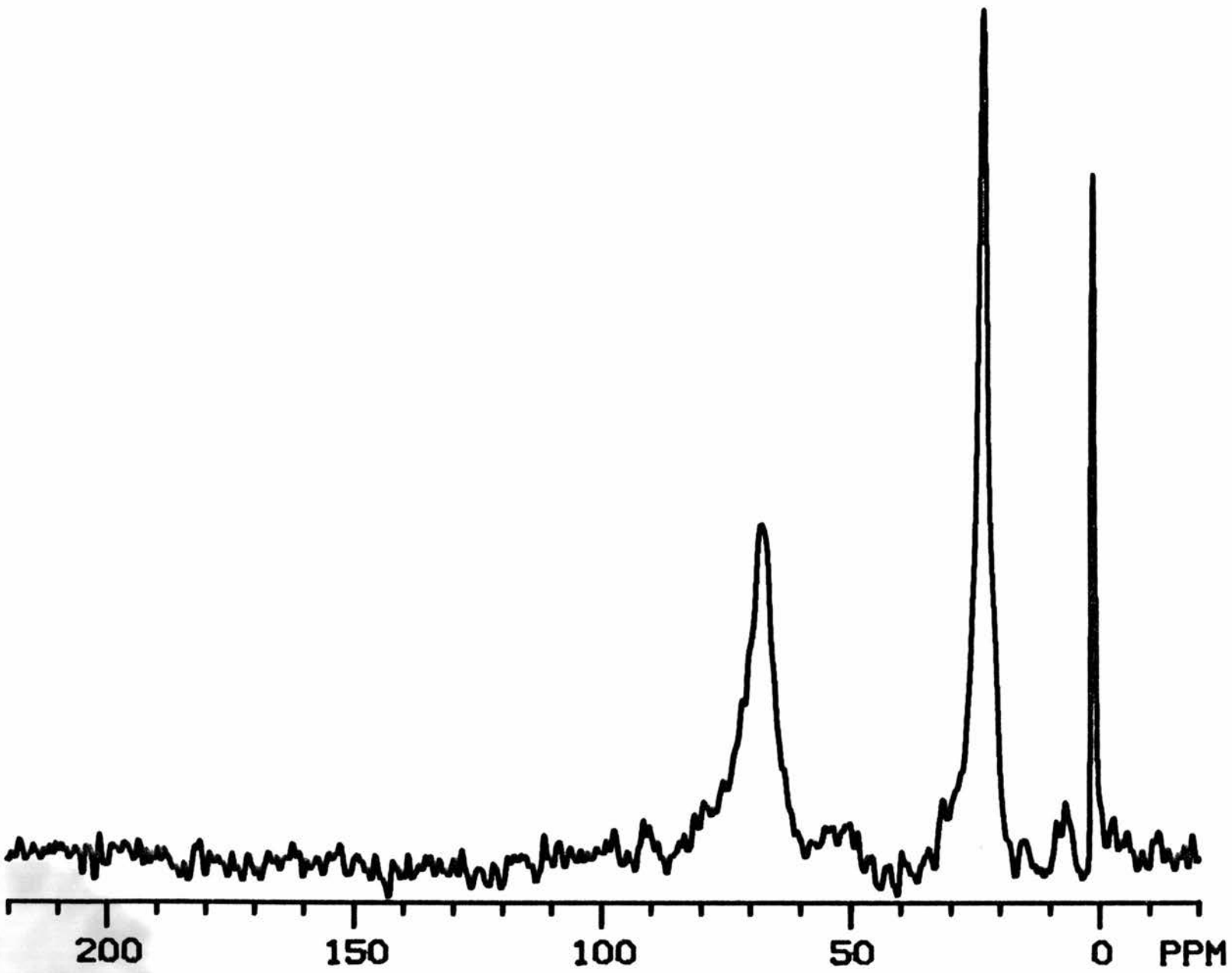
200
150
100
50
0
PPM

FIg. 20. Results of a variable contact time experiment on 15% 2-propanol adsorbed on HY(400). Open circles represent the CH_2OH carbon. Filled circles represent the CH_3 carbons.

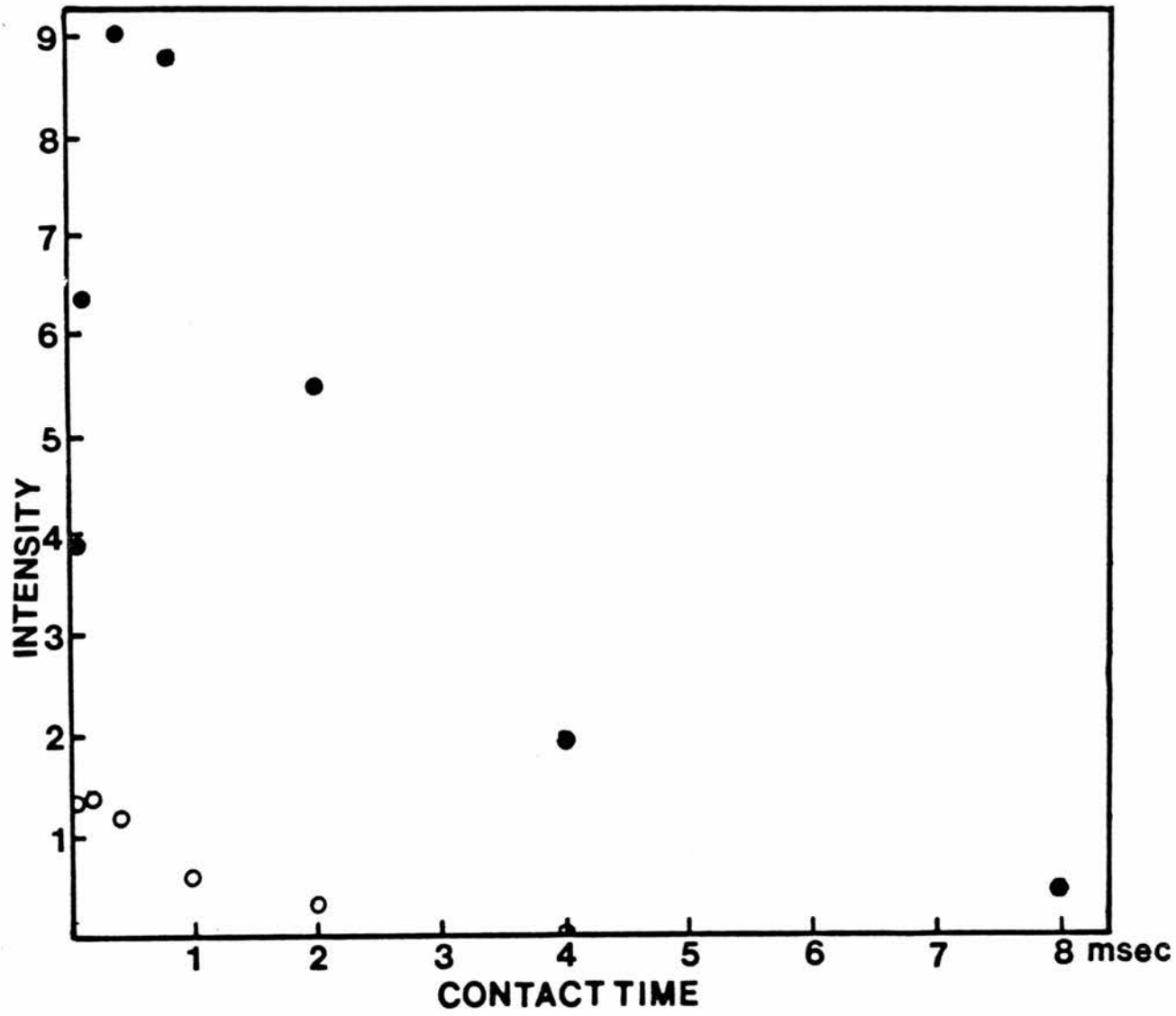
INTENSITY
9
8
7
6
5
4
3
2
1
1
2
3
4
5
6
7
8 msec
CONTACT TIME

Fig. 21. Results of a rotating-frame ^{13}C relaxation experiment on the methyl carbons of 15% 2-propanol on HY(400).

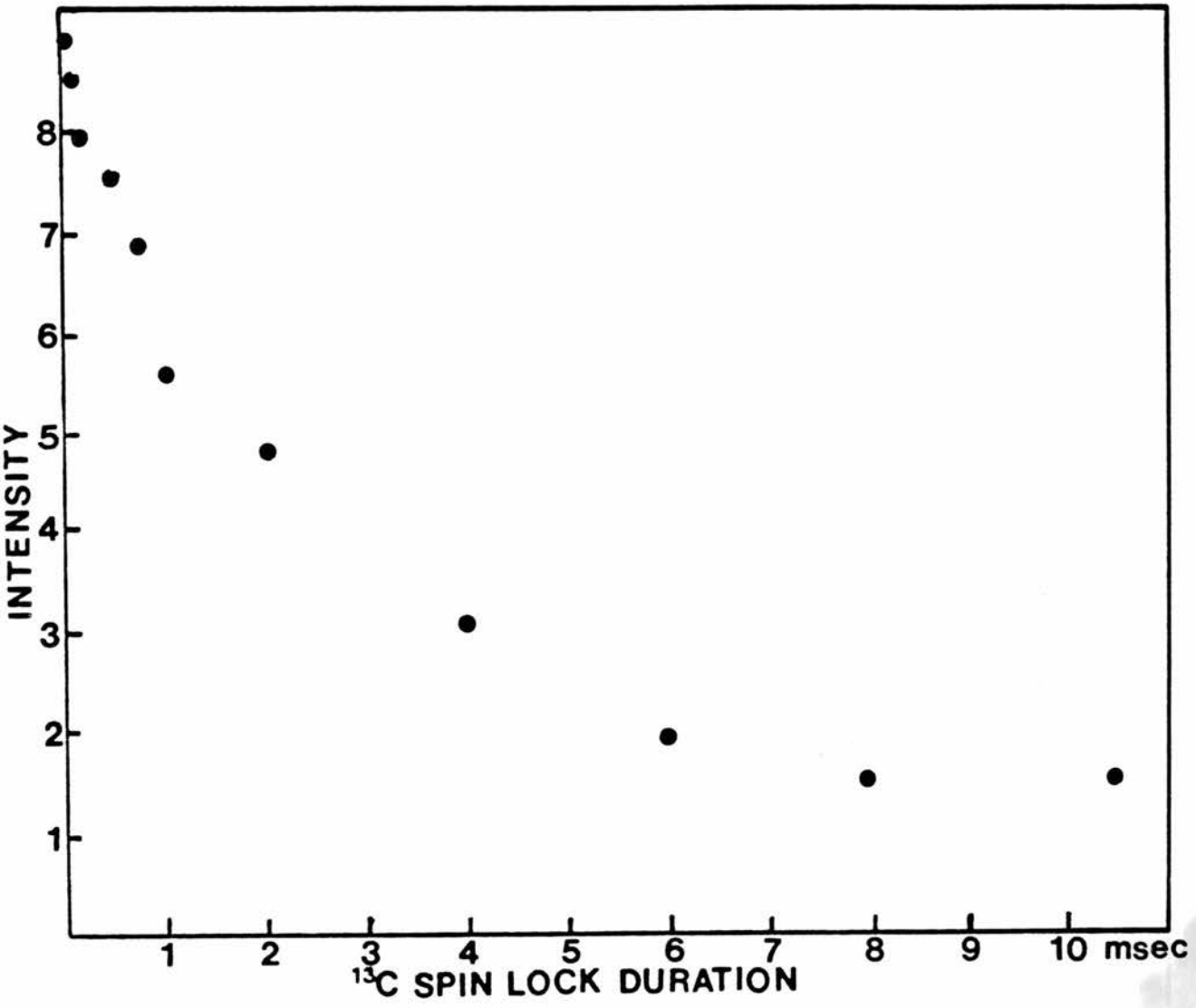
INTENSITY
8
7
6
5
4
3
2
1
1
2
3
4
5
6
7
8
9
10 msec
^{13}C SPIN LOCK DURATION

Fig. 22. Results of a rotating-frame ^{13}C relaxation experiment on the carbinol carbon of 15% 2-propanol on HY(400).

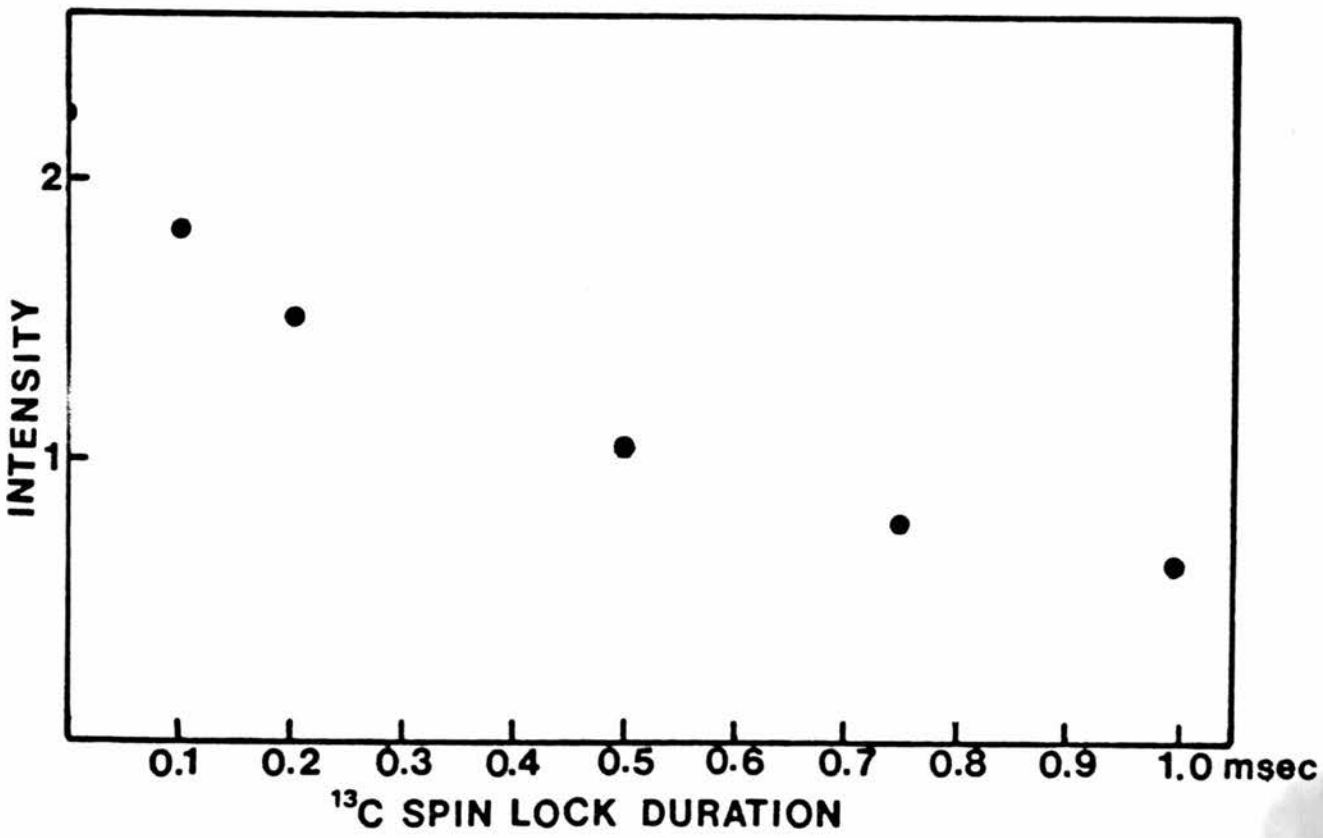
INTENSITY
2
1
0.1
0.2
0.3
0.4
0.5
0.6
0.7
0.8
0.9
1.0 msec
^{13}C SPIN LOCK DURATION

The results presented above suggest that small alcohols may be appropriate for a detailed investigation. The broadening and eventual disappearance of the carbinol resonance as one moves from methyl to tert-butyl alcohol is evidence that interactions between an alcohol and HY are in a regime in which changes in the nature of the alcohol result in substantial changes in rotating-frame spin dynamics. ^{13}C and ^{1}H rotating-frame relaxation rates are much faster in 2-propanol than in methanol. Relaxtion is particularly rapid for the carbinol ^{13}C and the corresponding proton in 2-propanol. It is possible that relaxation is so rapid in t-butanol that the carbinol resonance is not observable in a CP experiment.

Fig. 23. ^{13}C CPMAS spectrum of 8% t-butyl alcohol on HY(400).

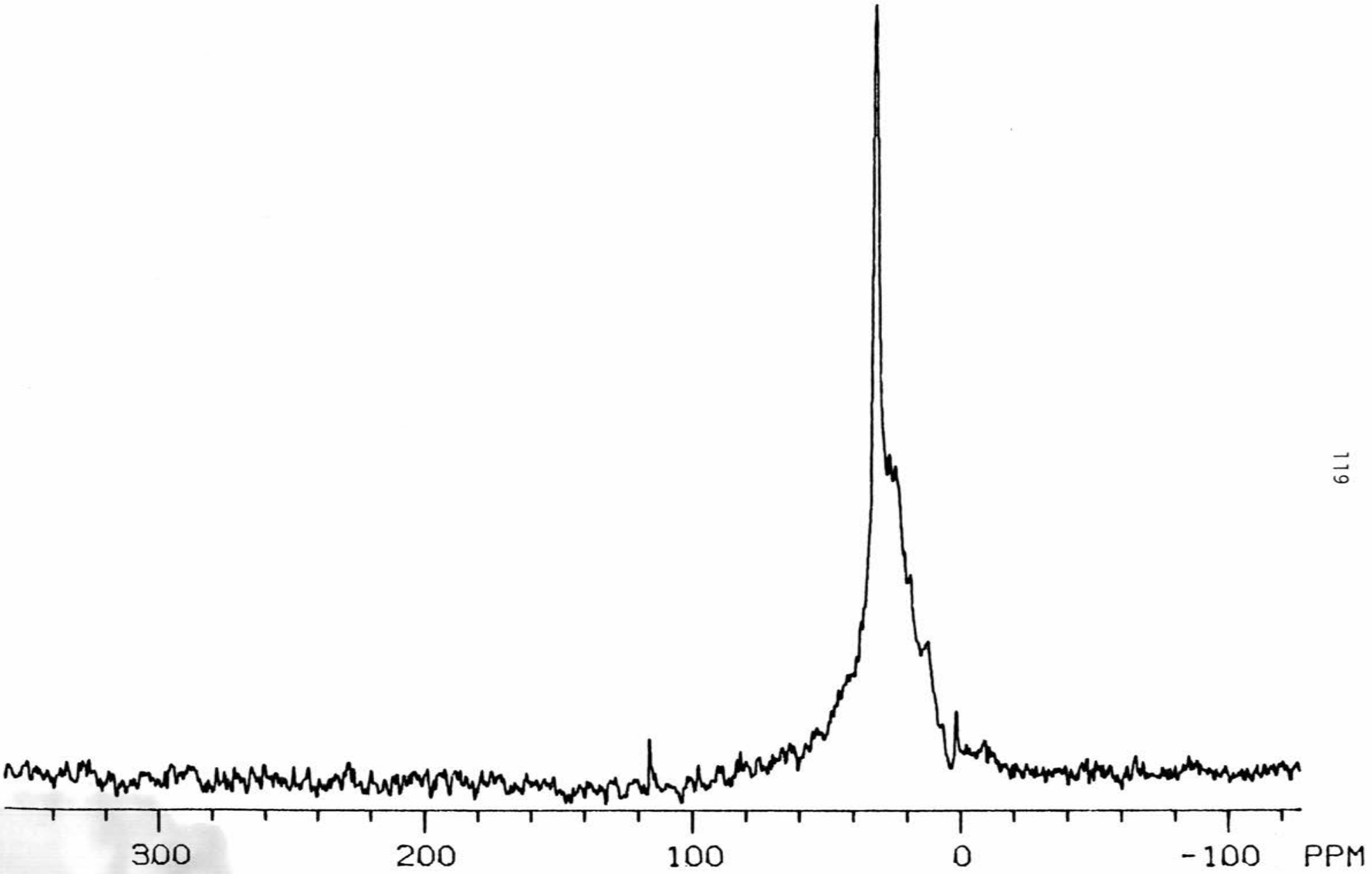
300
200
100
0
-100
PPM

CHAPTER 5

THE SYSTEM HY/METHANOL

The data from the previous section demonstrate the relative ease in obtaining ^{13}C CPMAS spectra in several zeolite/small molecule adsorbtion systems. Some fraction of the adsorbed molecules experience a static component of the ^{13}C-^{1}H dipolar interaction that permits cross polarization of the carbon spins. In the case of the alcohols surveyed, the dynamics of cross-polarization and of rotating-frame relaxation are quite different for different alcohols. This fact indicates that the low frequency processes responsible for these dynamics are sensitive to changes in the nature of the adsorbed alcohol, and thus may be controlled by the interaction between the alcohol and the zeolite. The interaction between the amines that were examined and the zeolite does not appear to be particularly sensitive to changes in the nature of the amine. One does not see correspondingly large changes in the rotating-frame spin dynamics of methyl amine and triethylamine in spite of the large difference in their K_b's.

5.1. $T_{1\rho C}$ Measurements.

An analysis of ^{13}C rotating-frame relaxation could be useful in the study of the interaction between an alcohol and HY. ^{13}C rotating-frame relaxation, characterized by the time constant $T_{1\rho_C}$, is in principle sensitive to fluctuations of the ^{13}C-^{1}H dipolar Hamiltonian with correlation times on the order of $1/(\gamma_C H_{1C})$, where H_{1C} is the strength

of the ^{13}C r.f. field that establishes the spin lock.[50] There are two possible sources for fluctuations of the dipolar Hamiltonian; these are 1) spatial reorientation of ^{13}C-^{1}H vectors, and 2) ^{1}H-^{1}H flip-flops. The former mechanism is a spin-lattice process that involves the exchange of energy between the spin-locked ^{13}C magnetization and the lattice (other, non-NMR modes of energy of the system), while the second effect is spin-spin in nature and involves equilibration between the spin-locked ^{13}C magnetization and the ^{1}H dipolar reservoir.[51] When operative, this spin-spin cross-relaxation can be very fast. It is most effective when the proton spins are strongly coupled to one another, e.g., in polyethylene,[52] and at lower ^{13}C r.f. field strengths. Roughly speaking, the former factor creates the spectral density of the ^{13}C-^{1}H dipolar interaction at the ^{13}C spin-lock frequency needed for the rotating-frame relaxation, and the latter effect reduces the frequency at which the ^{13}C transition occurs by reducing the precession frequency of the ^{13}C spins in the spin-locking field. In spin systems where spin-spin processes are important in rotating-frame relaxation it is difficult to extract motional information. Pulse sequences that quench the spin-spin mechanism are available,[53] but one should, if able, select a system that discriminates against spin-spin cross relaxation.

A priori one would expect that relaxation of a species adsorbed into a zeolite would favor spin-lattice processes over spin-spin cross-relaxation if ^{1}H-^{1}H dipolar coupling is reduced as a result of molecular motion or of relatively large interproton distances. Alcohols adsorbed into HY may experience such reduced dipolar coupling. In Fig.

20 it can be seen that in a T_{CH} experiment the two ^{13}C resonances of 2-propanol relax with different time constants. Unlike the case of triethylamine in Fig. 12, proton spin diffusion is not rapid enough in 2-propanol to average local differences in ^{1}H decay rates. The analogous experiment performed on the HY(400)/30% CH_3OH sample (Fig. 17) does not reveal anything about ^{1}H spin-diffusion rates, since there is only one methanol-based ^{13}C resonance relaxing, but one would expect methanol to be a good candidate for weak proton coupling. Internal rotation of the methyl group significantly reduces proton-proton coupling (see below). The hydroxyl proton is three bonds distant from the methyl protons, and its coupling to the methyl protons is also reduced by rotation of the methyl group.

Methyl alcohol is also a desirable choice for study because of its relative simplicity, both in terms of its NMR spectrum and the motional degrees of freedom available for relaxation of the ^{13}C polarization. For these reasons and the corresponding simplification anticipated for interpreting the data, methanol was chosen for detailed study.

A study of ^{1}H T_1 and T_2 relaxation using liquid state techniques has been reported for CD_3OH adsorbed onto HY(350).[54] No T_1 minimum could be found over the covered temperature range of -160°C to +80°C. It was concluded that relaxation of the hydroxyl proton is probably effected by a chemical exchange process involving the protonation of methanol by the acidic framework protons.

$$^{*}CD_3OH + CD_3OH_2^{+} \rightleftharpoons {}^{*}CD_3OH_2^{+} + CD_3OH \qquad (22)$$

Modulation of the C-H dipolar coupling as a result of proton transfer can induce spin-lattice relaxation if the hopping frequency of the

proton is on the order of the proton Larmor frequency. The absence of a T_1 minimum makes a complete analysis difficult, but the authors were able to calculate an activation energy of approximately 2.5-2.7 kcal/mole for the proton transfer, depending on the loading level. The authors speculate that a small fraction of the methanol in HY forms a strong hydrogen bond with structural hydroxyl groups, citing as evidence the perturbation of the hydroxyl stretching bands of HY upon the adsorption of methanol.

Fig. 24 shows the CPMAS spectrum of HY(400) loaded with 15% methanol by weight. The HY zeolite was generated by calcination at 400°C as described above. The spectrum contains a single peak at 50 ppm, much as in the case of 30% loading (Fig. 16). The optimal contact time for observation of the spectrum was found to be 2 ms, a value that would be considered typical of an organic solid.

A variable temperature study of $T_{1\rho C}$ was performed on this sample at 37.735 MHz, using a prototype variable-temperature probe constructed by Dr. James Frye. Stable spinning could be achieved over a range of +30°C to -70°C with the prototype probe. The carbon precession frequency in the spin-locking field, $\omega_{1C} = \gamma_C H_1$, for this set of experiments was set to 2.24×10^5 rad/sec, corresponding to a 90° pulse width of 7.0 μs, at each temperature. This procedure was essential, as the probe tuning and efficiency were found to change significantly with temperature. The data for this set of experiments are summarized in Fig. 25. Unlike the proton T_1 values, the value of $T_{1\rho_C}$ was found to pass through a minimum at -35 °C.

As a first step towards interpreting the relaxation, the $T_{1\rho_C}$ data were fit with a very simple model. It was assumed that only

Fig. 24. ^{13}C CPMAS spectrum of 15% methyl alcohol by weight on HY(400).

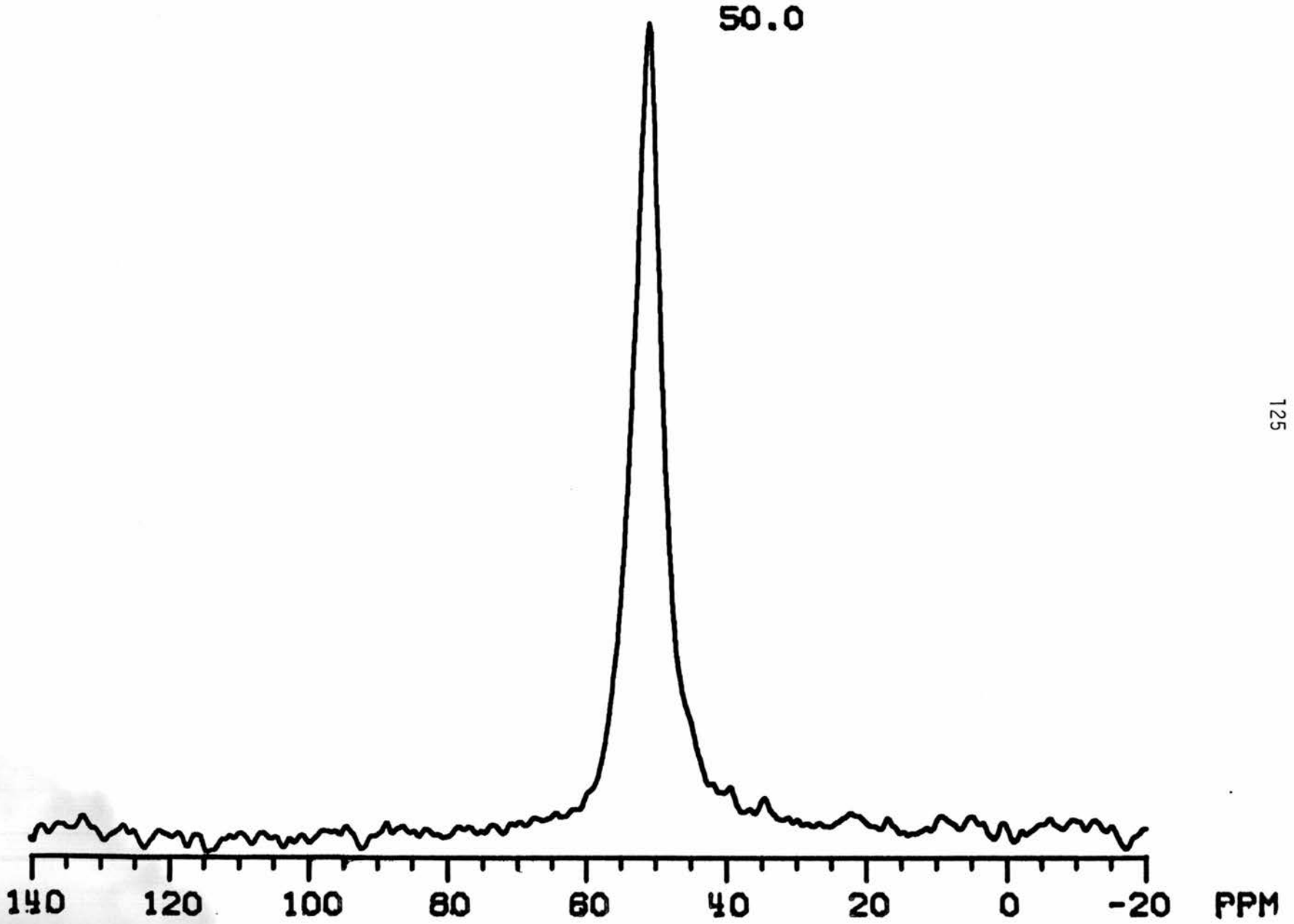
50.0
140
120
100
80
60
40
20
0
-20
PPM

Fig. 25. Plot of the $T_{1\rho C}$ values measured on a sample of 15% methanol by weight on HY(400) vs. $10^3/T$.

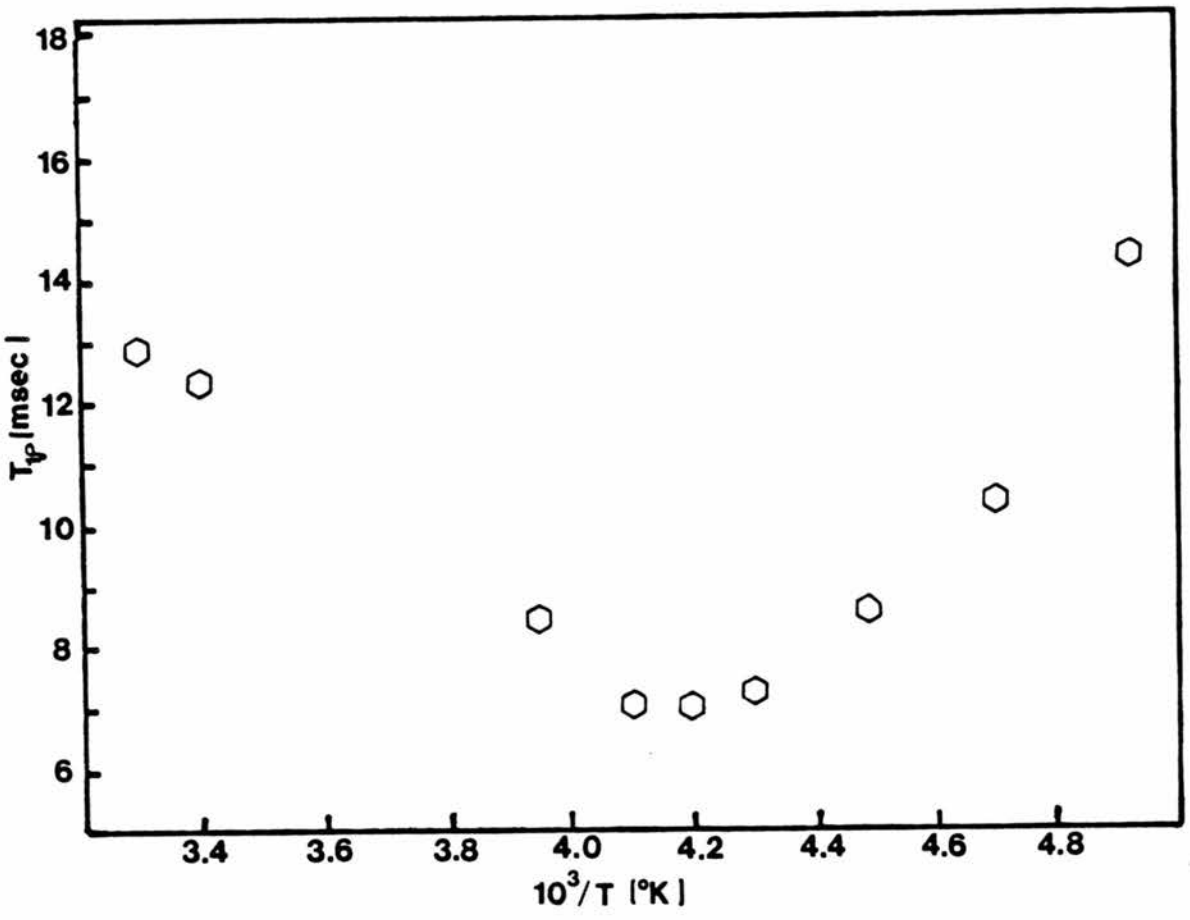
18
16
14
12
10
8
6
T_{φ} (msec)
3.4
3.6
3.8
4.0
4.2
4.4
4.6
4.8
$10^3/T$ (°K)

fluctuations of C-H couplings at ω_{1C} are effective in relaxing the spin-locked carbon magnetization and that these fluctuations arise only from molecular motion and are characterized by a single correlation time τ_c. The development outlined below would be inappropriate for spin-spin processes, for which a model dealing with T_{CH} would be more appropriate. Although these assumptions are severe, we felt that the results of a fit to this model would be helpful in deciding the nature of more detailed models that might be appropriate.

For the on-resonance condition, $T_{1\rho_C}$ for ^{13}C relaxation induced by motional modulation of the ^{13}C-^{1}H dipole coupling may be expressed as a sum of contributions from the various elements of the dipolar coupling Hamiltonian.[55]

$$\frac{1}{T_{1\rho_C}} = \frac{1}{4}\left\{\frac{2}{3}j_{20}(\omega_{1C}) + j_{21}(\omega_H) + \frac{1}{6}j_{20}(\omega_H - \omega_C) + \frac{1}{2}j_{21}(\omega_C) + j_{22}(\omega_H + \omega_C)\right\} \tag{23}$$

In this equation ω_{1C} is the precessional frequency of the ^{13}C spins in the ^{13}C rf field; ω_H and ω_C are the Larmor frequencies of the ^{1}H and ^{13}C spins in the large static (H_o) field, $\gamma_H H_o$ and $\gamma_C H_o$, respectively. The $J_{kg}q(\omega)$ are the so-called generalized spectral functions.

$$j_{kq}(\omega) = (-1)^q \mathrm{Re}\int_0^\infty dt\langle A_{kq}(t)A_{k-q}(0)\rangle e^{-i\omega t} \tag{24}$$

The A_{kq} contain the spatial dependence of each term of the dipolar Hamiltonian. These are listed for reference in Table I.

Table I. Elements of H_D^{IS} expressed as $\sum_{q=-2}^{+2} (-1)^q A_{2q} T_{2-q}$.

A_{2q}	T_{2-q}
$A_{20} = \frac{\gamma_I \gamma_S}{2\hbar} \sqrt{6} \frac{(1-3\cos^2\theta)}{r^3}$	$T_{20} = \frac{1}{\sqrt{6}}(3I_zS_z - \underset{\sim}{I} \cdot \underset{\sim}{S})$
$A_{2\pm1} = \pm\frac{3\gamma_I \gamma_S}{\hbar} \frac{\sin\theta\cos\theta e^{\pm i\phi}}{r^3}$	$T_{2\pm1} = \mp \frac{1}{2}(I_zS_\pm + I_\pm S_z)$
$A_{2\pm2} = \frac{3}{2} \frac{\gamma_I \gamma_S}{\hbar} \frac{\sin^2\theta}{r^3} e^{\pm 2i\phi}$	$T_{2\pm2} = \frac{1}{2} I_\pm S_\pm$

Each term in Eqn. 23 corresponds to a distinct mechanism for the relaxation of the carbon spins. The arguments, ω, indicate the frequency of the photon that is supplied to the spins by the lattice. Thus, for example, $j_{20}(\omega_{1C})$ corresponds to a transition of the ^{13}C spin along $\underset{\sim}{H}_1$ for which the energy supplied by the lattice is $\hbar\omega_{1C}$. The term $j_{21}(\omega_H)$ corresponds to simultaneous transitions of carbon spins along $\underset{\sim}{H}_{1C}$ and of proton spins along $\underset{\sim}{H}_o$ with the lattice supplying $\hbar(\omega_{1C} + \omega_H) \tilde{=} \omega\hbar_H$. These two terms are not found in expressions for laboratory-frame spin lattice relaxation. They are the result of the presence of the spin-lock applied to the carbon spins.

The remaining three terms in Eqn. 23 describe contributions to spin-locked rotating-frame ^{13}C relaxation due to relaxtion of the ^{13}C spins along $\underset{\sim}{H}_o$ by T_1 processes. Laboratory frame relaxation will alter the carbon polarization along $\underset{\sim}{H}_1$, although T_1 is usually much larger than $T_{1\rho}$ and is thus usually neglected. A transition of a ^{13}C spin from a state of quantization along $\underset{\sim}{H}_1$ to quantization along H_o produces half the change in polarization along $\underset{\sim}{H}_1$ as does a ^{13}C transition involving population differences along $\underset{\sim}{H}_1$ only. Thus, T_1-type processes are half as efficient as are transitions along $\underset{\sim}{H}_1$.

$$\frac{1}{T_{1\rho_C}} = \frac{1}{4}\left(\frac{2}{3}j_{20}(\omega_{1C}) + j_{21}(\omega_H)\right) + \frac{1}{2T_1} \qquad (25)$$

where the contributions from relaxation along $\underset{\sim}{H}_o$ are given by the last three terms in Eqn. 23.

$$\frac{1}{2T_1} = \frac{1}{4}\left(\frac{1}{6}j_{20}(\omega_H - \omega_C) + \frac{1}{2}j_{21}(\omega_C) + j_{22}(\omega_H + \omega_C)\right) \qquad (26)$$

It is now assumed that high-frequency motions are not important for relaxation near the $T_{1\rho_C}$ minimum. In effect this amounts to neglecting all but the $j_{20}(\omega_{1C})$ term in Eqn. 23. For a solid this is a good approximation, since measured ^{13}C T_1s are generally two to three orders of magnitude greater than $T_{1\rho_C}$[56]. ^1H T_1's of molecules adsorbed in zeolites when measured using liquid techniques are frequently on the order of 50-100 ms near the T_1 minimum.[57] However, a species observable by cross-polarization must experience a static dipolar coupling. This in turn suggests the presence of interactions that restrict molecular motions and a corresponding decrease in spectral density at high frequencies compared to a liquid-like species. Eliminating the high frequency terms from Eqn. 25 leads to Eqn. 20.

$$\frac{1}{T_{1\rho_C}} = \frac{1}{6} j_{20}(\omega_{1C}) \tag{27}$$

The simplest form for the spectral function $j_{20}(\omega_{1C})$ is obtained by assuming that the ^{13}C-^1H vector reorients isotropically with a single correlation time. In this case $j_{20}(\omega_{1C})$ for a single C-H pair can be expressed as[58]

$$j_{20}(\omega_{1C}) = \frac{6}{5} \frac{\gamma_C^2 \gamma_H^2 \hbar^2}{r_{CH}^6} \quad \frac{\tau_C}{1 + \omega_{1C}^2 \tau_C^2} \tag{28}$$

The data from the variable-temperature $T_{1\rho_C}$ experiment were initially fit to Eqn. 27 under the assumption that methyl C-H coupling is responsible for $T_{1\rho_C}$ relaxation. If the correlation between the motion of the three ^{13}C-^1H vectors of a methyl group is ignored, the total relaxation may be expressed as the sum of three independent contributions from the three ^{13}C-^1H pairs of the methyl group.[59]

Fig. 26. Plot of $\ln(\tau_c)$, calculated from Eqn. 22 vs. $10^3/T$.

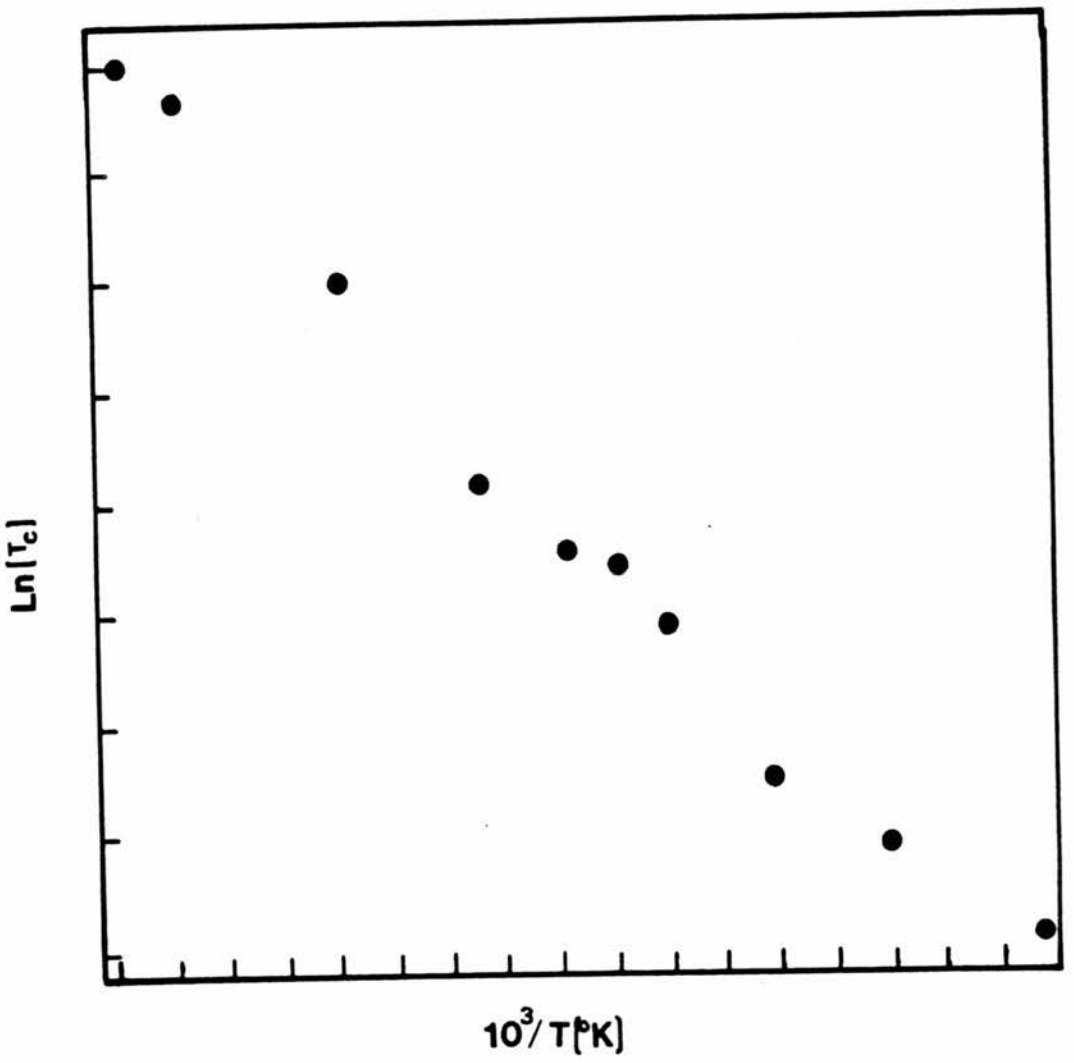
Ln[τc]
10³/T[°K]

Fig. 27. Experimental $T_{1\rho}$ data for the sample HY(400)/15% MeOH (hexagons) along with the predicted $T_{1\rho}$ for a process obeying E_a = 3.0 kcal/mole (open circles).

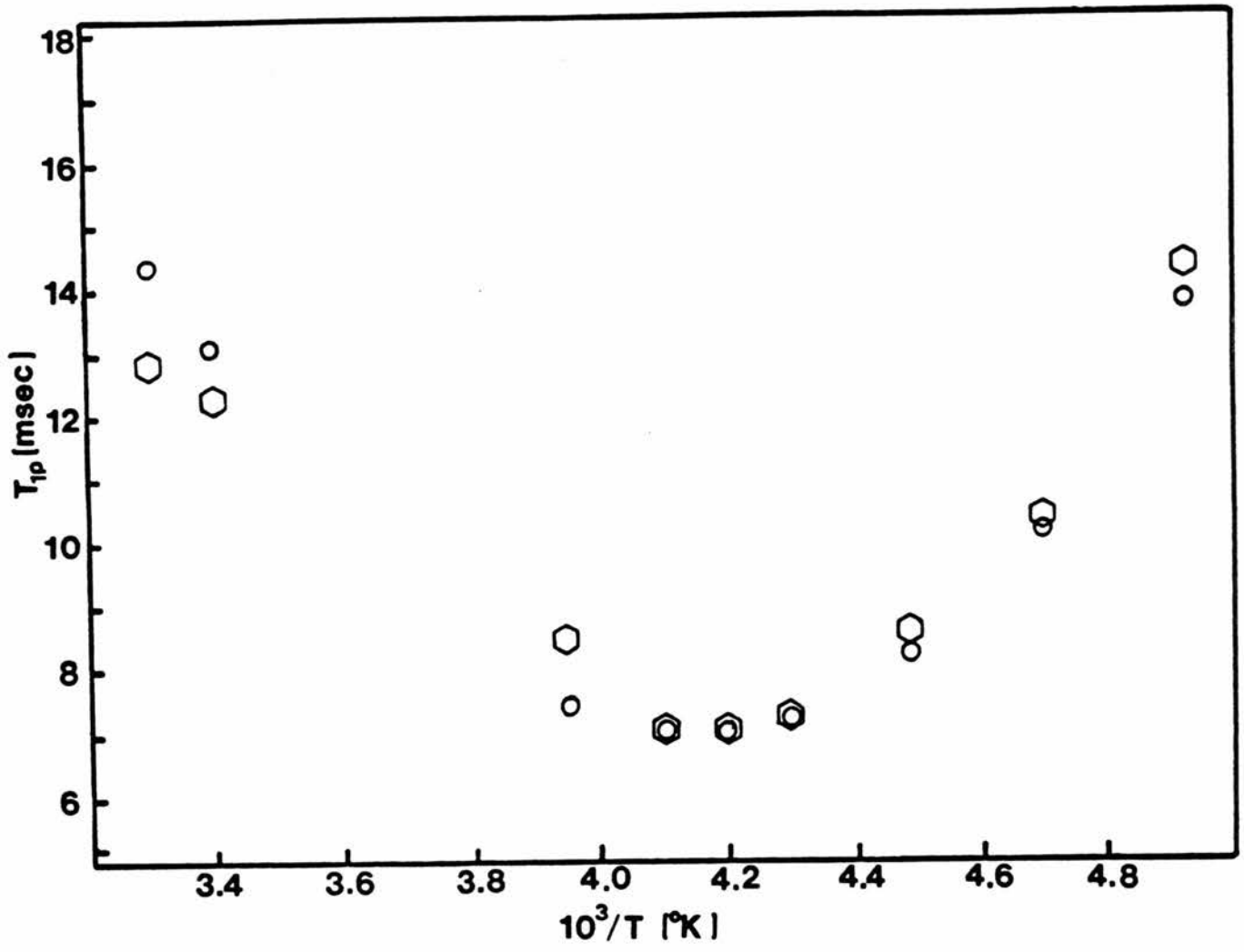
18
16
14
12
10
8
6
$T_{1\rho}$ [msec]
3.4
3.6
3.8
4.0
4.2
4.4
4.6
4.8
$10^3/T$ [°K]

$$j_{20}(\omega_{1C}) = \sum_{i=1}^{3} j^{i}_{20}(\omega_{1C}) \qquad (29)$$

The end result of the above approximations is a particularly simple equation for $T_{1\rho_C}$.

$$\frac{1}{T_{1\rho_C}} = \frac{3}{5}\frac{\gamma_C^2\gamma_H^2\hbar^2}{r_{CH}^6}\quad\frac{\tau_C}{1+\omega_{1C}^2\tau_C^2} \qquad (30)$$

Eqn. 30 predicts that at the $T_{1\rho_C}$ minimum $\omega_{1C}\tau_C = 1$, so that $\tau_C = 1/\omega_{1C}$. This value for τ_C can then be inserted into Eqn. 30 and the constant factor involving r_{CH} and the γ's thereby evaluated. After this constant is obtained, τ_C at each temperature can be calculated from the measured value of $T_{1\rho_C}$. Assuming that $\tau_C^{-1} = \tau_0^{-1} e^{-E_a/R\tau}$, an activation energy can then be obtained from the slope of a plot of $\ln(\tau_C)$ vs. $1/T$.

Fig. 26 shows a plot of $\ln(\tau_C)$ vs. $1/T$. The activation energy was calculated to be 3.0 kcal/mole, which is comparable to the value obtained from the study of relaxation of the hydroxyl group cited earlier.

Fig. 27 shows the experimental $T_{1\rho_C}$ data, along with predicted values of $T_{1\rho_C}$ obtained from Eqn. 30 assuming an activation energy of 3.0 kcal/mole. Considering the level of approximation involved in obtaining Eqn. 23, the fit is really quite good. The low temperature data are better reproduced than are the high temperature data. At the highest temperature, 30°C, the divergence between the data and the fit is rather large. Based on this limited set of data one might suspect

that a second relaxation mechanism is being manifested at higher temperatures, causing $T_{1\rho_C}$ to be shorter than anticipated in the assumed model. It could be that at higher temperatures processes involving shorter correlation times, i.e., the T_1-type terms neglected on the way to Eqn. 30, may become important. A quick check on this is to measure T_1 for the methyl carbon at room temperature. This was done for HY(400)/15%MeOH and a value of 50 ms was obtained. 50 ms is not completely negligible compared to the measured $T_{1\rho}$ of 9.7 ms at 20°C, even when the factor of 1/2 in Eqn. 25 is incorporated. Hence, a complete $T_{1\rho_C}$ study must include T_1 measurements. It will also be necessary to observe relaxation at temperatures above 30°C in order to more completely investigate the discrepancy at higher temperatures. This type of measurement will require the use of different rotor materials, since KEL-F rotors will distort at temperatures much above 30°C.

The value of r_{CH} obtained from Eqn. 30 is 2.58 Å, which is clearly inconsistent with the C-H bond distance in a methyl group ($r_{CH} \simeq 1.09$ Å). If one returns to Eqn. 27 and assumes that a single C-H pair is responsible for the relaxation, r_{CH} is then calculated from Eqn. 30 to be 2.15 Å. This value is relatively close to the C-O-H distance of 1.92 Å in free methanol.[60] Thus, it is possible that $T_{1\rho_C}$ relaxation is controlled by proton exchange of the hydroxyl proton rather than by intra methyl dipolar coupling.

In any event, the relative success of these preliminary experiments was encouraging. A $T_{1\rho_C}$ minimum was observed. Near the minimum and on the low temperature side of the minimum the data seem reasonably well fit with the very simple model developed above. At temperatures above the $T_{1\rho_C}$ minimum, the fit predicts a more rapid increase in $T_{1\rho_C}$

with temperature than is observed, possibly as a result of more efficient T_1 relaxation of the methyl carbon at these temperatures.

The results of this preliminary $T_{1\rho C}$ study indicate that the choice of a spectral function corresponding to a random diffusion model may be appropriate if applied to a more complete relaxation equation, i.e., Eqn. 26 rather than Eqn. 30. The assumption that relaxation is controlled by methyl group rotation is questionable. On the basis of the calculated values for r_{CH} and E_a, the data appear to be more consistent with relaxation induced by chemical exchange of the hydroxyl protons of CH_3OH. There is some evidence to support this possibility in the data collected on 2-propanol, Figs. 19-22. The carbinol resonance of 2-propanol is broader than the methyl resonances. This fact implies the existence of T_2 (low frequency) processes that are specific to the carbinol resonance. Secondly, the carbinol resonance is seen to relax much more rapidly than the methyl resonance in a $T_{1\rho C}$ experiment, which also is consistent with the idea of a relaxation mechanism specific to that carbon.

5.2. HY(400)/10%MeOH).

Variation in the loading level of methanol on HY(400) should, by virtue of changing the relative numbers of acid sites and methanol molecules, help reveal the importance of specific methanol-zeolite interactions in the relaxation of the methanol resonance. In particular, samples prepared at lower loading levels of methanol may display relaxation that is more characteristic of a stronger interaction with the surface. Other than the implications of a static component of the ^{13}C-^1H dipolar coupling that allows cross-polarization, there are no data to indicate that the species observed in the CPMAS spectrum of

HY(400)/15% MeOH is any different from that seen with liquid state techniques. The activation energy and correlation times obtained from the $T_{1\rho_C}$ analysis are quite similar to those reported in the liquid-state study cited above.

Accordingly, a sample loaded with 10%-by-weight methanol (HY(400)/10%MeOH) was prepared. The room temperature ^{13}C CPMAS spectrum of this sample, recorded on the NT-200, is shown in Fig. 28. There are two lines in this spectrum, one at 50.1 ppm, as in the case of the samples at higher loading levels, and one at 55.7 ppm. There are two spinning sidebands on either side of the lines. These are spaced roughly 5 ppm from one another. The presence of these sidebands tells us that there are two species constrained from executing rapid random motion in the framework. There must be a distribution of orientations of the methanol molecules with respect to $\underset{\sim}{H}_o$ that remains static for at least several spinner periods (roughly 500 μs for the low speed bullet design) in order for the chemical shift anisotropy to be manifested in spinning sidebands. The combination of higher magnetic field and lower spinning rate on the NT-200 allows the observation of spinning sidebands that arise from this distribution of chemical shifts.

The resolution of a second resonance (55.7 ppm) at this lower loading level is consistent with the proposition that this second resonance is due to a species that is interacting strongly with the active sites in the zeolite. One can imagine that the relatively large perturbation in the chemical shift of this species relative to the liquid methanol chemical shift might be due to the effects of such a strong interaction. At higher loading levels this resonance at 55.7 ppm is

Fig. 28. ^{13}C CPMAS spectrum of 10% methanol by weight on HY(400).

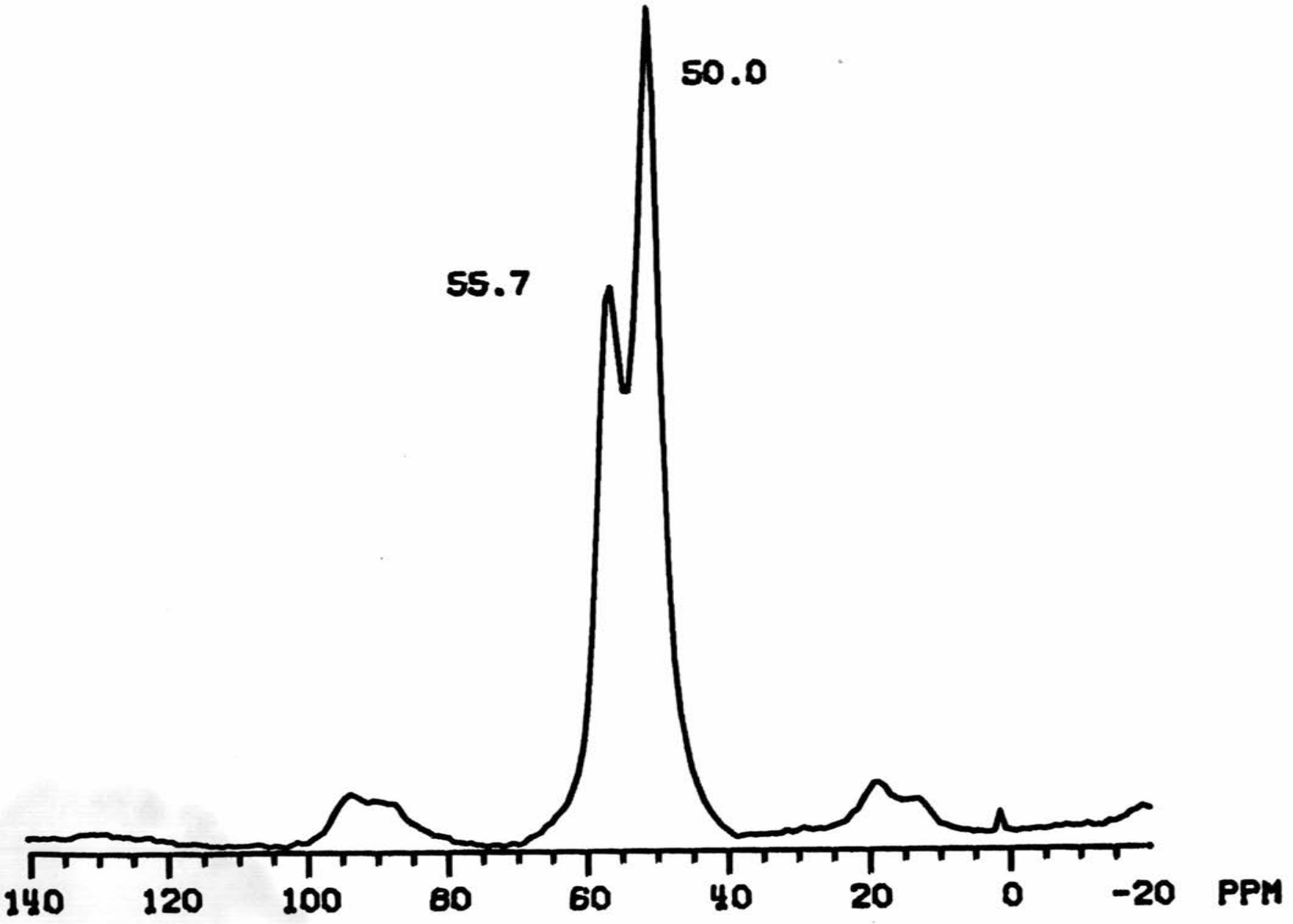
50.0
55.7
140
120
100
80
60
40
20
0
-20
PPM

overlapped and largely obscured by the 50.1-ppm resonance. If this newly resolved species does correspond to methanol strongly interacting with the zeolite, then it may be less mobile than the species at 50.1 ppm. To explore this issue, a variable contact time experiment was carried out on HY(400)/10%MeOH in order to determine the pertinent CP dynamics. A stacked plot of the data is given in Fig. 29. The 56-ppm resonance does appear to come up a bit more quickly than the 50-ppm resonance, and it decays a bit more slowly. The 56-ppm line reaches its maximum intensity at a contact time of 250 μs, while the 50.1-ppm line reaches maximum intensity at 1.5 ms. At a contact time of 8 ms, the 56-ppm line is at roughly half its maximum intensity compared to one quarter maximum for the 50.1-ppm line. Although both features would be expected for a species with reduced mobility, the differences are not great.

A ^{13}C T_1 experiment was also performed. A contact time of 100 μs was used in order to emphasize the 55.7-ppm resonance. The results are presented in Fig. 30 as a plot of the logarithm of signal intensity vs time. As discussed in Chapter 1, such a plot should yield a straight line for relaxation governed by a single T_1. A fit of the data from the 55.7-ppm resonance to a single exponential decay yields a value of T_1 on the order of 1.5 s. The data from the 50-ppm resonance show a pronounced curvature that is not consistent with single exponential relaxation. The data for this resonance can be fit with a double exponential.

$$\dot{M}_A(t) + \dot{M}_B(t) = 2[M_A(o)e^{-t/T_{1A}} + M_B(o)e^{-t/T_{1B}}] \qquad (31)$$

Fig. 29. Stacked plot of the results of a variable contact time ^{13}C CPMAS experiment on the sample HY(400)/10%MeOH.

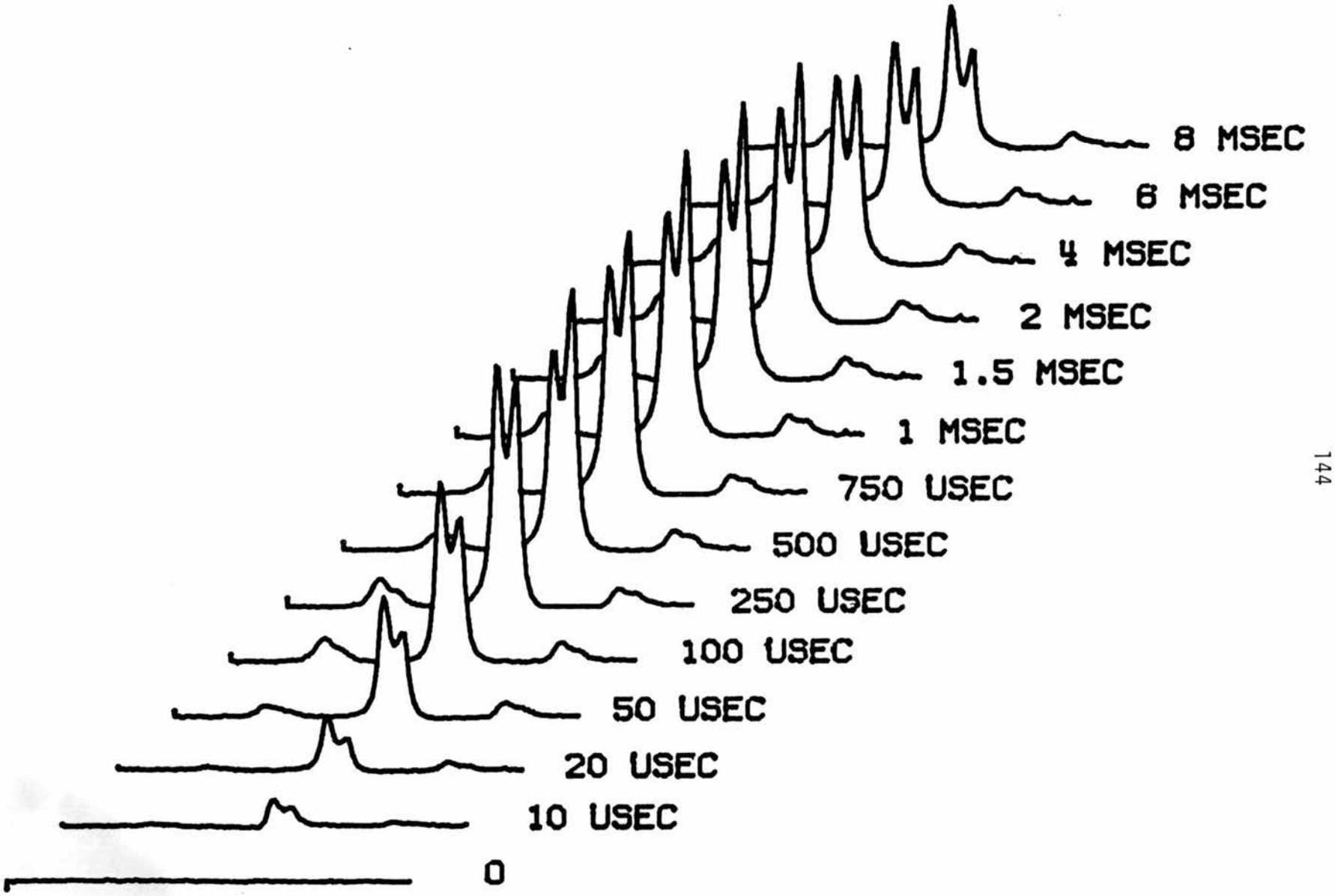
8 MSEC
6 MSEC
4 MSEC
2 MSEC
1.5 MSEC
1 MSEC
750 USEC
500 USEC
250 USEC
100 USEC
50 USEC
20 USEC
10 USEC
0

Fig. 30. Results of a laboratory-frame ^{13}C relaxation measurement on the sample HY(400)/15% MeOH. Filled circles represent species resonating at 55.7 ppm. Open circles represent species at 50.1 ppm.

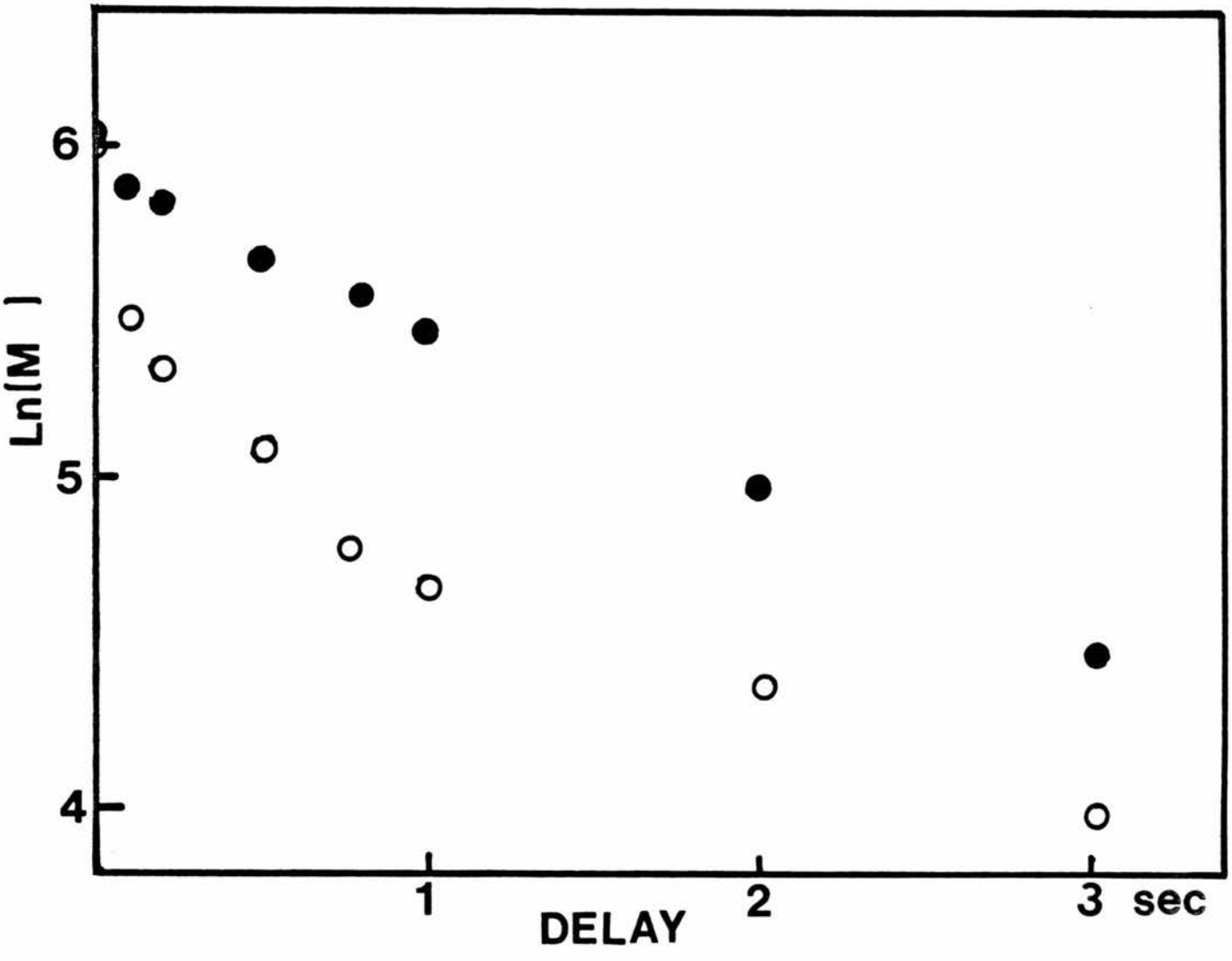
6
5
4
Ln(M)
1
2
3 sec
DELAY

The result of a double exponential fit is a value of 50 ms for one component, corresponding to the measured T_1 in HY(400)/15%MeOH and a roughly equal contribution which is also on the order of 1.5 s (1.7 ± 0.5). It now appears that there are actually two "new" resonances found at 10% loading, one at 55.7 ppm and the other at 50.1 ppm.

In summary, the samples at higher loading levels of methanol (30% and 15% by weight) have CPMAS spectra which are dominated by a single broad resonance at 50.1 ppm (see Figs. 16 and 24). At a loading level of 10% a second resonance, which appears at 55.7 ppm, is resolved, and there is strong reason to suspect that a third resonance remains unresolved from the 50.1-ppm line. The major component at higher loading levels could be due to "intracrystalline fluid" methanol of the sort one would expect to see in a liquid state experiment, i.e., relatively mobile, liquid-like material that resides in the supercages of the zeolite but which is not experiencing a specific interaction with an acid site. The results of the $T_{1\rho_C}$ experiment on HY(400)/15%MeOH tend to support this idea, as does the relatively short T_1 value measured for this species. However, the ease with which this species can be observed by cross-polarization, even with a contact time as short as 100 μs, remains unexplained. Mobile species have been observed using cross-polarization;[61] due to motional averaging of the dipolar coupling, such species usually cross-polarize very slowly and are sensitive to mismatching of the Hartmann-Hahn condition. When working with highly mobile species, the stability of the spin-locking fields is often inadequate to ensure reproducible CP results over a period of hours. However, the HY/methanol system shows no indication of such behavior. Signal intensities are reproducible to approximately ±10%

over a 24 hour period, which is typical of the overall stability of the instrument used. No particular effort is needed to locate the Hartmann-Hahn match, and cross-polarization is readily achieved. If this dominant component at higher loading levels is in fact such a highly mobile species, it is unusually easy to observe.

5.3. Cross-polarization of the 50-ppm Line.

It is possible to obtain a qualitative picture of the dipolar processes responsible for the cross-polarization of the species at 50 ppm by determining the cross-polarization efficiency as a function of the proton decoupling field strength. In the case of ^{13}C-^{1}H cross-polarization in a rigid solid with the ^{13}C spin-locking field on resonance, the rate constant for magnetization transfer from ^{1}H to ^{13}C is approximately given by[62]

$$\frac{1}{T_{CH}} = M_2^{CH} \left\{\cos^2\Theta_H J_z(\omega_{1C}) + \frac{1}{2}\sin^2\Theta_H \left(J_x(\omega_{eH} - \omega_{1C}) + J_x(\omega_{eH} + \omega_{1C})\right)\right\} \tag{32}$$

In Eqn. 32, M_2^{CH} is the second moment of the ^{13}C-^{1}H dipolar interaction.[63]

$$M_2^{CH} = \frac{1}{4}\gamma_C\gamma_H\hbar \sum_{k'} \frac{(1 - 3\cos^2\Theta_{jk'})^2}{r_{jk'}^6} \tag{33}$$

The sum in Eqn. 33 is over the ^{1}H spins interacting with the ^{13}C spin. Θ_H represents the angle in the rotating frame made by the proton rf field with respect to $\vec{H}_o$.

$$\Theta_H = \tan^{-1}\left(\frac{\omega_{1H}}{\Delta\omega_H^o}\right) \tag{34}$$

The terms J_x and J_z are spectral density functions describing the frequency distribution of the processes responsible for modulation of the dipolar coupling. ω_{1C} is the precession frequency of the ^{13}C spins in the ^{13}C rf field. ω_{eH} is the precession frequency of the ^{1}H spins in the effective field generated by an off-resonance ^{1}H rf field.

$$\omega_{eH} = \sqrt{\omega_1^2 + (\Delta\omega_H^o)^2} \tag{35}$$

In the case of a rigid solid, the modulation described by the spectral density functions arises from the evolution of the protons under proton-proton dipolar coupling. As the ^{1}H rf field is not necessarily parallel to the^{13}C rf field in the tilted rotating frame,[64] fluctuations in the proton magnetization both parallel and perpendicular to the decoupling field may be effective in inducing the transfer of magnetizaton. Thus there are two spectral density functions, J_x and J_z, in the expression for T_{CH}.

Both magic-angle spinning and molecular motion will complicate the cross-polarizaton process through their effect on the ^{13}C-^{1}H and ^{1}H-^{1}H dipolar coupling. Their general effect is a reduction in, or modulation of the ^{13}C-^{1}H dipolar coupling which slows the transfer, and a damping or modulation of ^{1}H-^{1}H flip-flops, which steepens the shape of the spectral density function; thus, the sensitivity to offset in the Hartmann-Hahn is increased. Experimentally one finds that the match is difficult to locate in such mobile systems and, once found, it is sensitive to amplifier drift and fluctuations in probe tuning.

In Fig. 31 is shown a plot of the intensity of the 50-ppm peak of the HY(400)/7%MeOH spectrum as a function of the frequency of the proton rf field. It is evident that there is not an abrupt change in

Fig. 31. Plot of the intensity of the ^{13}C CPMAS resonance at 50 ppm in HY(400)/10%MeOH sample as a function of the frequency offset of the ^{1}H rf field.

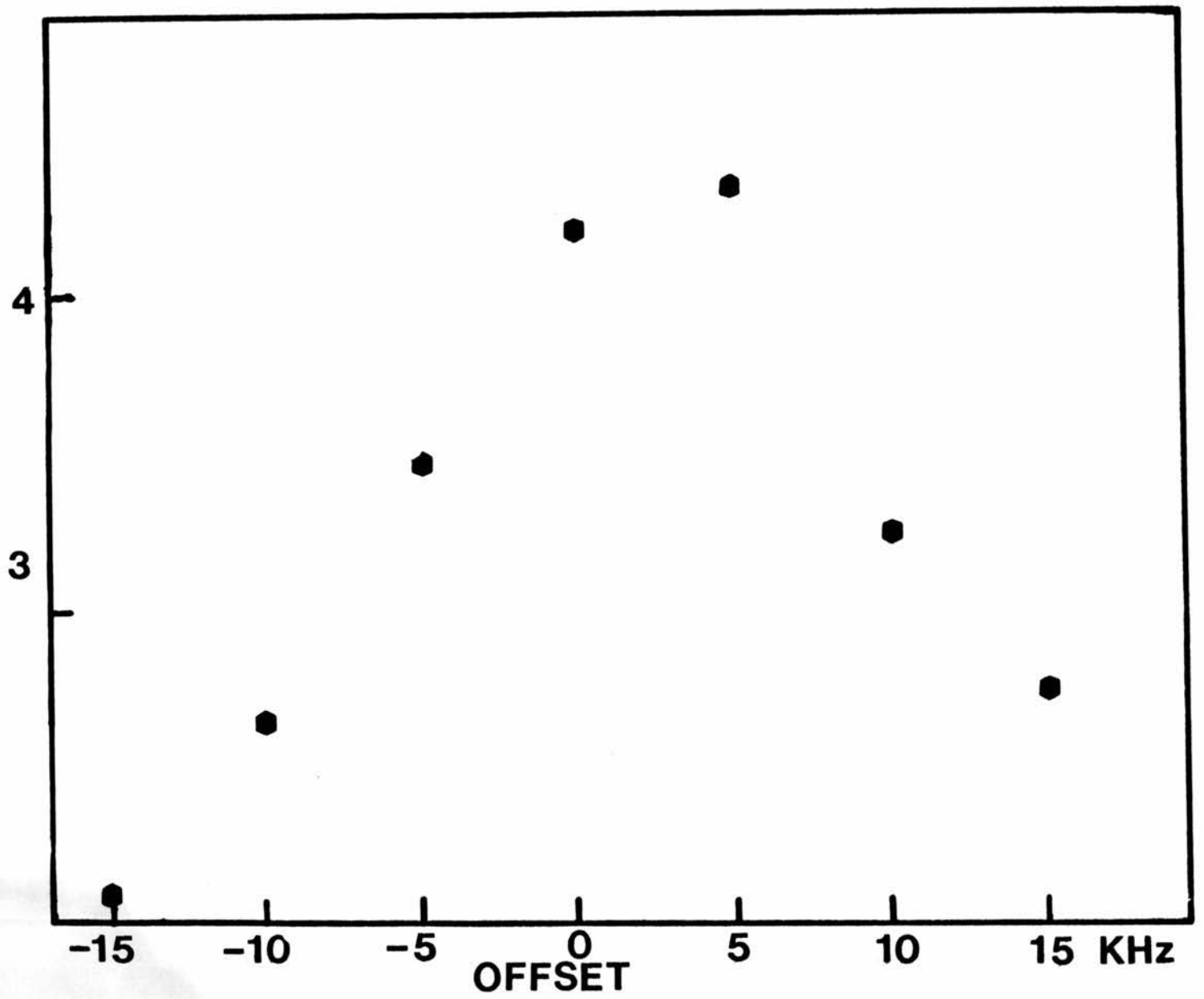
4
3
-15
-10
-5
0
5
10
15 KHz
OFFSET

T_{CH} as $\Delta\omega_H^\circ$ is changed; a sharp change would be expected for a weakly coupled proton reservoir. It follows that the protons involved in the cross-polarization of the 50-ppm species are themselves relatively immobile and in dipolar contact with other protons, even if part of the 50-ppm peak is due to a mobile species. The 56-ppm peak behaves similarly; it also cross-polarizes over a large range of decoupler frequencies.

It cannot be concluded from these data that the species at 50 ppm are themselves immobile. It is possible that an "intracrystalline fluid" species with relatively high mobility is being cross-polarized via dipolar coupling to protons that are immobilized on the zeolite framework. In such a case no amount of rotation or translation of the mobile species within a cavity would completely remove a dipolar coupling of the methanol ^{13}C's to the framework-attached protons.

5.4. FTMAS (or Bloch-Decay Experiments).

A cross polarization spectrum does not generally yield quantitative intensities. If the CP dynamics are characterized, then one can extract quantitative intensities, but such an analysis can become fairly involved. The simple FT (Bloch Decay) spectrum is preferable, if T_1 relaxation is rapid enough to make it feasible. As the longest T_1's in the HY/MEOH system are about 1 s, the Bloch-decay spectrum can be easily obtained.

A series of Bloch-decay spectra of HY(400)/10% MeOH are presented in Fig. 32. The bottom spectrum is the routine Bloch-decay spectrum, with high-power proton decoupling applied during acquisition of the FID. From the relative intensities it is clear that the resonance at 50 ppm is dominant, comprising some 90% of the total signal intensity. The second spectrum is a Bloch-decay spectrum recorded without proton

Fig. 32. Top: ^{1}H-coupled ^{13}C FTMAS spectrum of HY(400)/10%MeOH with a 1 ms preacquisition delay.

Middle: ^{1}H-coupled ^{13}C FTMAS spectrum of HY(400)/10% MeOH acquired immediately after the ^{13}C 90° pulse.

Bottom: ^{1}H decoupled ^{13}C FTMAS spectrum of HY(400)/10%MeOH.

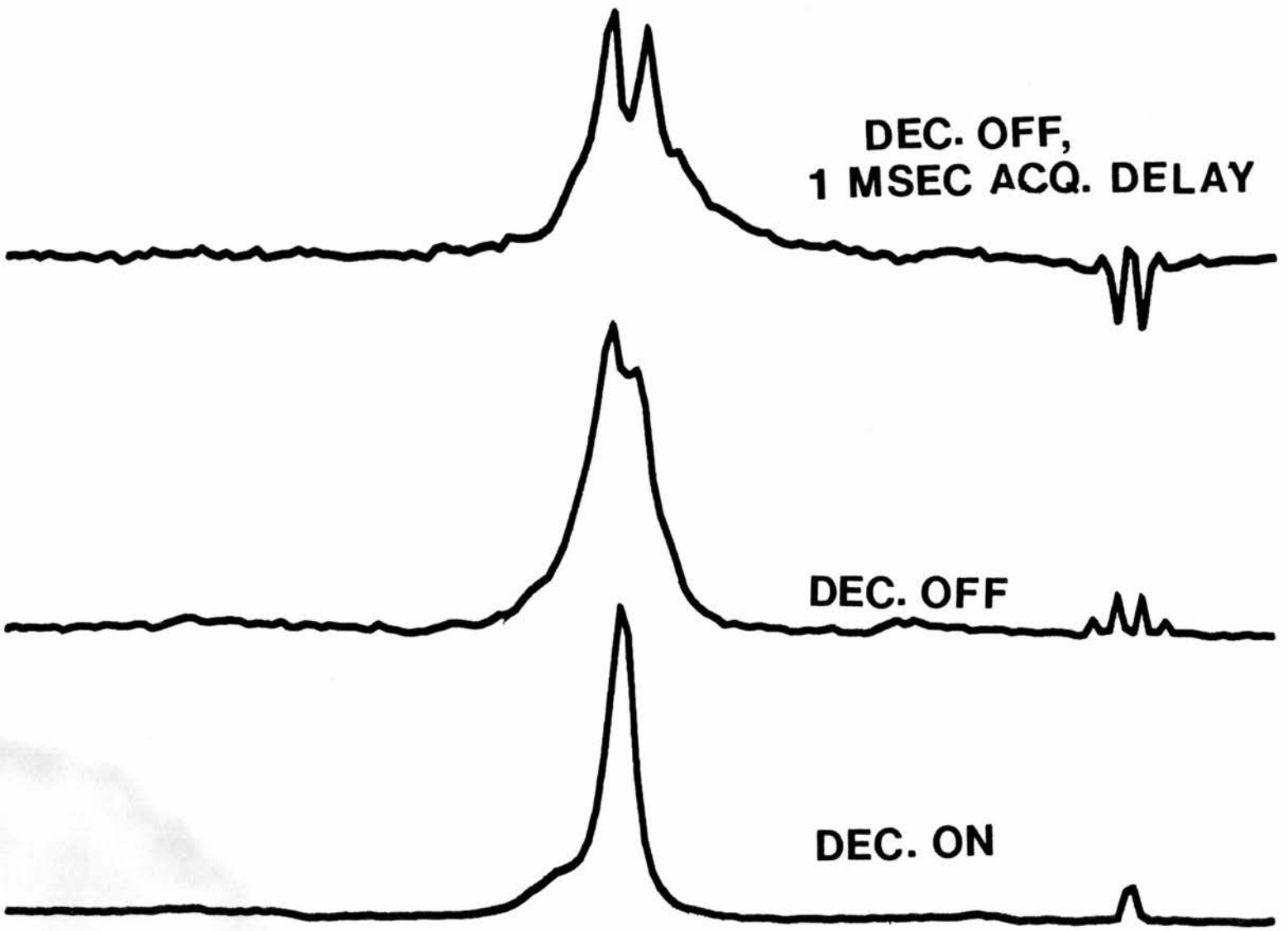
DEC. OFF,
1 MSEC ACQ. DELAY
DEC. OFF
DEC. ON

decoupling. The resonance at 50 ppm has apparently split into a partially-resolved J quartet, while the resonance at 56 ppm is no longer visible. The top spectrum in Fig. 32 is the proton-coupled Bloch-decay spectrum obtained with a delay of 1 ms after the ^{13}C 90° pulse and before acquisition of the FID. The resolution of the multiplet at 50 ppm is quite a bit better than in the spectrum obtained with no delay, taking on the appearance of a broadened quartet.

This ability to resolve J coupling in the spectra described above indicates that molecular motion averages ^{13}C-^{1}H dipolar coupling to near zero. In this sense, the 50-ppm resonance corresponds to a species of liquid-like mobility. It may be the same mobile component that was detected at lower relative intensity in the CP spectrum. The enhanced resolution of the J quartet in the delayed acquisition experiment is caused by a distribution of T_2's at this chemical shift; such a distribution might be caused by a distribution of motional correlation times in the mobile species or from the presence of a second, immobile species. If there are two or more T_2 value represented in a line, then delaying acquisition will allow the resonance(s) with smaller T_2 values to dephase, leaving behind the narrower resonance.

5.5. Dipolar Coupling.

If the 50-ppm peaks in the CP and Bloch Decay spectra are due to the same species, then the J coupling should appear in the proton-coupled CPMAS spectrum. Fig. 33 shows the proton-coupled CPMAS spectrum of HY(400)10%MeOH. There is a sideband pattern extending some 10 KHz from the 50-ppm region. It is not possible to pinpoint the origin of the sideband pattern as being at either 50 or 56 ppm. The two peaks

Fig. 33. ^{1}H-coupled ^{13}C CPMAS spectrum of HY(400)/15%MeOH.

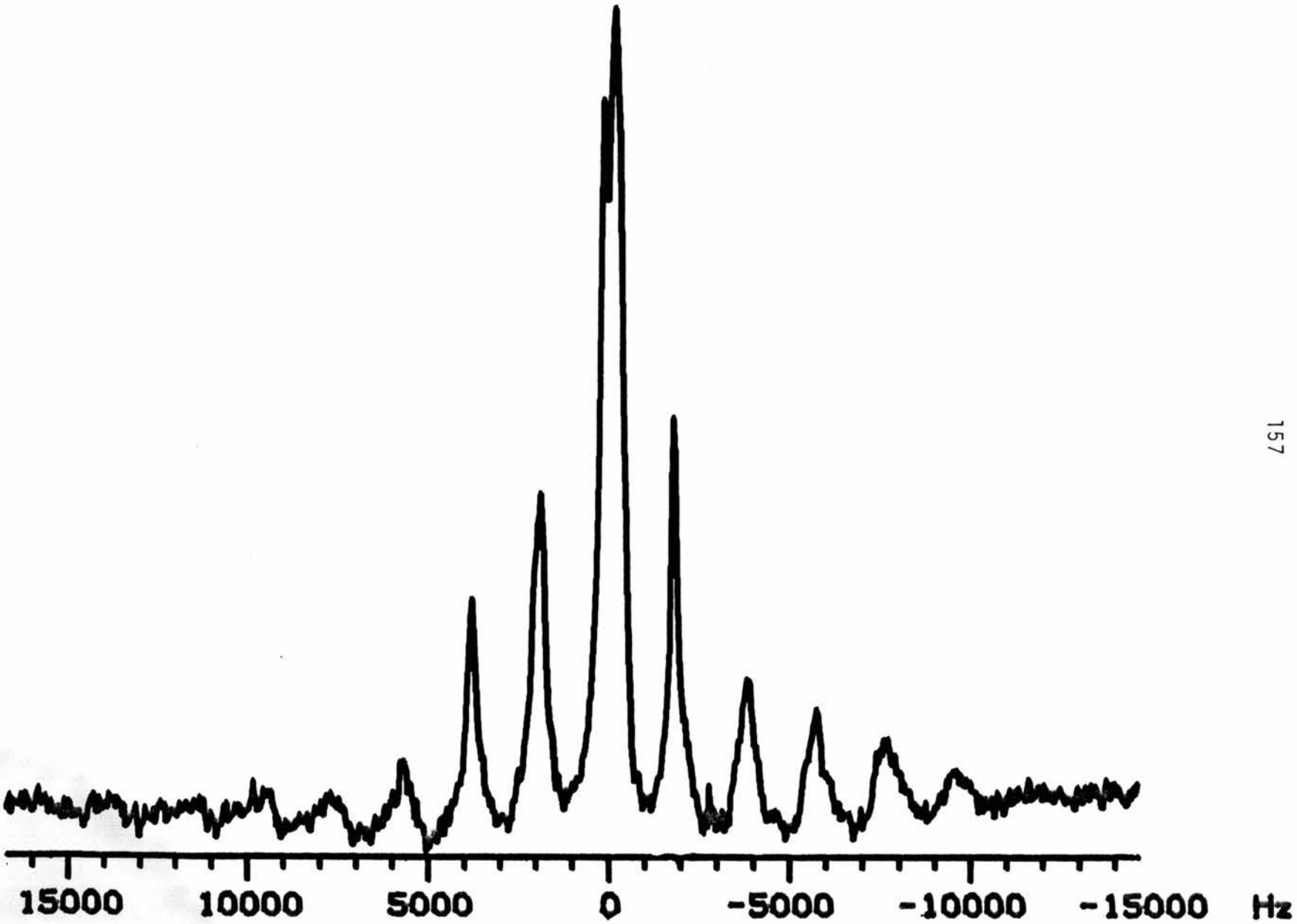
15000
10000
5000
0
-5000
-10000
-15000
Hz

overlap and the observed position of the sideband maxima depends critically on the choice of phasing parameters. The spectrum can be phased to make the origin of the sideband pattern appear to be at either position. In any case, this kind of pattern can occur only if one or both of the species has an inhomogeneous C-H coupling, i.e., the proton local field experienced by ^{13}C is time-independent (apart from modulation under MAS) over the duration of one or more spinner periods.

The spinning sidebands in the proton-coupled spectrum are characteristic of an inhomogeneous ^{13}C resonance, one which is completely described by the zeroth-order term in the Average Hamiltonian expansion of the "spinning Hamiltonian".[65,66] Normally the proton-proton dipolar coupling renders the total dipolar Hamiltonian homogeneous, with the result that the proton-coupled carbon spectrum is broad and featureless. In the following paragraphs some features of inhomogeneous dipolar coupling are examined.

Consider a ^{13}C-^{1}H system in which only dipolar interactions are exerted (which is equivalent in the rotating frame to observation at exact resonance for both spins). The secular dipolar Hamiltonian can be written as

$$H_D = H_D^{HH} + H_D^{CH} \tag{36}$$

where

$$H^{HH} = \frac{1}{4}\gamma_H^2\hbar^2 \sum_{j,k} \frac{(1 - 3\cos^2\Theta_{jk})}{r_{jk}^3} (3I_{zj}I_{zk} - \underset{\sim}{I}_j \cdot \underset{\sim}{I}_k) \tag{37}$$

$$H_D^{CH} = \gamma_C\gamma_H\hbar \sum_{i,m} \frac{(1 - 3\cos^2\Theta_{im})}{r_{im}^3} I_{zi}S_{zm} \tag{38}$$

In these equations r_{jk} is the magnitude of the internuclear vector connecting the j^{th} and k^{th} spins and θ_{jk} is the angle that the internuclear vector makes with the z axis. It will be sufficient for the purposes of this discussion to consider the first two terms of the expansion of the Hamiltonian given by Average Hamiltonian Theory (AHT) in the case of magic-angle spinning

$$H_D^{(0)}(t) = \frac{1}{t}\int_0^t dt_1 (H_D^{HH}(t_1) + H_D^{CH}(t_1)) \tag{39}$$

$$H_D^{(0)}(t) = \frac{-i}{2t}\int_0^t dt_2 \int_0^{t_1} dt_1 [H_D^{HH}(t_2) + H_D^{CH}(t_2), H_D^{HH}(t_1) + H_D^{CH}(t_1)] \tag{40}$$

The time-dependence of H_D is contained in the geometric factors which are modulated by spinning. If for all t_1 and t_2 $[H_D(t_2), H_D(t_1)] = 0$, then $H_D^{(1)}$ and all higher order terms in the expansion are zero and the average Hamiltonian is given by $H_D^{(0)}$. Then, if the integration is carried out over an integral number of spinner periods, $H_D^{(0)}$ will be exactly zero. What this means is that, if the magnetization is sampled at integral intervals of the rotation period, there would be no evidence of the dipolar coupling in the spectrum for the commuting case specified above. One is usually forced to sample a great deal faster than this in order to satisfy the sampling theorem, and the signal is seen to decay and then refocus at times corresponding to the reciprocal of the spinner frequency. Qualitatively one can consider this to be a phase modulation of the proton-decoupled signal at the spinner frequency. It is this modulation that generates the spinning sidebands in the frequency domain spectrum.

H_D^{CH} is itself inhomogeneous in the AHT sense, but the total Hamiltonian, $H_D^{CH} + H_D^{HH}$, is not. The problem lies in commutators of the H_D^{CH} with H_D^{HH} in the first-order and higher-order terms in the AHT expansion. The first-order terms involve the commutators,

$$[H_D^{CH}(t_2) + H_D^{HH}(t_2),\ H_D^{CH}(t_1) + H_D^{HH}(t_1)] \tag{41}$$

which, according to Eqns. 39 and 40, generate the first-order terms,

$$H_D^{(1)}(t) = \frac{-i}{2t}\int_o^t dt_2 \int_o^{t_2} dt_1 \left\{ \frac{1}{4}\gamma_C^3 \gamma_H \hbar^4 \sum_{ijkm} \frac{(1 - 3\cos^2\theta_{im}(t_2)(1 - 3\cos^2\theta_{jk}(t_1))}{r_{im}^3 r_{jk}^3} \right. \tag{42}$$

$$\left. - \frac{(1 - 3\cos^2\theta_{jk}(t_1))(1 - 3\cos\theta_{im}(t_1))}{r_{im}^3 r_{jk}^3} \right\} \times \left\{ [3I_{zj}I_{zk} - \underset{\sim}{I}_j \cdot \underset{\sim}{I}_k, I_{zi}S_{zm}] \right\} \tag{43}$$

Rewriting the geometric terms in a more compact form leads to Eqn. 44.

$$H_D^{(1)}(t) = \frac{-i}{2t}\int_o^t dt_2 \int_o^{t_2} dt_1 \frac{1}{4}\gamma_C^3 \gamma_H \hbar^4 \sum_{ijkm} \left\{ f_{im}(t_2)g_{jk}(t_1) - f_{im}(t_1)g_{jk}(t_2) \right\}$$

$$\left\{ [3I_{zj}I_{zk} - I_j I_k, I_{zi}S_{zm}]) \right\} \tag{44}$$

Evaluating the commutators leaves only 3-body terms.

$$H_D^{(1)}(t) = \frac{-i}{2t}\int_o^t dt_2 \int_o^{t_2} dt_1 \frac{1}{4}\gamma_C \gamma_H \hbar^4 \sum_{jkm} (f_{2m}(t_2)g_{jk}(t_1) - f_{2m}(t_1)g_{jk}(t_2))$$

$$(I_j^+ I_k^- - I_j^- I_k^+)S_{zm} \tag{45}$$

The product operators $I_j^+ I_k$ and $I_j^- I_k^+$ are "responsible" for "flip-flops" among the ^1H spins. The coupling $S_{zm} I_{zk}$ will thus be modulated by the flip-flopping of proton spin k with nearby protons j, which destructively interferes with the modulation of the C_m-H_k coupling by spinning. In another manner of speaking, the strong proton-proton dipolar coupling makes the azimuthal quantum number of the proton spin angular momentum a bad quantum number. As a result there is an uncertainty introduced into the ^{13}C-^1H coupling that makes for a homogeneous carbon resonance, which cannot be averaged properly by spinning. To overcome the effects of the ^1H-^1H flip-flops requires spinning at rates sufficiently rapid to damp the higher order-terms in the expansion; this has not yet been technically feasible in any laboratory.

From the above discussion it follows that proton spin-diffusion must not be interfering significantly with the MAS averaging of the heteronuclear coupling of one or more species in HY(400)/MeOH, as evidenced by the appearance of dipolar sidebands in the proton-coupled CPMAS spectrum. The methyl protons of the corresponding species must be isolated from other protons in the system, isolated enough to limit intermoleculear proton coupling to substantially less than the spinning rate of 2 KHz.

Implicit in the discussion to this point has been the assumption that intramethyl ^1H-^1H flip-flops also must not affect the net ^{13}C-^1H dipolar coupling. This is in fact that one would expect as the result of rapid internal rotation of the methyl group. Qualitatively, methyl group rotation "equalizes" the three methyl ^{13}C-^1H couplings; and flip-flops among the methyl protons leave the net ^{13}C-$^1H_3$ coupling unchanged. This case can also be treated by AHT.

The effect of internal rotation of the methyl group will now be incorporated into the AHT formalism developed above. The rotation will be treated classically; i.e., the rotation will be assumed to proceed continuously, not by rotational jumps, and will be described by a single correlation time, the inverse of which is the rotational frequency, ω_{rot}. As far as the dipolar Hamiltonian is concerned, such a classical treatment is equivalent to the full quantum-mechanical treatment.[67]

Typical correlation frequencies for the internal rotation of methyl groups fall in the range of 10^9-10^{12} Hz.[68] This sort of time scale for modulation of the dipolar Hamiltonian is far removed from the time scales of other processes, such as MAS or intermolecular ^1H-^1H flip-flops that may occur in the system. Hence averaging over the rotation can be carried out independently of these slower processes.

Consider an isolated methyl group with an orientation fixed with respect to the angle α between the external magnetic field (H_0) and the C_{3v} axis (see Fig. 34). Each ^{13}C-^1H pair is characterized by an internuclear vector (magnitude r_{im}) at an angle $\gamma_{im} \tilde{=} 54.7°$ to the axis of methyl group rotation. Each proton pair is separated by an internuclear vector, of magnitude r_{jk}, at an angle $\gamma_{jk} = 90°$ to the axis of rotation. The methyl rotational frequency, ω_{rot}, is much greater than the static dipolar linewidth, which allows the problem to be described in zeroth order of AHT.

Fig. 34. Coordinates for averaging dipolar coupling over the internal rotation of a methyl group.

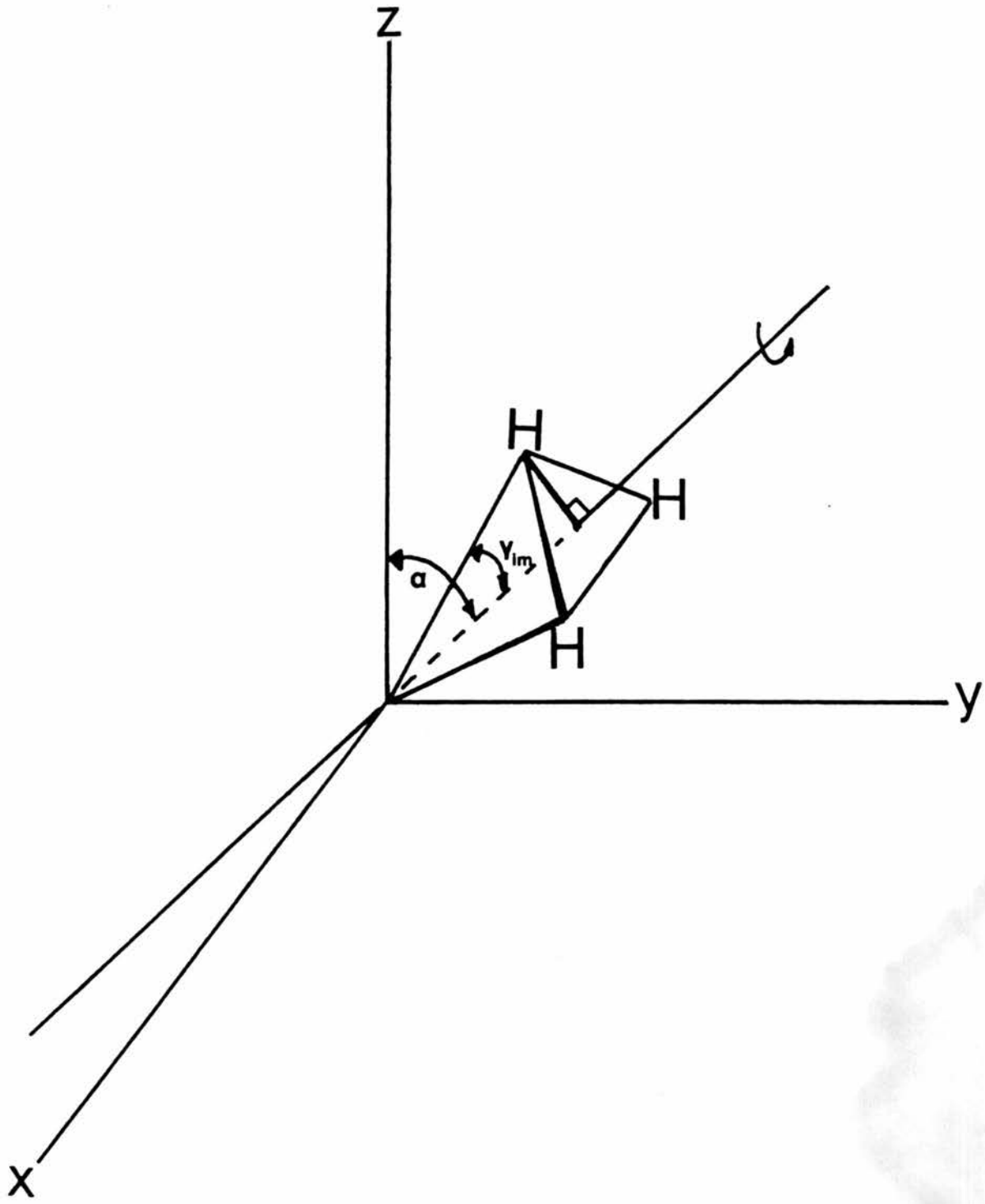
Z
H
H
H
α
γ_{im}
y
x

$$H_{CH}^{(0)} = \omega_{rot}\int_{0}^{1/\omega_{rot}} dt_1 H_{CH}(t_1) \tag{46}$$

$$H_{HH}^{(0)} = \omega_{rot}\int_{0}^{1/\omega_{rot}} dt_1 H_{HH}(t_1) \tag{47}$$

Carrying out the integration, one finds

$$H_{CH}^{(0)} = \frac{1}{2}\gamma_C\gamma_H\hbar^2(3\cos^2\alpha - 1)\sum_{z,m}\frac{(1-3\cos^2\gamma_{im})}{r_{im}^3} I_{zi}S_{zm} \tag{48}$$

$$H_{HH}^{(0)} = \frac{1}{8}\gamma_H^2\hbar^2(3\cos^2\alpha - 1)\sum_{j,k}\frac{(1-3\cos^2\gamma_{jk})}{r_{jk}^3}\left[\frac{3I_{zj}I_{zk} - \mathbf{I}_j\cdot\mathbf{I}_k}{r_{jk}^3}\right] \tag{49}$$

Both couplings are scaled by the motion, and more importantly they now carry the same orientational dependence. Hence, when the motionally averaged Hamiltonians are entered into the expression for magic-angle spinning (Eqn. 37), the term

$$f_{im}(t_2)g_{jk}(t_1) - g_{jk}(t_2)f_{im}(t_1) \tag{50}$$

in Eqn. 45 is zero, as are the corresponding terms in the higher-order corrections. Therefore, the average Hamiltonian is given by the zeroth order term, which predicts periodic refocussing of the magnetization at the spinner frequency.

Fig. 35. Pulse sequence for the rotationally-synchronized interrupted-decoupling experiment.

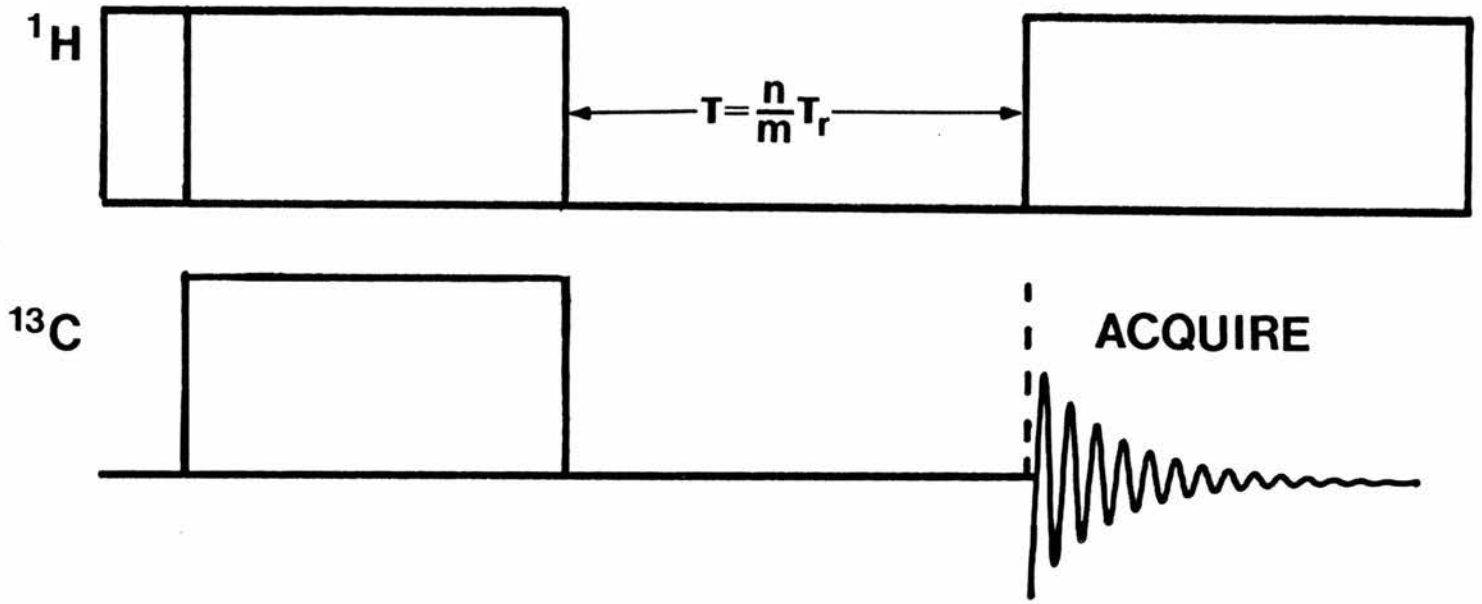
^{1}H
$T=\frac{n}{m}T_r$
^{13}C
ACQUIRE

Fig. 36. Evolution of the ^{13}C resonances of HY(400)/10%MeOH during the rotationally-synchronized interrupted-decoupling experiment.

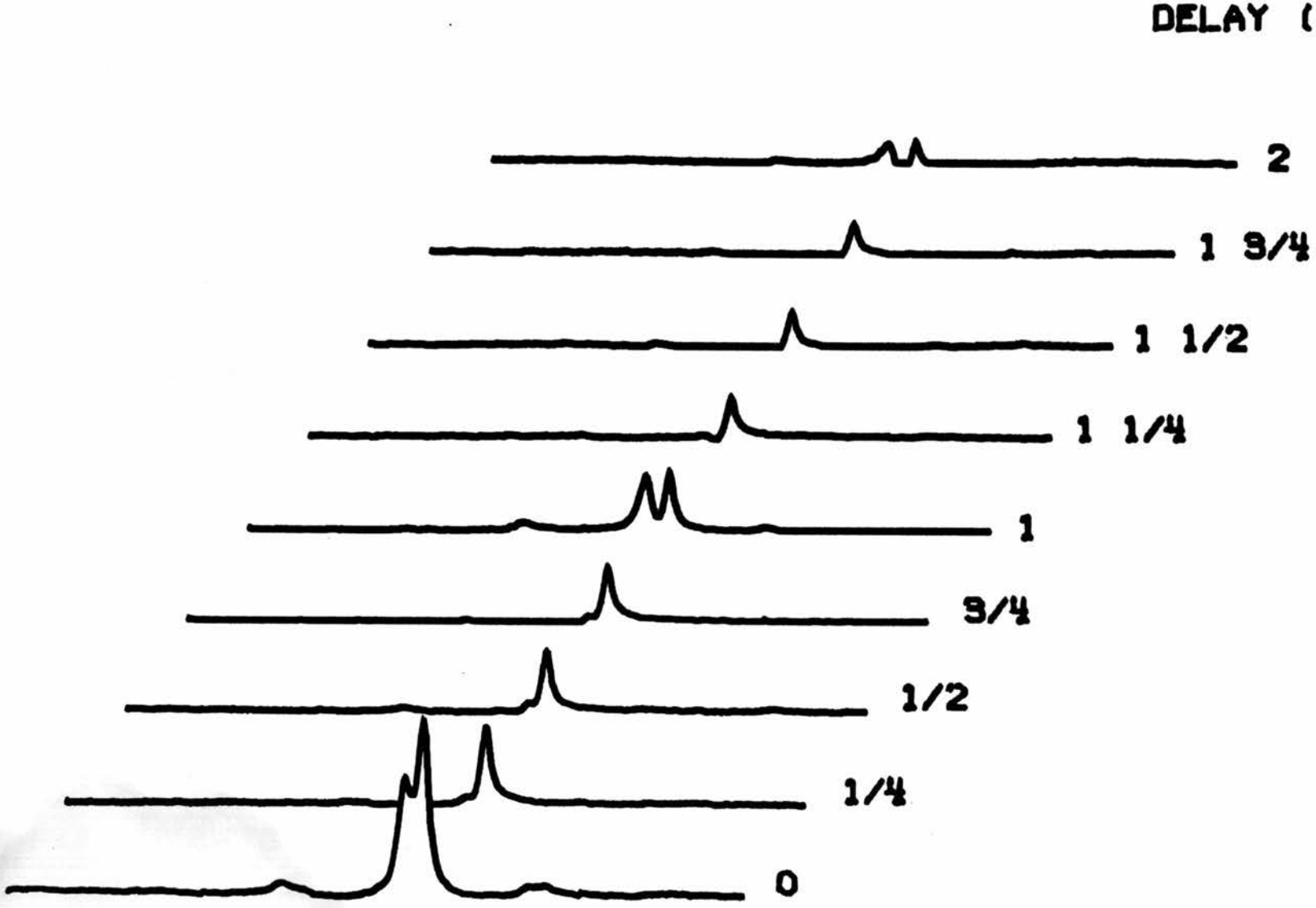
DELAY (ROTOR PERIODS)
2
1 3/4
1 1/2
1 1/4
1
3/4
1/2
1/4
0

The periodic refocussing of an inhomogeneous resonance can be seen clearly in a rotationally-synchronized interrupted-decoupling experiment. This experiment is diagrammed in Fig. 35. In this experiment, the magnetization is prepared by cross polarization and allowed to evolve without proton decoupling for an incremented time, t_d, prior to the data acquisition period, during which high-power proton decoupling is employed. The size of the increment in t_d is chosen to be a fraction of the rotor period, so that $t_d = nt_{rot}/m$, where n and m are integers. During the evolution period the ^{13}C magnetization evolves under both the chemical shift and dipole-dipole Hamiltonians, which are both modulated by magic-angle spinning. The effect of a pre-acquisition delay on evolution of the spins under the isotropic part of the chemical shift Hamiltonian is merely to introduce a phase shift into the spectrum, which may be removed by applying a phase correction to the frequency-domain spectrum. When the decoupler is turned on for accumulation of the signal, the dipolar coupling is removed and the magnetization retains the dephasing accumulated during the evolution under dipolar coupling. A homogeneous line will show a rapid decay as a function of t_d and the intensity will not refocus at $t_d = nt_{rot}$. In contrast, the intensity of an inhomogeneously broadened resonance will refocus at $t_d = nt_{rot}$. The results of a series of rotatonally-synchronized interrupted-decoupling experiments with $t_d = nt_{rot}/4$ are displayed in Fig. 36. The 56-ppm resonance demonstrates the rotational dipolar echo expected of an inhomogeneous dipolar Hamiltonian. There is clearly a two-phase pattern in the behavior of the 50-ppm peak. One component of this peak decays quickly over the first 100 μs delay and a second component persists with only slight decay over the duration of that segment of the experiment (roughly 1 ms). The rapid decay of the

first component is what one expects from a homogeneous interaction. The second, persistent behavior is characteristic of a species with liquid-like mobility.

5.6 Summary.

The NMR spectrum of methanol adsorbed onto HY(400) contains two resolved peaks, one at 55.7 ppm and one at 50.1 ppm. At higher loading levels, the 50-ppm resonance dominates the spectrum and the presence of the 56-ppm resonance can be inferred only from the presence of spinning sidebands. The 50-ppm peak apparently has contributions from two distinct species. This point was first brought out by the biphasic T_1 relaxation of this resonance and later confirmed in the rotationally-synchronized interrupted-decoupling experiment just described, in which the two components exhibit completely different ^{13}C-^{1}H dipolar coupling behavior. One species decays in a manner characteristic of a typical strongly-coupled organic solid, while for the other species the protons are almost completely decoupled from one another.

The Bloch-decay spectrum confirms the presence of a signal arising from mobile methanol molecules (50.1 ppm), which are seen to be the predominant species in the system. The comparatively weak intensity of this signal in the CP experiment reflects a weak residual ^{13}C-^{1}H dipolar coupling that results in poor cross-polarization efficiency. The ^{13}C-^{1}H dipolar coupling is actually reduced to the point where it is possible to observe J coupling. This would lead one to think that the cross-polarization rate for this species would be very sensitive to the quality of the Hartmann-Hatch match. However, it is not. One can move several KHz off resonance and stil achieve cross polarization. Cross

polarization of the mobile species must therefore proceed via intermolecular dipolar contact to a reservoir of strongly-coupled protons.

The second species at 50 ppm behaves more like a solid. It displays chemical shift anisotropy, which means it is immobilized to some degree, and it displays homogeneous dipolar coupling. The homogeneous nature of the ^{13}C-^{1}H dipolar coupling indicates that the methyl protons of this species are involved in flip-flops with some other protons that have a non-equivalent dipolar coupling to the methyl ^{13}C.

The third resonance, at 56 ppm, also behaves like a bound species. The ^{13}C-^{1}H dipolar coupling is inhomogeneous, which can occur only if there is no appreciable ^{1}H spin-diffusion from the methyl protons to other protons in the system. This species must be relatively isolated.

In the following pages several "models" are presented and discussed as explanations for the observations presented above. The models are not mutually exclusive. Rather they offer one or more possibilities for some aspect of the description of HY/MEOH that can be resolved by an appropriate experiment or series of experiments. After a presentation of the models and discussion of the experiments, the most appropriate linear combinaton of these models will be offered as a description of the HY/MEOH system.

5.7. Models.

5.7.1. Adsorption into the beta cage.

The 56-ppm resonance may correspond to methanol adsorbed into the beta cages of HY(400). Species adsorbed into the beta cages would be isolated from the bulk of the adsorbed methanol and thus may not partake in ^{1}H-^{1}H flip-flops.

As the diameter of the 6-ring aperature of the beta cage in NaY is approximately 2.2 Å,[69] compared to a 4 Å diameter for a methyl group,[70] the adsorption of methanol into the beta cage would seem to require expansion of the aperature. Such a mechanism, called "breathing", has been proposed to account for an observed increase in the uptake of ammonia (diameter 3.8 Å) by NaY at elevated temperatures.[71] More recently the adsorbtion of small amounts of methanol onto zeolite ZSM-5 has been found to cause profound changes in the crystal structure of the zeolite.[72]

The possibility of adsorption of methanol into the beta cages has been previously offered as a possible explanation for an observed increase in the adsorption of methanol by HY as compared to NaY, but the data are contradictory in this regard.[73] The adsorption characteristics of a particular framework structure will depend on the size and chemical nature of the counterion.[74] The effect of changing the counterion can be quite dramatic.[75] Apparent pore volumes can vary by as much as 20%-30% upon change of the cation. Thus, although a measured increase in the adsorption of methanol onto HY over NaY is suggestive of adsorption into the beta cages, it is not conclusive in the absence of direct spectroscopic evidence, such as may be supplied by NMR.

5.7.2. Formation of Si-O-CH_3 units

When methanol is desorbed from HY at 150 - 200°C and the IR spectrum taken, absorption bands characteristic of the methoxysilane linkage are seen.[76] One could envisage the formation of such species as follows:[77]

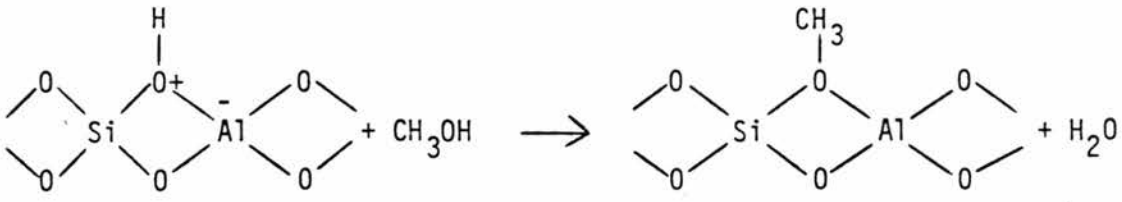

(51)

It is not clear whether these species are present in the zeolite prior to heating or are generated during the heating process. The region in which the methoxysilane resonance appears in the IR spectrum is dominated by the signal arising from mobile methanol in the unheated sample, and would thus not be resolved in a sample loaded at room temperature. The ^{13}C chemical shift of the methoxysilane group should fall in the region of 50 to 60 ppm, and it may be that one or both of the immobile species are methoxysilanes of this general type.

The two immobile species have chemical shifts differing by about 5 ppm. If this chemical shift difference is due to their being chemically distinct species (i.e., in the sense of CH_3OH vs $CH_3OSi\lesssim$) and not due to their being in different regions of the framework, then it is reasonable to suppose that their different proton spin-diffusion properties are related to this chemical difference. The formation of water in the reaction to make the methoxysilane unit results in the loss of two protons from the immediate environment of the methyl protons that might otherwise be involved in flip-flops with the methyl protons. This may account for the reduced dipolar coupling the in the species at 56 ppm.

5.7.3. Heterogeneous filling of the cages.

It is possible that methanol, both the mobile and immobile forms, is heterogeneously distributed throughout the framework. In principle, variations in the populations of the various species from region to region could affect ^{1}H spin-diffusion and the ^{13}C chemical shift of these species.

The ^{1}H spin diffusion rate and ^{13}C chemical shift of the immobile species could be affected by interactions with free methanol or with other immobilized methanol molecules. In the first case, a type of "solvent effect" model, it would be supposed that ^{1}H spin-diffusion occurs as a result of dipolar coupling between bound and mobile methanol molecules. The 56 ppm resonance would then correspond to species in relatively empty supercages and the 50-ppm resonance to species bound in relatively full supercages. The chemical shift of bound methanol molecules could also depend on the availability of other methanol molecules to act as a "solvent". For example, it may be that methanol molecules cluster about an active site, much as water is found to cluster about some cations in zeolites.[78] The chemical shift would then be a function of the number of methanol molecules available in a particular location within the framework. As one does not observe a continuous range of chemical shifts between 50.1 ppm and 55.7 ppm there would have to be an abrupt change in the chemical shift at some critical number of methanol molecules in order to account for the distinct 5.6 ppm shift difference that is observed.

In the second, and perhaps more likely case, interactions betwen adjacent bound species might be proposed to affect the behavior of the ^{13}C resonance. The protons of two neighboring species could undergo

flip-flops. A situation in which there are two neighboring bound methanol molecules requires that there is a pair of close aluminum neighbors. Such aluminum neighbors are thought to be associated with weaker acidity in the zeolite,[79] and interaction of methanol with such sites may thus result in a smaller perturbation of the ^{13}C chemical shift than would interaction with a more isolated acid site.

5.7.4. Chemical exchange.

Chemical exchange processes are frequently observed in adsorption systems.[80] It is important here to consider possible exchange mechanisms as a means of determining the nature of the interaction between the zeolite and adsorbed methanol.

One possibility is that cross-polarizaton of the mobile species occurs because of chemical exchange of this species with bound species. According to this view, the bound species undergoes cross-polarization and then carries ^{13}C magnetization into the mobile through chemical exchange. In order for this mechanism to be effective, the exchange lifetime must be smaller than or comparable to the cross-polarization contact time of 1-5 ms. In the case where exchange is rapid relative to T_1 relaxation rates of the exchanging species one should observe a weighted average of the T_1 values of the exchanging species. In HY(400)/10% MeOH we were able to measure quite different T_1 values for bound and mobile species at 50.1 ppm. Thus, we conclude that chemical exchange between bound and mobile species, if present, is too slow to affect cross-polarization dynamics.

Another possibility is that the immobile species are involved in exchange processes that do not involve the mobile species, e.g., exchange between various sites in the framework or between different

orientations of a methanol molecule with respect to a single site. Such processes will in general affect the observed chemical shift and powder pattern of a randomly oriented material.[86] Determination of their presence or absence will be of importance in understanding the nature of the interaction of methanol with the framework.

5.7.5. Adsorption on the exterior of the zeolite.

Wherever the zeolite framework terminates at the boundary of a microcrystallite there must be surface hydroxyl groups. Typically these surface hydroxyls account for about 1% of the total hydroxyl content of the zeolite.[82] The 56-ppm resonance could be due to methanol interacting with such sites, in which case the relatively slow spin-diffusion of this species would be the result of its isolation from the bulk of the ^{1}H-containing material of the system. If this is the case, the relatively large intensity of this resonance must be explained.

5.7.6. Chemically distinct sites.

Both Lewis and Bronsted acid sites are generated in the activation of NH_4Y. Methanol will in principle interact with both types of sties. Lewis acid sites necessarily occur at or near structural defects that result from dehydroxylation of the framework (see structures IX, XI or XIII) so that methanol interacting with such sites might be isolated from the bulk of the adsorbed material. Structure IX predicts the loss of hydroxyl protons upon the formation of tricoordinate aluminum, which, if true, would result in reduced intermolecular dipolar coupling in methanol moieties intracting with those sites. However, ^{27}Al and ^{1}H

NMR data indicate that species similar to those in structures XI and XIII are more likely to be responsible for Lewis acidity.[83]

5.8. Further Experiments.

The strategies and results of a series of experiments addressing the questions raised above in terms of the six models are now described.

5.8.1. Steric restriction.

The interaction of an alcohol with a beta cage site, and possibly with Lewis sites and close pairs of sites will be limited to those alcohols capable of accessing the sites. Adsorption of alcohols of differing sizes and structures may determine whether or not there is a steric restriction associated with one of the resonances in the methanol/HY system. A set of experiments was carried out in which a series of alcohols, all of which are small enough to pass the 12-ring aperture of the supercage, were adsorbed onto HY(400) and the NMR spectra were recorded. The spectra are presented in Figs. 37-41. Results are tabulated in Table II. Only methyl and ethyl alcohols yield spectra which contain a "splitting" that is indicative of interaction with two distinct sites. The ^{13}C resonances of the remaining alcohols are only slightly displaced from their corresponding liquid-state spectra, whereas the second alpha carbon resonance of methyl and ethyl alcohols is relatively strongly shifted from the liquid state value (by 6.7 ppm and 11.7 ppm, respectively).

There does appear to be a steric restriction on interaction with one of the sites in the zeolite. Interaction with this site produces a relatively large perturbation of the chemical shift. This steric

Fig. 37. ^{13}C CPMAS spectrum of 12.9% (by weight) ethanol on HY(400).

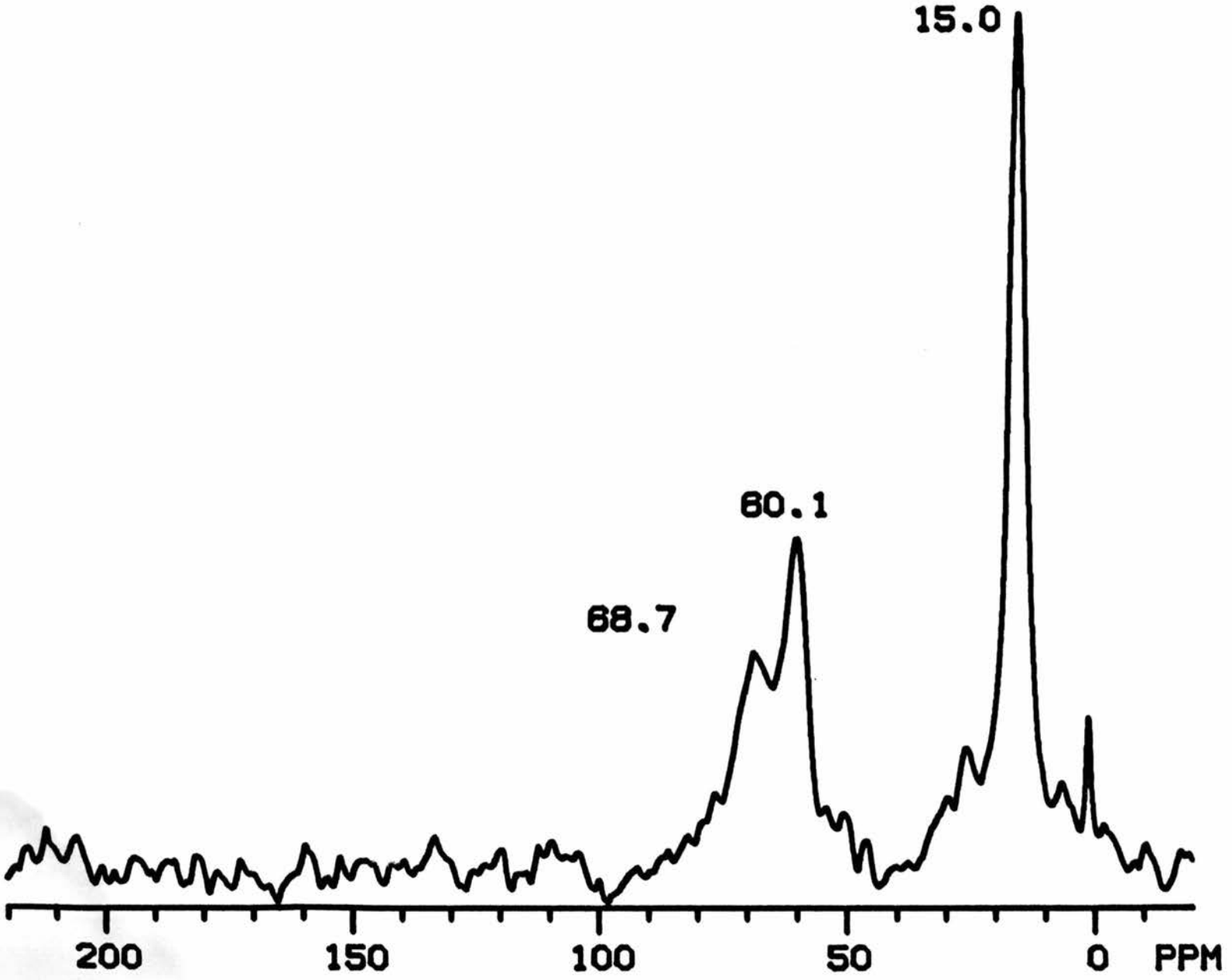
15.0
60.1
68.7
200
150
100
50
0
PPM

Fig. 38. ^{13}C CPMAS spectrum of 5.7% (by weight) n-propanol on HY(400).

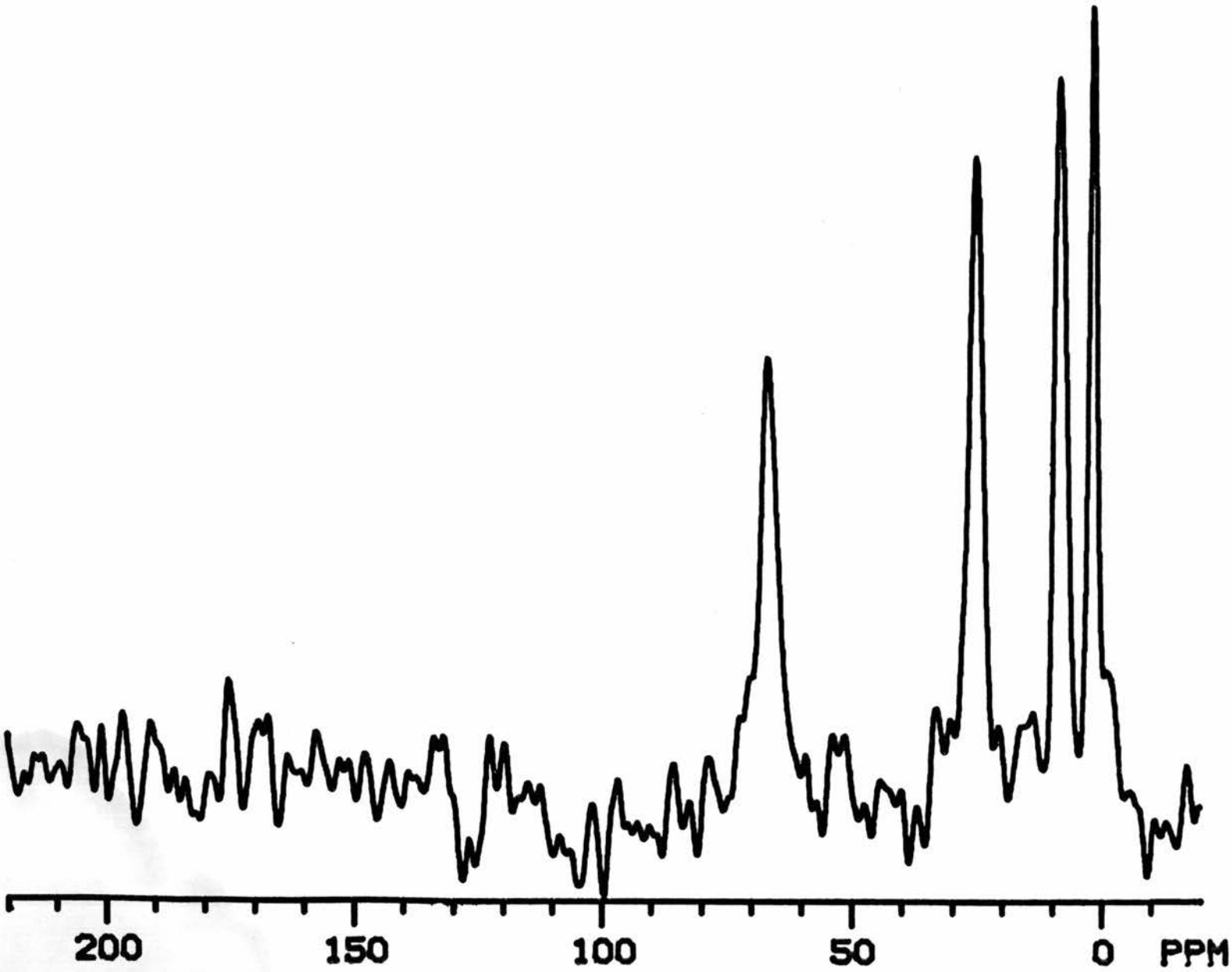
200
150
100
50
0
PPM

Fig. 39. ^{13}C CPMAS spectrum of 8% (by weight) isobutyl alcohol on HY(400).

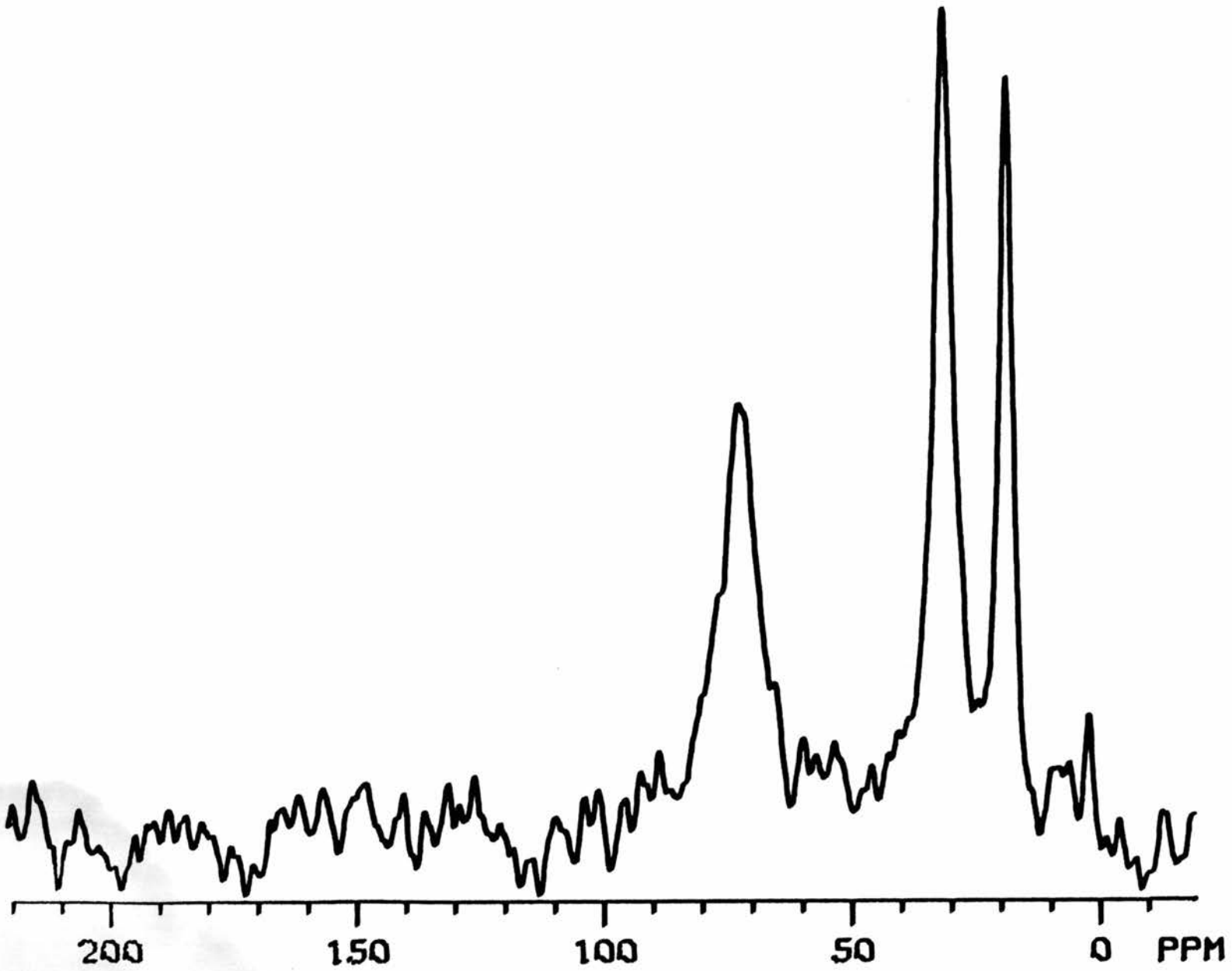
200
150
100
50
0
PPM

Fig. 40. ^{13}C CPMAS spectrum of 11.9% (by weight) sec-butyl alcohol on HY(400).

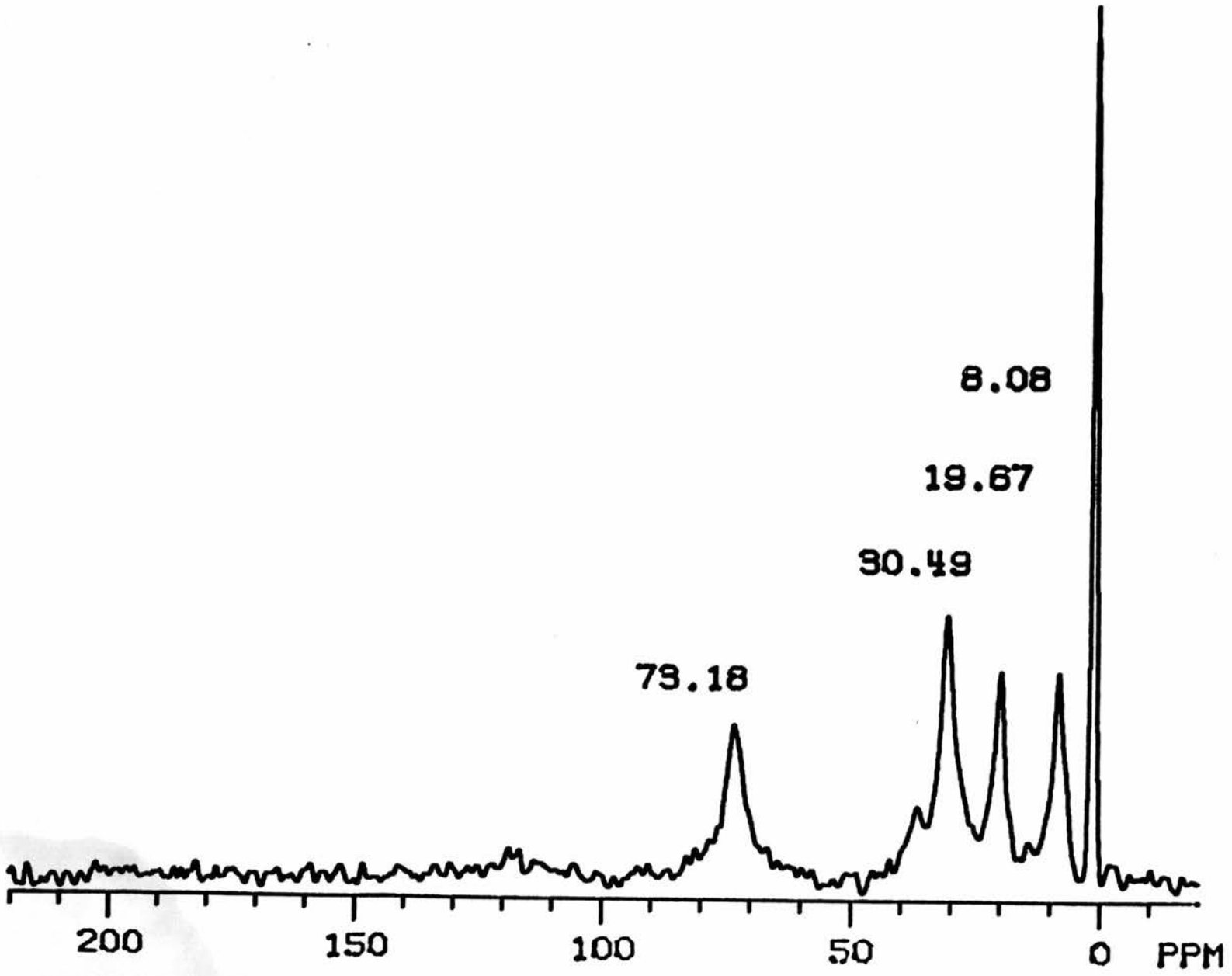
8.08
19.67
30.49
73.18
200
150
100
50
0
PPM

Fig. 41. ^{13}C CPMAS of 12% (by weight) n-butyl alcohol on HY(400).

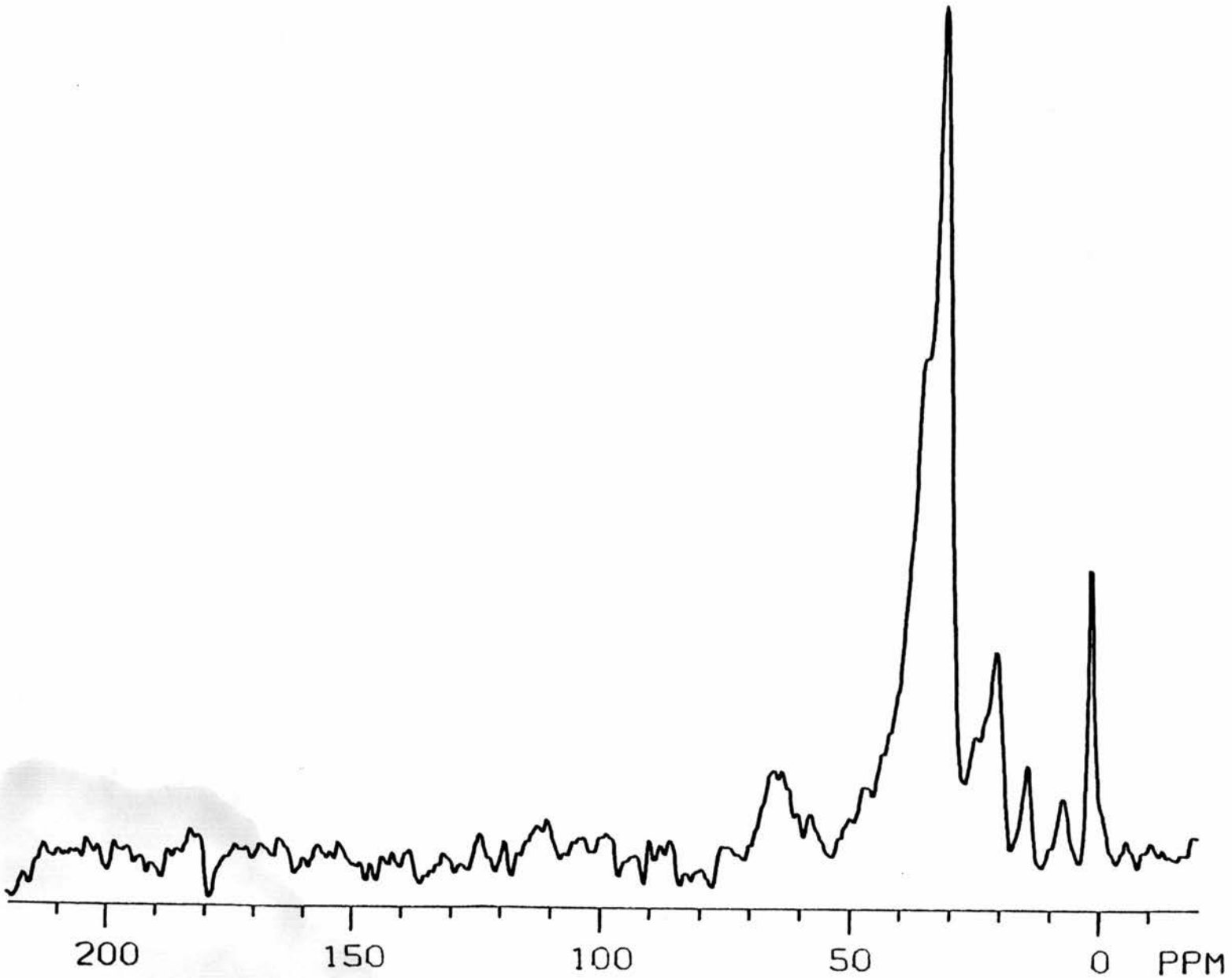
200
150
100
50
0
PPM

Table II. ^{13}C Chemical Shifts (ppm from TMS) of several alcohols on HY(400).

	C1	C2	C3	C4
Methanol	55.7 (+6.4)[a] 50.1 (+0.8)			
Ethanol	68.7 (+11.4) 60.1 (+2.8)	15.0 (-2.9)		
1-Propanol	66.6 (+2.7)	24.9 (-1.20)	8.08 (-2.12)	
2-Propanol	23.8 (-1.6)	67.3 (+3.6)		
2-Butanol	19.67 (-3.23)	73.18 (+4.2)	30.49 (-1.8)	8.08 (-2.1)
Isobuanol	71.67 (+2.5)	29.77 (-1.3)	19.77 (-0.6)	

[a]Difference in ppm from values for pure liquids gives in parenthesis.

Fig. 42. Pulse sequence for the two-dimensional spin-exchange experiment.

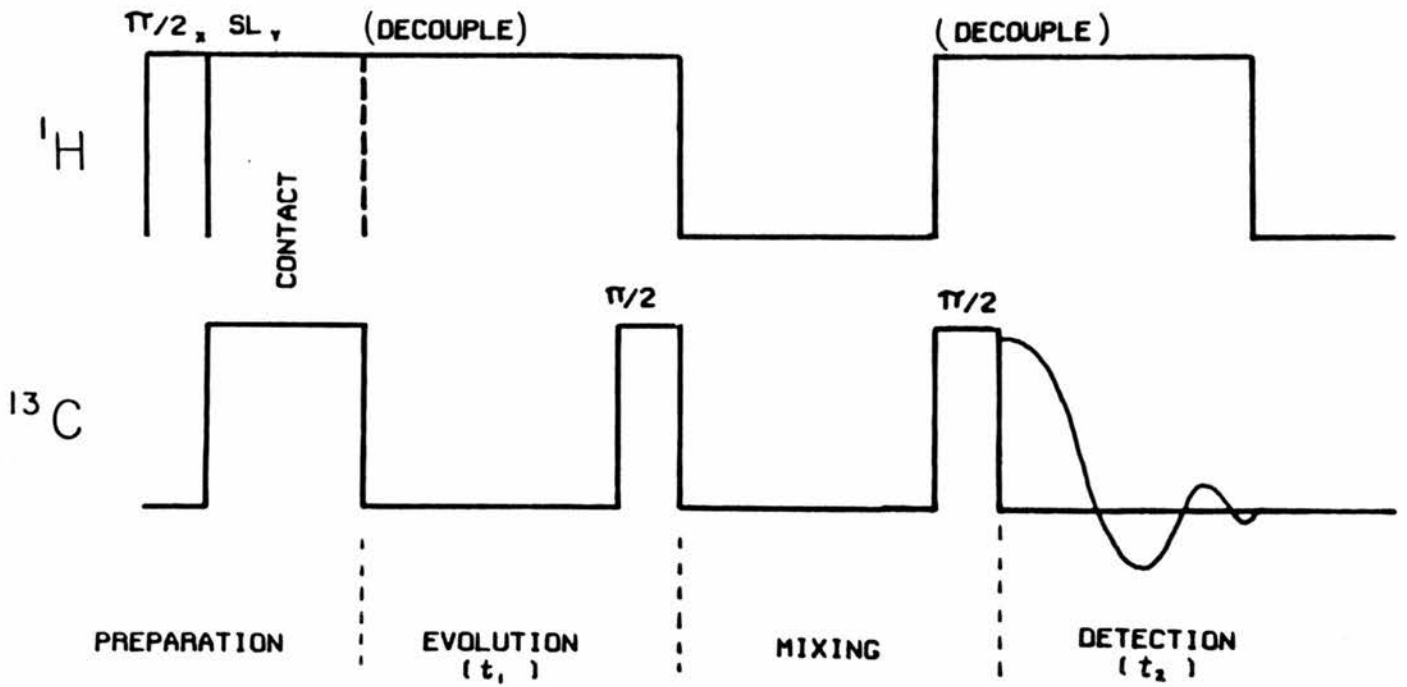
π/2 x SL y
(DECOUPLE)
(DECOUPLE)
^{1}H
CONTACT
π/2
π/2
^{13}C
PREPARATION
EVOLUTION
(t1)
MIXING
DETECTION
(t2)

restriction is inconsistent with this site's being an external site. The steric restriction also does not appear to originate from closely paired sites. Whereas one would expect the closely paired molecules to be those showing signs of proton-proton dipolar coupling, it is the more strongly shifted of the two resonances that is limited to smaller molecules. In methanol it is this species that is isolated from proton-proton coupling. The possibilities of the interaction of methanol with a Lewis site and of adsorption of methanol into the beta cage are not inconsistent with these data.

5.8.2. Chemical exchange.

An experiment was next performed to determine the presence or absence of chemical exchange between the various components of the system. On the basis of the separate measured T_1 values of the mobile and immobile species (see sec. 5.2), it is known that exchange between the two types of molecules is too slow to effect the cross-polarization process in the CPMAS experiment.

A non-spinning two-dimensional spin exchange experiment provides complete information on the possible spin exchange processes.[84] In this experiment (pulse sequence given in Fig. 42) the CP signal is generated using a fairly short contact time of 100 us in order to favor intensity from the bound species at 55.7 and 50.1 ppm, which will be spread out over a powder pattern. If during the mixing time the molecules generating a particular spin isochromat reorient or migrate to another site, there will be a correlation between the relevant resonance frequencies in the evolution and detection periods. This kind of correlation appears in the two-dimensional Fourier transform as off-diagonal intensity. This situation is indicated schematically in Fig.

Fig. 43. Illustration of the type of correlation expected for a system undergoing orientational exchange.

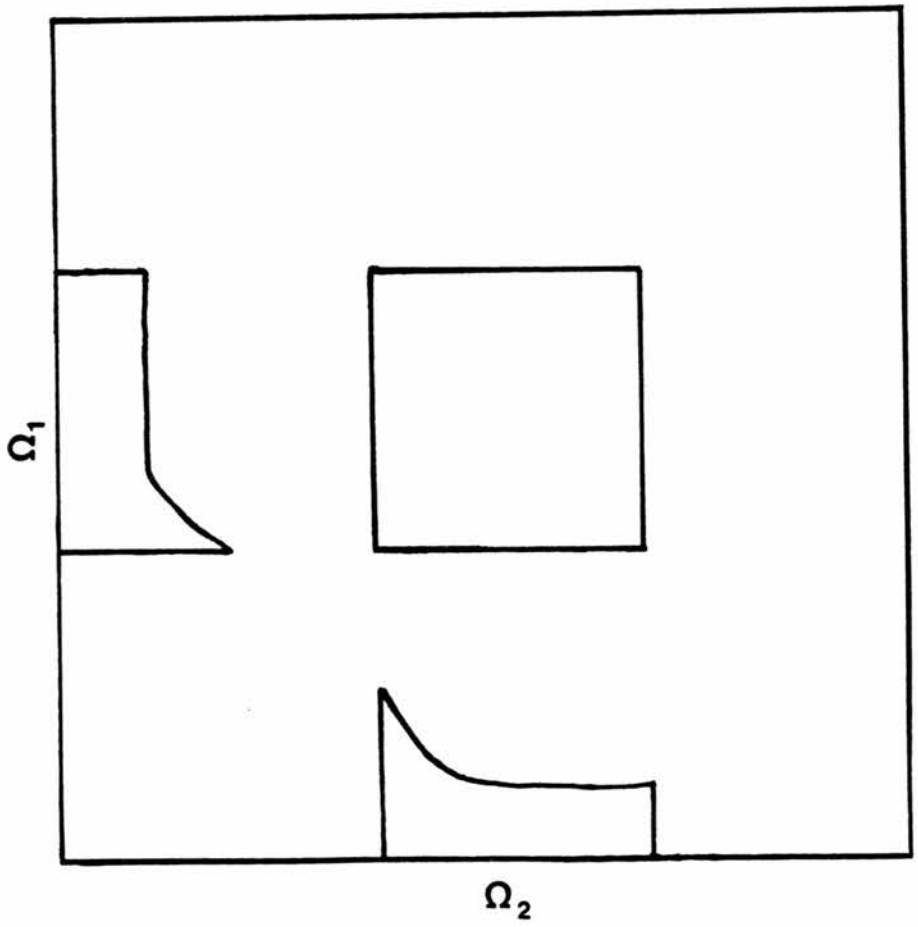
Ω_1
Ω_2

43. The experiment could also reveal exchange between bound and mobile species as a mapping of the powder pattern into the isotropic peak of the mobile species and vice versa.

The spectrum in Fig. 44 is for a mixing time of 200 msec and shows no cross-peak intensity for any of the three resonances. Therefore, we conclude that the immobile species are rigidly attached to the framework over this period of time.

5.8.3. Loading level.

In order to determine whether the appearance and/or properties of the 56-ppm resonance are a function of the loading level of methanol in the zeolite, a sample of 22% by weight methanol on HY(400) was prepared. The CPMAS spectrum of this sample, shown in Fig. 45 is dominated by the signal arising from the mobile species at 50.1 ppm. If the 56-ppm resonance is present in this sample and remains inhomogeneously coupled to its methyl protons, then the proton-coupled CPMAS spectrum will contain dipolar spinning sidebands. As shown in Fig. 46, this is the case, and we can conclude that it is not the presence or absence of the mobile species that determines the nature of dipolar coupling in the 56-ppm species.

In another set of experiments the role of the mobile species in determining spin diffusion in the second bound species was explored. Both the routine CPMAS and rotationally-synchronized interrupted-decoupling experiments were performed on a sample that was evacuated at progressively higher temperatures. If ^{1}H spin diffusion in the immobile 50-ppm species occurs with the mobile species, then removal of the mobile species should result in the formation of rotational dipolar

Fig. 44. Two-dimensional exchange spectrum for the HY(400)/10%MeOH sample obtained with a 200 ms mixing time.

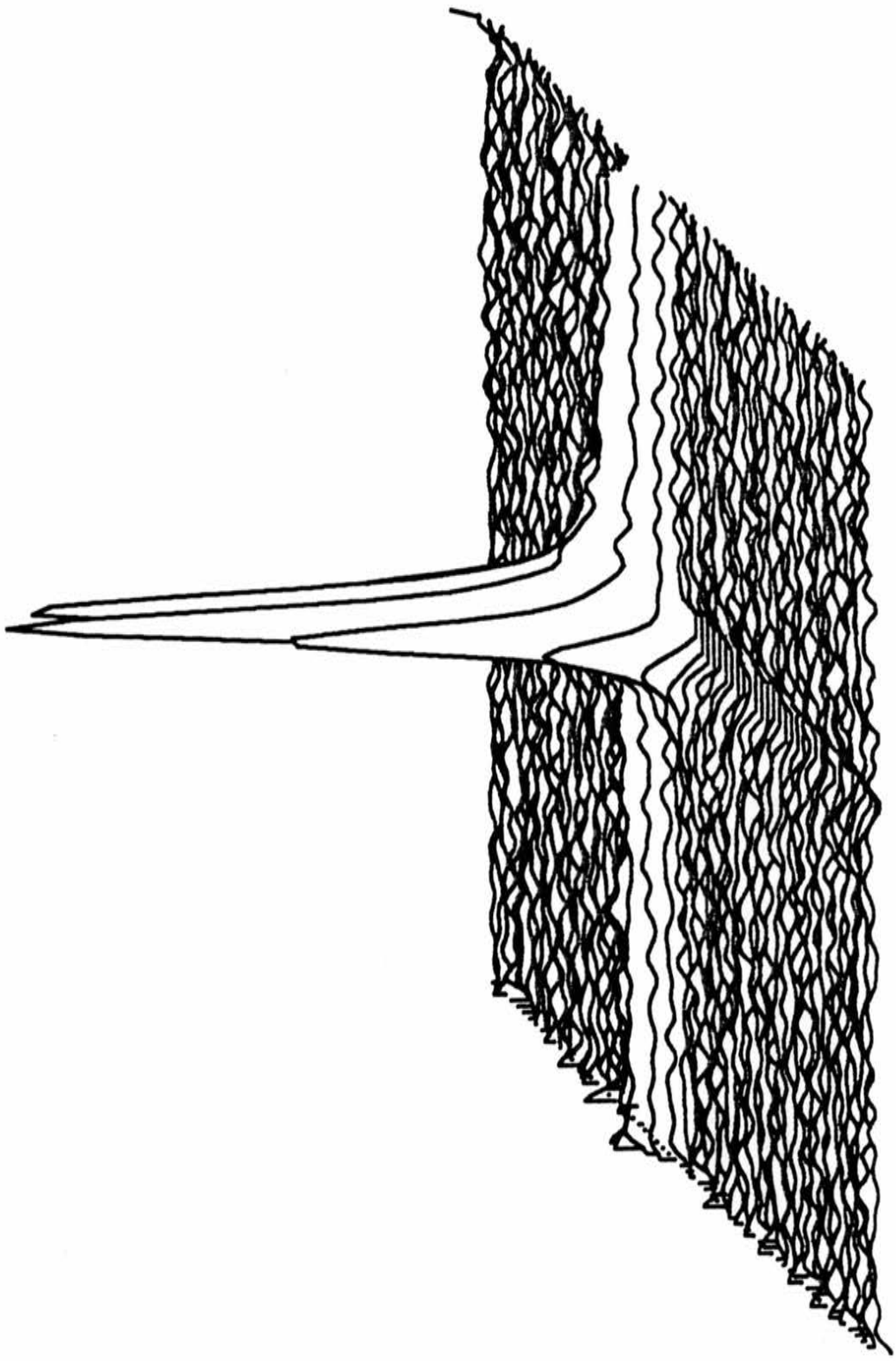

Fig. 45. ^{13}C CPMAS spectrum of 22% methyl alcohol (by weight) on HY(400).

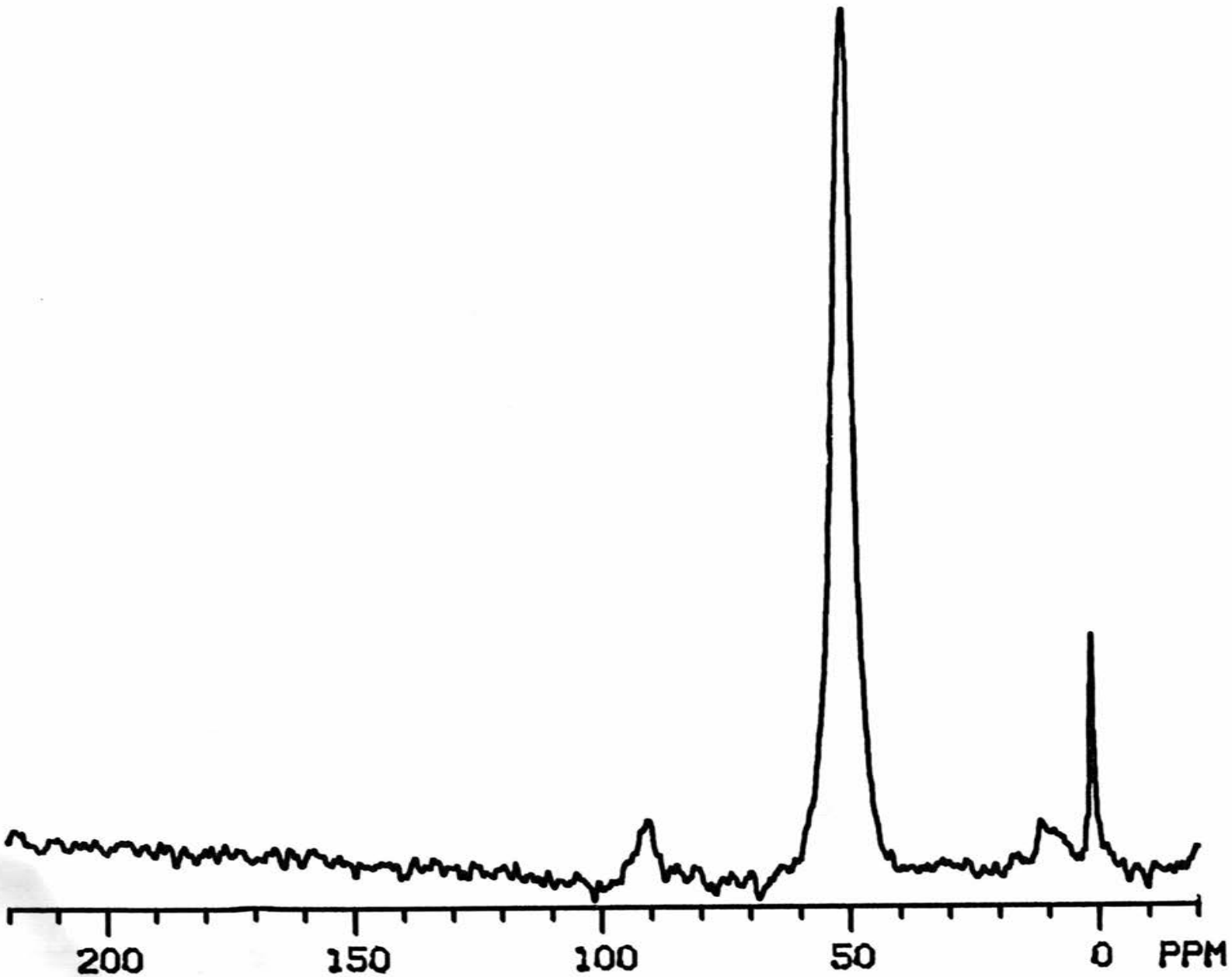
200
150
100
50
0
PPM

Fig. 46. ^{1}H-coupled ^{13}C CPMAS spectrum of 22% methyl alcohol (by weight) on HY(400).

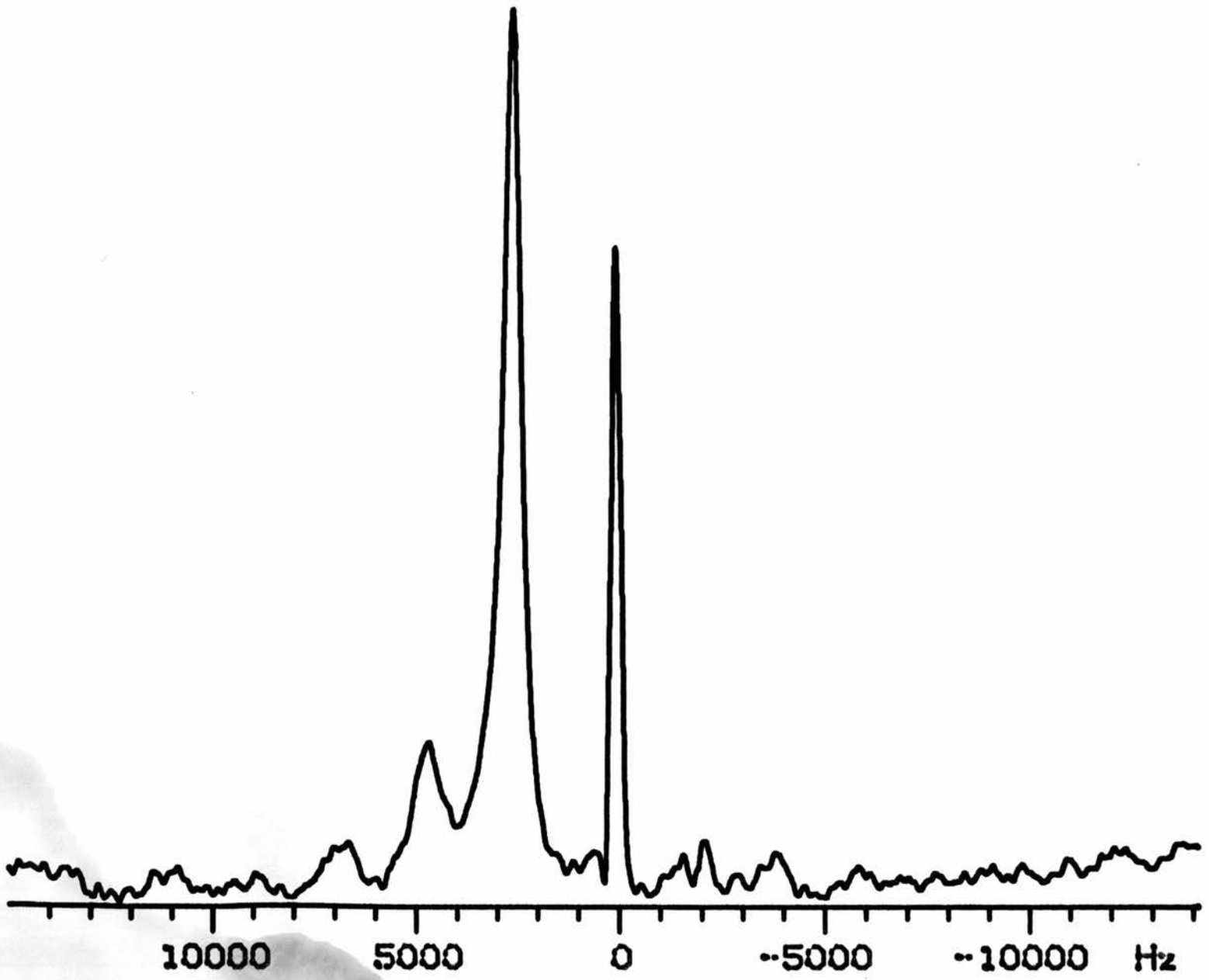
10000
5000
0
-5000
-10000
Hz

echoes. Removal of the mobile material may also allow resolution of the signal due to the immobile species in the 50-ppm region.

The original sample containing 10% methanol by weight was evacuated for 12 hr at 40°C, 90°C and 140°C, and the experiments performed at each stage. The results for the sample evacuated at 40°C are shown in Fig. 47. A slight rotational echo can be seen in the 50-ppm region, superimposed upon the unmodulated decay of the liquid-like resonance. The CP spectrum of the sample evacuated at 90°C is shown in Fig. 48. There is a newly resolved peak at 51.4 ppm which, as shown in Fig. 49, echoes in the rotationally-synchronized interrupted-decoupling experiment. The echo is hard to see, but real. By the fourth time interval of the experiment, the shoulder at 51.4 ppm can no longer be resolved from the 50-ppm line, but at the end of one rotor period it reappears.

Evacuation at 140°C results in the spectrum in Fig. 50. The 56-ppm resonance dominates. The other two resonances have been attenuated to such a degree that the interrupted-decoupling experiment cannot yield useable data over a reasonable experimental time span.

Evacuation at 40°C, as shown in Fig. 47, results in partially inhomogeneous behavior in the 50-ppm line. Further evacuation at 90°C results in the resolution of a signal at 51.4 pm (Fig. 48), which is seen to echo in the rotationally-synchronized interrupted-decoupling experiment (Fig. 49). These observations are consistent with a model in which proton spin-diffusion in the homogeneously coupled bound species (now identified as resonating at 51.4 ppm) occurs with mobile methanol. As the mobile methanol is removed by evacuation, the spin-diffusion rate decreases and rotational echoes are observed in the 51.4-ppm resonance.

Fig. 47. Evolution of the ^{13}C magnetization of a sample evacuated at 40°C under a rotationally-synchronized interrupted-decoupling experiments.

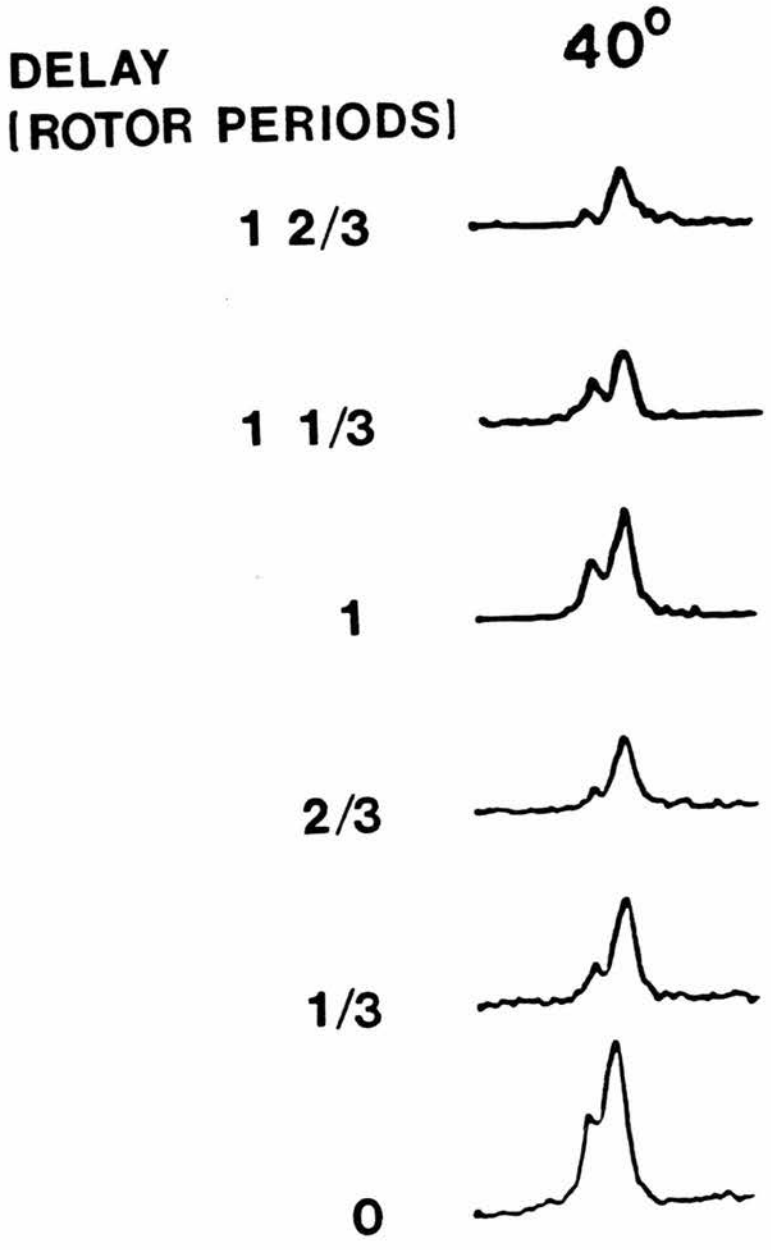
40°
DELAY
(ROTOR PERIODS)
1 2/3
1 1/3
1
2/3
1/3
0

Fig. 48. ^{13}C CPMAS spectrum of methanol on HY(400) after evacuation at 10^{-6} microns at 90°C for 12 hr.

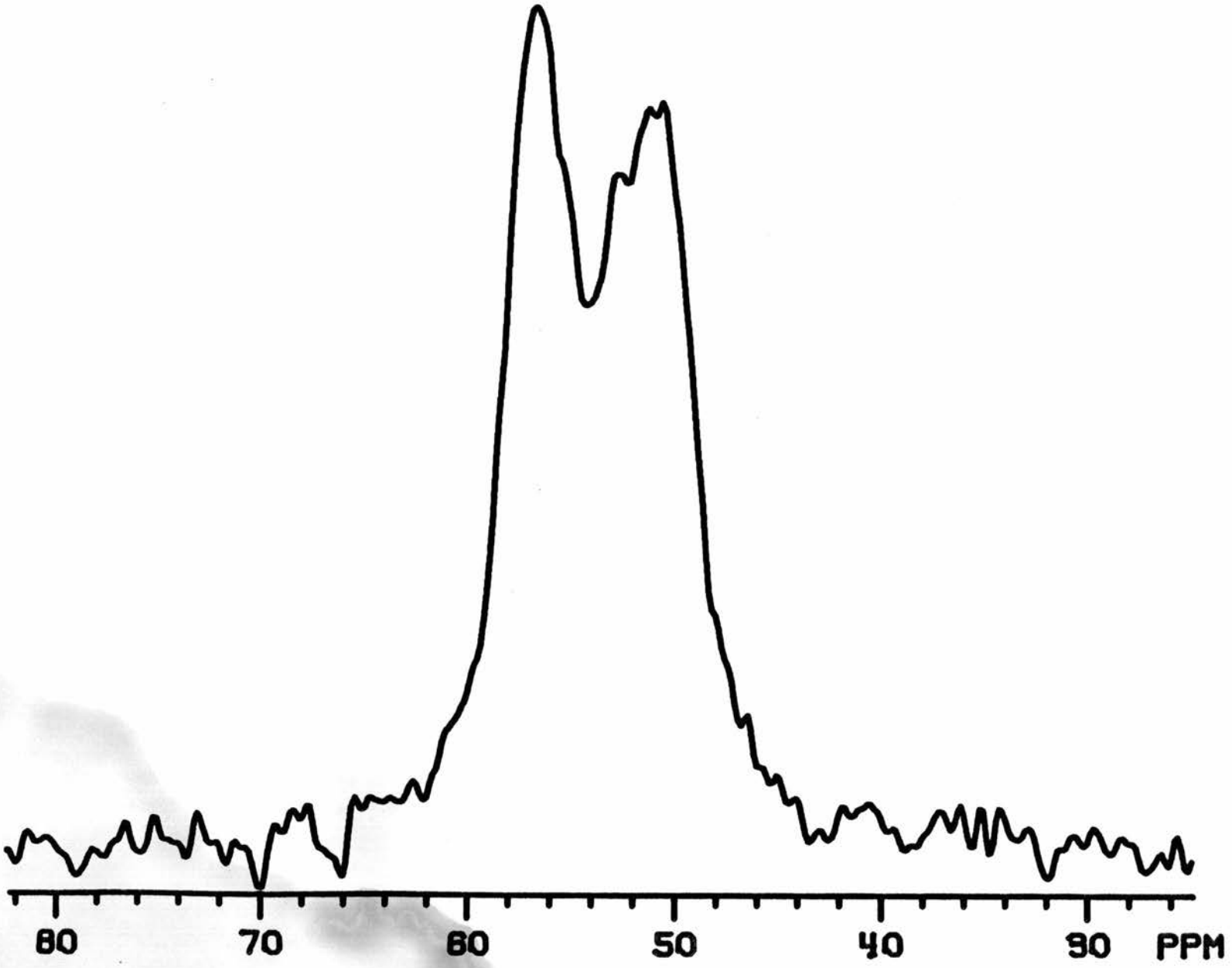
80
70
60
50
40
30
PPM

Fig. 49. Results of a rotationally-synchronized interrupted-decoupling experiment on a sample of methanol on HY(400) evacuated at 10^{-6} torr at 90°C for 12 hr.

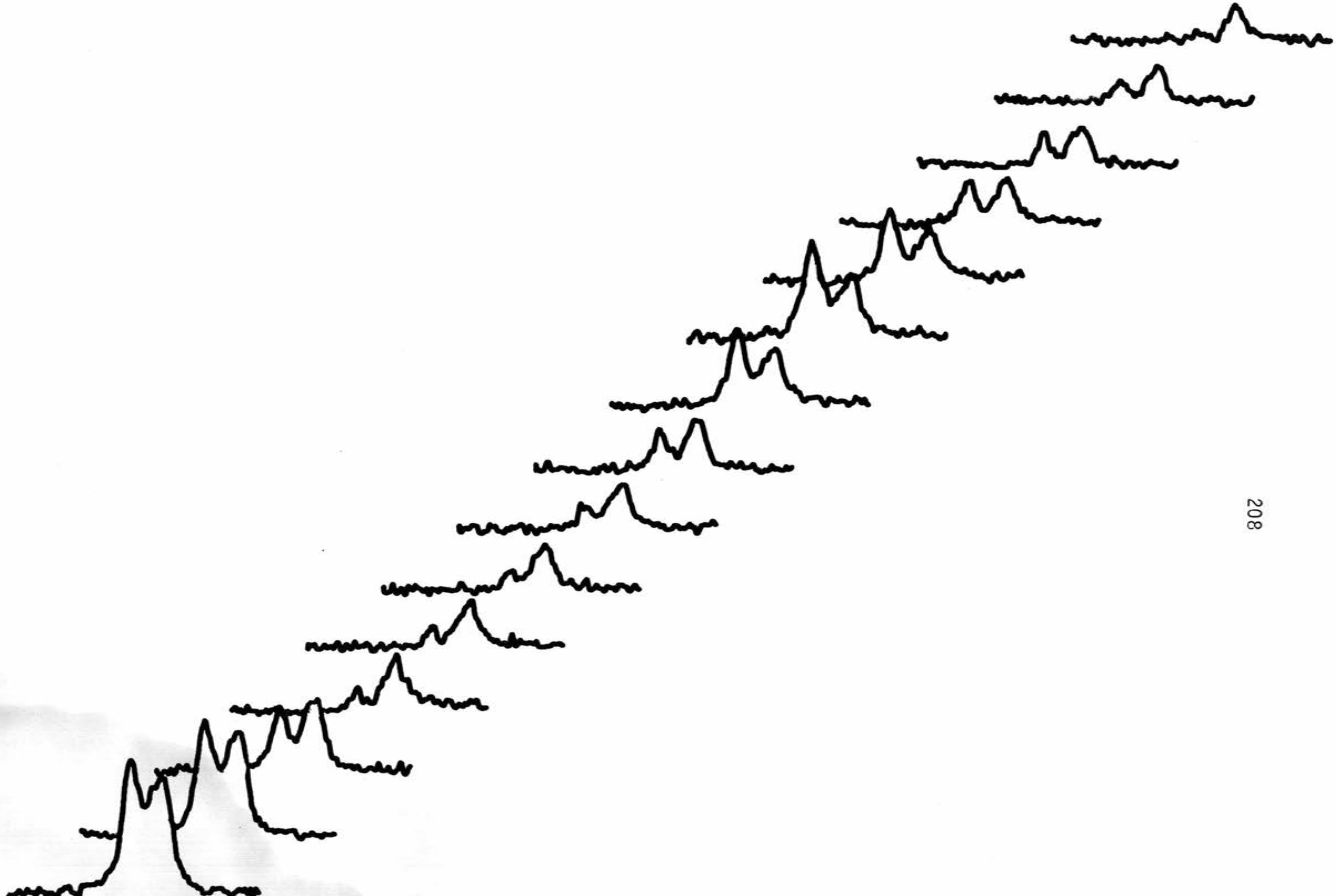

Fig. 50. ^{13}C CPMAS spectrum of a sample of methanol on HY(400) evacuated at 10^{-6} micron at 140°C for 12 hr.

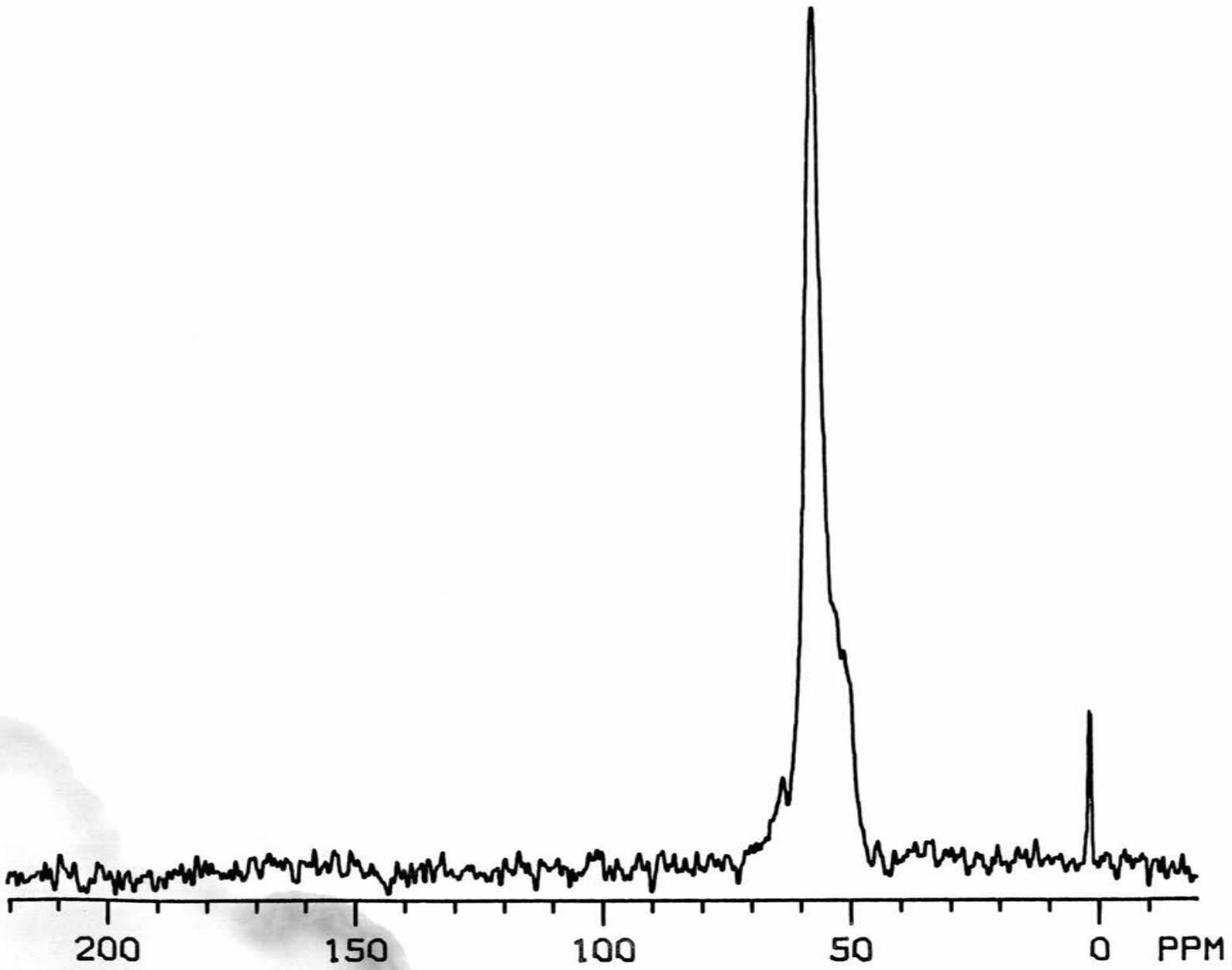
200
150
100
50
0
PPM

5.8.4. Effect of activation temperature.

As NH_4Y is heated beyond 400°C, the number of Lewis acid aluminum sites should increase as framework dehydroxylation proceeds (see sec. 1.4.1.). Activation at temperatures much below 400°C should strongly favor Bronsted sites. If the spectra of HY/MEOH are due to a mixture of these two types of sites, then samples prepared at different activation temperatures should reflect the changing distribution of these sites in the relative ^{13}C intensities observed. Accordingly, samples of NH_4Y were activated at 300°C, 500°C and 600°C and loaded with methanol.

The CPMAS spectra of methanol adsorbed onto these samples are shown in Figs. 51-54. The notable feature of this series is the loss of the resonance at 56 ppm in the spectra of samples activated at 500°C and 600°c. The non-spinning spectrum of methanol on HY(500) (Fig. 53) contains a powder pattern characteristic of immoble species. This is also confirmed by the presence of weak spinning sidebands in the CPMAS spectra of methanol on HY(500) and HY(600) in Figs. 52 and 54.

From these results we conclude that either the site associated with the 56-ppm resonance has been destroyed in the activation, or access of methanol to the site is denied as a result of structural change within the zeolite. It has been observed that activating NH_4Y at temperatures above 400°C results in the removal of some aluminum from the framework (see section 1.4.1). In the initial stages of this dealumination process the extra-lattice aluminum cations are thought to

Fig. 51. ^{13}C CPMAS spectrum of HY(300)/5%MeOH.

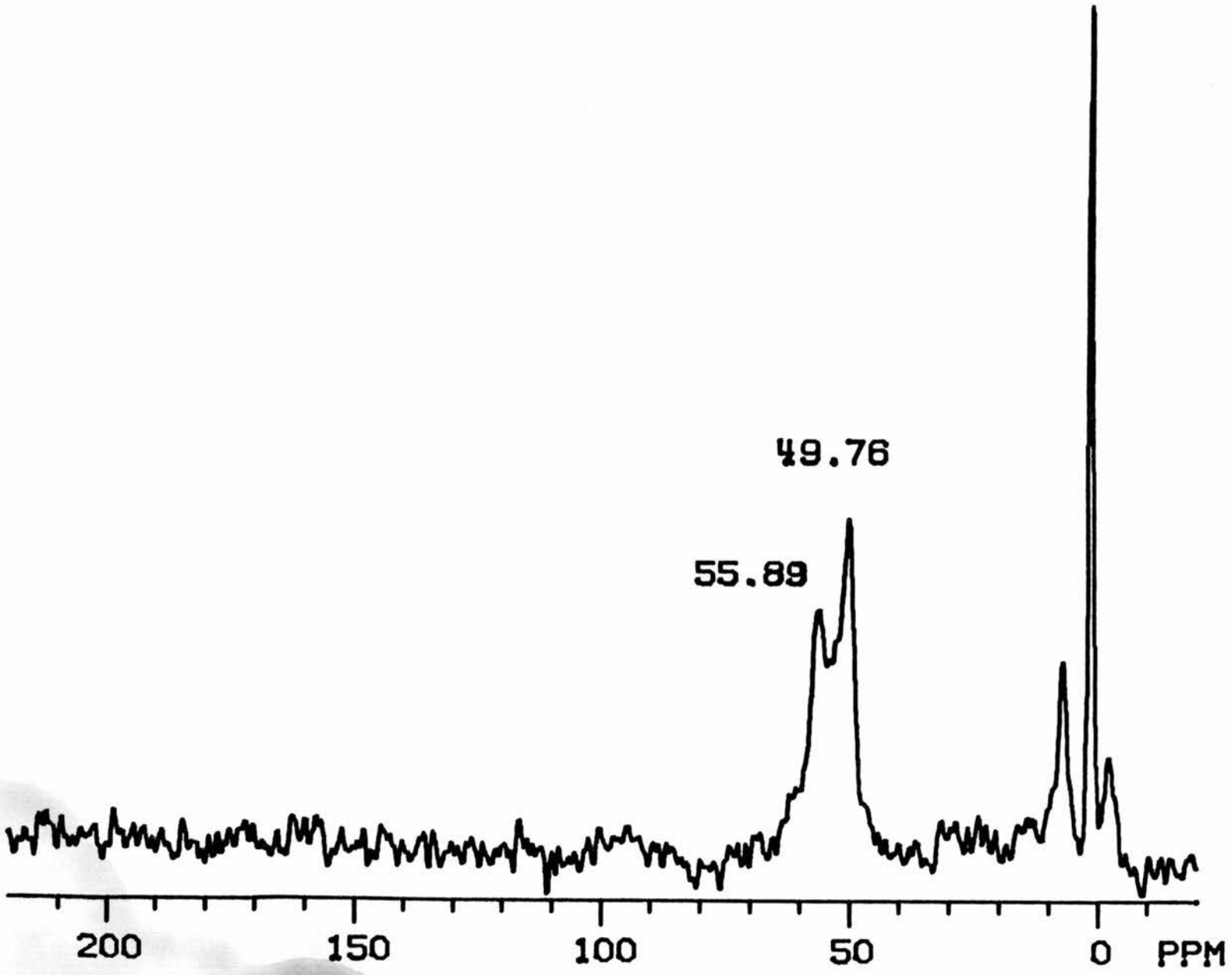
49.76
55.89
200
150
100
50
0
PPM

Fig. 52. ^{13}C CPMAS spectrum of HY(500)/8% MeOH.

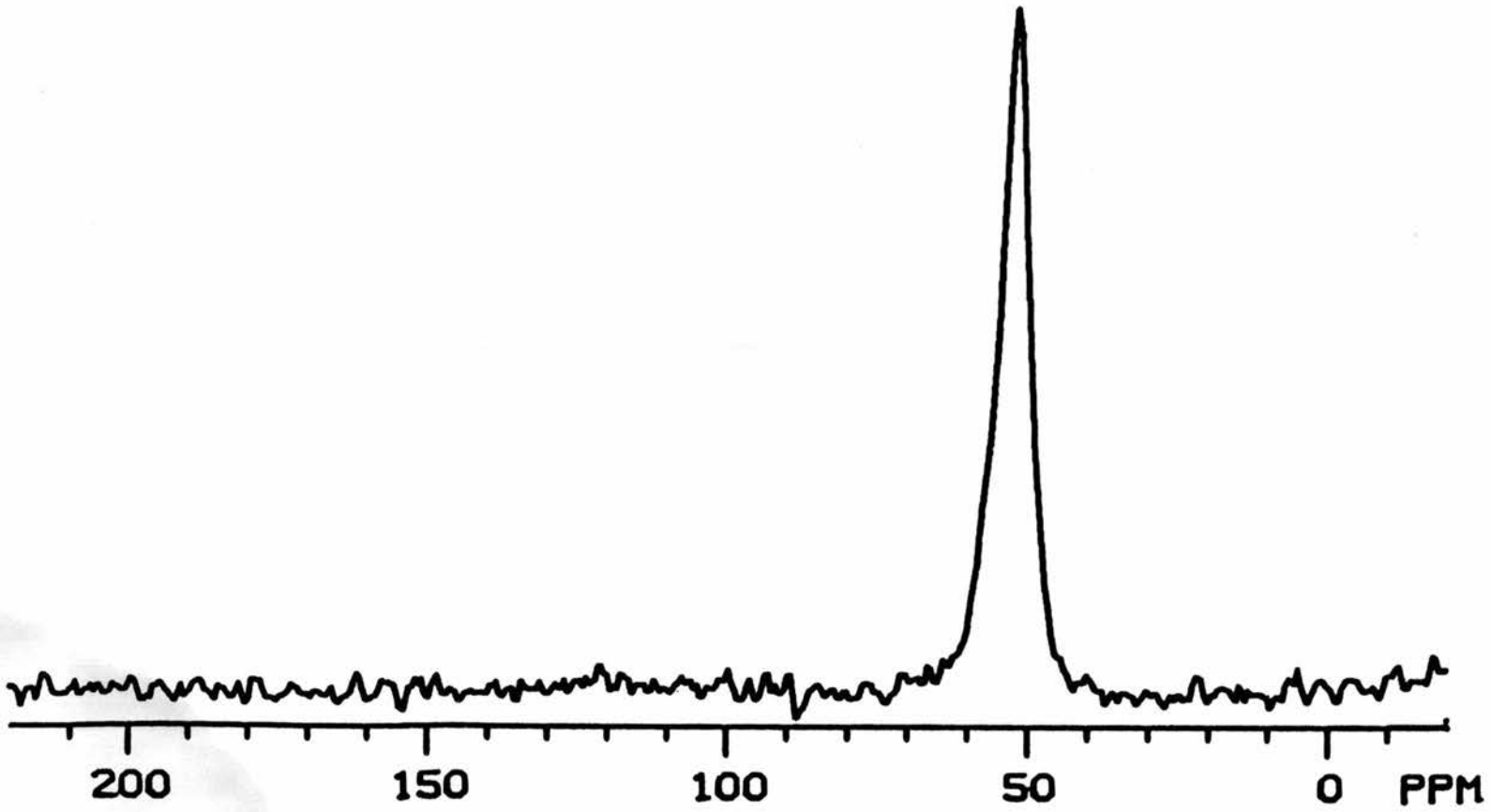
200
150
100
50
0
PPM

Fig. 53. Non-spinning ^{13}C CP spectrum of HY(500)/8% MeOH. A chemical shift anisotropy powder pattern is displayed as well as a motionally narrowed resonance.

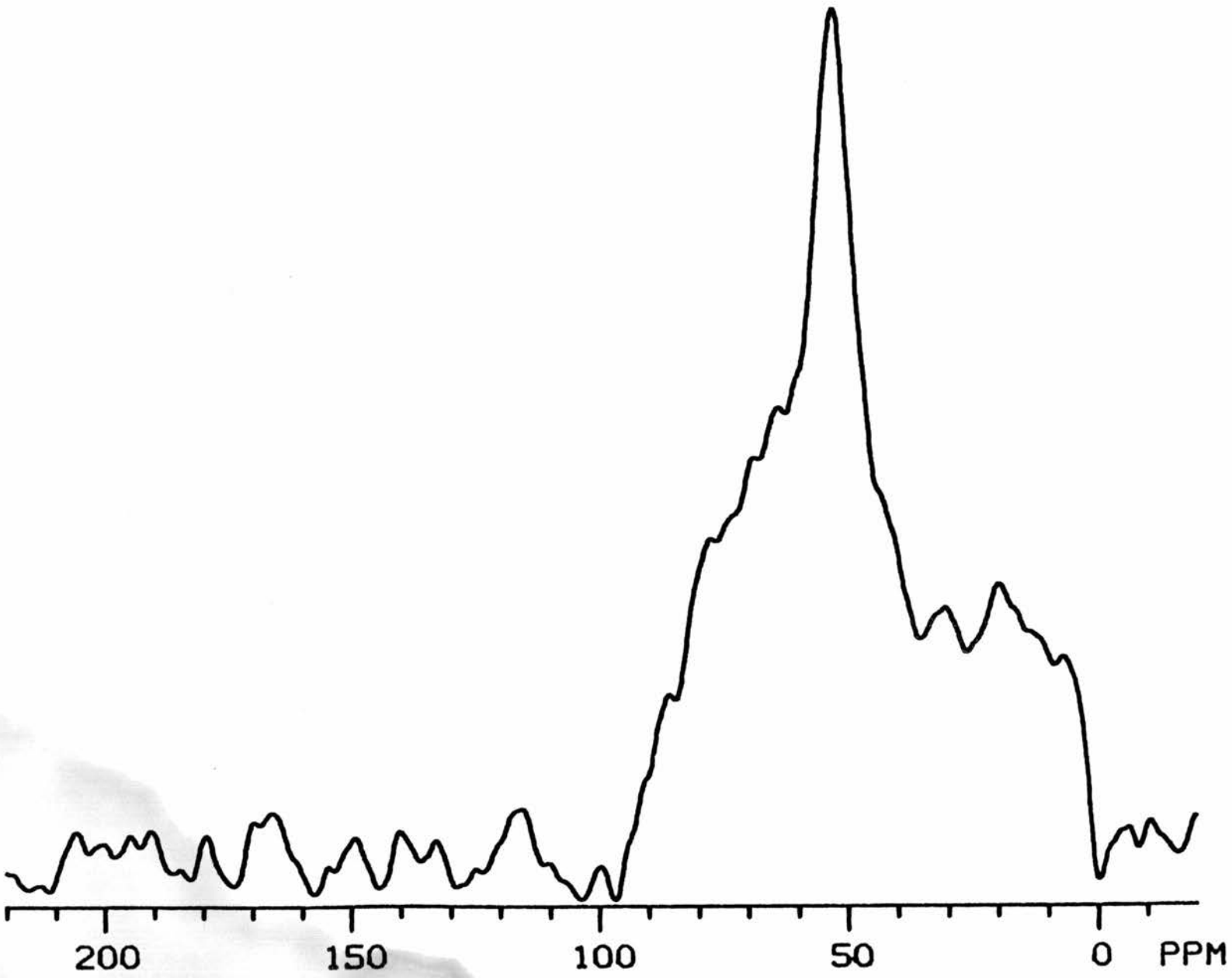
200
150
100
50
0
PPM

Fig. 54. ^{13}C CPMAS spectrum of HY(600)/11.2% MeOH.

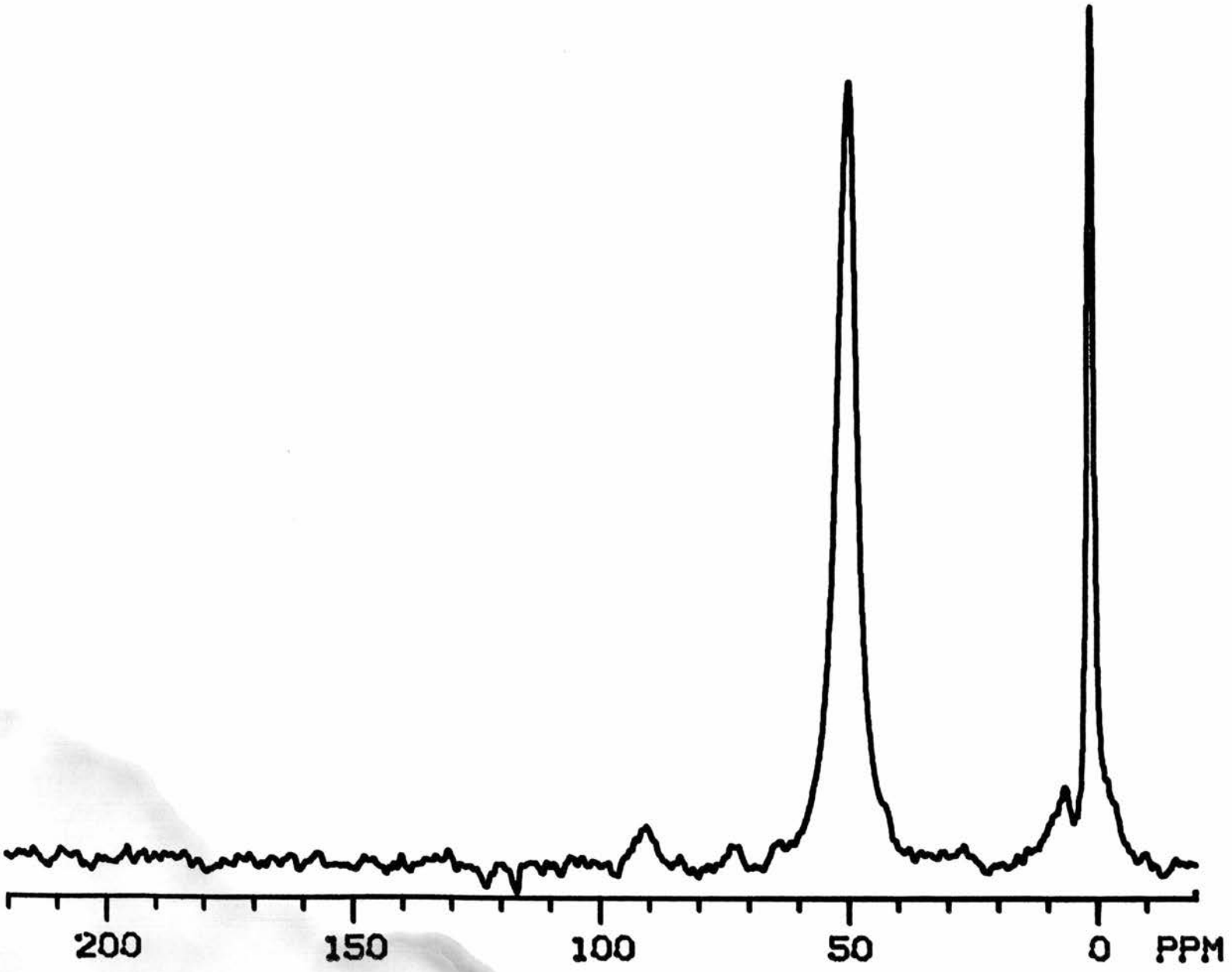
200
150
100
50
0
PPM

Fig. 55. ^{13}C CPMAS spectrum of HY(600)/11.2% MeOH after evacuation at torr at 90°C for 12 hr.

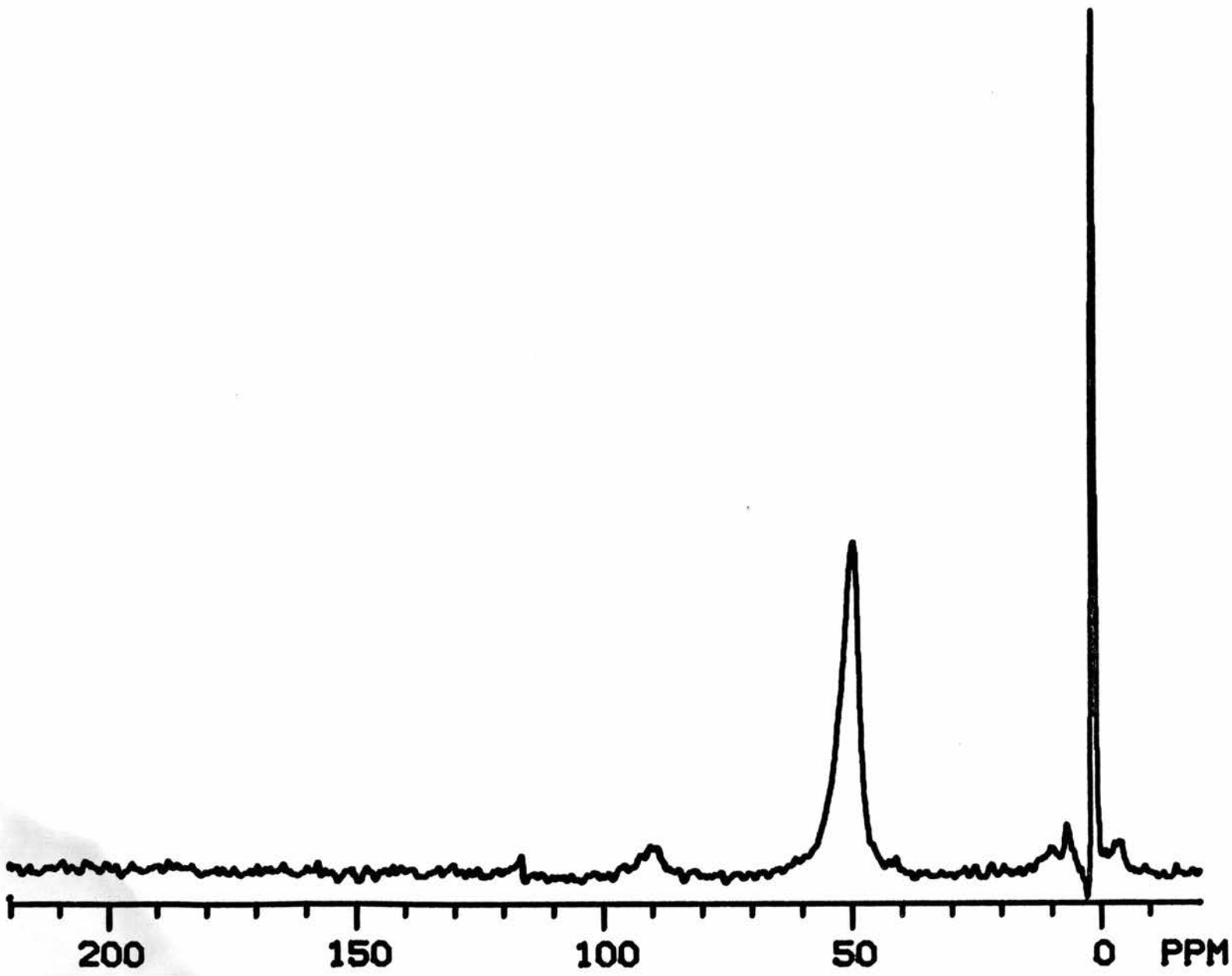
200
150
100
50
0
PPM

reside predominantly in the β cages.[84] Adsorbtion of methanol into the β cage would presumably be blocked by the presence of aluminum cations.

5.9. Discussion.

The experimental results discussed above provide sufficient data for a consistent description of the methanol/HY system. The greatest difficulty in this description lies in the identification of the two "solid-like" species, both of which could in principle be due to interaction with Bronsted or Lewis sites or the product of a dehydration reaction with the framework. Either of these species may exist in the beta cage, supercage or both cages. The chemical shift is not a definitive diagnostic tool for such a problem. It would be very difficult to separate the effects of adsorption into different regions of the zeolite from the typically small changes in the chemical shift of the methyl carbon that one would expect for interactions with different acid functions or as a result of chemical reaction. Fortunately, the dynamics associated with the NMR signals prove to be informative.

The ^{13}C CPMAS spectra of HY(400)/MEOH at methanol loading levels of 15% and 30% by weight display a single peak at 50 ppm. The optimal contact time for observation of this peak is about two ms, and $T_{1\rho_C}$ is about 10 ms at room temperature. These values are not unusual for an organic solid. A variable temperature study of $T_{1\rho_C}$ yields an activation energy of 3.0 kcal/mole for the process responsible for the rotating-frame relaxation. This is in the range of hydrogen-bond energies.

At 10% (by weight) loading of methanol two more resonances can be detected. These are characterized by larger $T_{1\rho_C}$ and T_1 relaxation times, and display chemical shift anisotropy which suggests that these

resonances may correspond to less mobile species. A Bloch-decay spectrum of this sample proves that methanol exists predominantly as a mobile, liquid-like species. Only a fraction of the adsorbed material exists as the more slowly relaxing forms.

It isn't clear from the above pattern of data whether the dominant 50-ppm resonances in the CP and Bloch-decay spectra correspond to the same species. Intuitively one would suspect that they do not; the degree of mobility necessary to allow the resolution of J coupling in the Bloch-decay spectrum seems inconsistent with the relative ease of cross-polarization of the 50-ppm resonance in the CP spectra. An attempt to observe J coupling in the 50-ppm resonance in a CPMAS spectrum instead revealed an array of sidebands arising from inhomogeneous ^{13}C-^{1}H dipolar coupling. A rotationally-synchronized interrupted-decoupling experiment indicates that the three species have three types of dipolar coupling. The peak at 50 ppm is a superposition of a rapidly-decaying component, as occurs in the case of homogeneous dipolar coupling, and a slowly-decaying component that must correspond to the mobile species seen in the Bloch-decay spectrum. The species at 56 ppm echoes at the rotor frequency, which identifies it as the inhomogeneously coupled resonance.

From the 2D spin exchange experiment, we have seen that none of the species show any sign of chemical exchange with one another, nor do the immobile species undergo orientational exchange.

Evacuating the sample at 90°C allows the resolution of the second immobile species at 51.4 ppm and leads to the formation of rotational dipolar echoes in this species under the rotationally-synchronized interrupted-decoupling experiment. It is thus dipolar coupling between

the 51.4-ppm methanol and the mobile methanol that renders the dipolar coupling in the 51.4 ppm resonance homogeneous in the unevacuated sample.

Whereas the methyl protons of the bound species with resonance at 51.4 ppm are in dipolar contact with protons of mobile methanol, this is not the case for the 56-ppm species. This 56-ppm signal must correspond to methanol interacting with a site in the beta cage of the zeolite. Only methyl and ethyl alcohols, both with molecular volumes less than the approximately 120 A volume of the beta cage, display a separate low-shielding resonance that we believe to be characteristic of interaction with this second site. Activation at 500°C and above results in the loss of this signal from the NMR spectrum. Thus, it is not likely that this site is a Lewis site, because Lewis site concentration should be relatively high in samples activated at 500-600°C. On the other hand, Bronsted sites are not completely destroyed until activation temperatures above 600°C are reached.[88] However, it is known that activation in the 500°C to 600°C range does remove some aluminum from the framework and that some of the displaced aluminum resides in the beta cages, where it would block methanol from entering.

Proton spin-diffusion in the 51.4-ppm species occurs with mobile methanol. This fact demonstrates the existence of a static component of the ^{1}H-^{1}H dipolar coupling between the bound species at 51.4 ppm and the mobile species at 50.1 ppm. It follows that there is also a static ^{13}C-^{1}H dipolar coupling between these two species that allows for the cross-polarizaton of the mobile methanol molecules. Dipolar coupling to framework-attached protons will not be averaged to zero by motion of

the adsorbed methanol. The primary evidence for this mechanism is the slowing of proton spin-diffusion upon evacuation of the sample.

As mentioned earlier, heating HY/MEOH at 150°C results in the appearance of bands in the IR spectrum that have been assigned to the methoxysilane linkage.[89] Similar results have been obtained upon heating HX and H-mordenite loaded with methanol.[90] It is significant, then, that heating HY/MeOH did not result in the appearance of new ^{13}C resonances of solid-like species in this study. It must be that, if the earlier studies are correct, the methoxysilane linkage is already present in the samples prepared at room temperature in the current project, and is responsible for one or both of the resonances attributed to solid-like species. Apart from a chemical shift separation of 4.3 ppm, the differences between the two resonances can be interpreted by assigning the resonance at 55.7 ppm to species in the beta cage. It does not seem appropriate to propose separate chemical structures for the two species. There are no data to suggest that either resonance corresponds to interaction with Lewis sites. The most direct interpretation of the data is that the two resonances attributed to solid-like species correspond to the same general type of species and their chemical shift separation is a result of the different physical environments in which they are located, i.e., electric fields or solid-state "solvent effect". Both the solid-like species must be methoxysilane units. This leaves unresolved the question of the origin of the differing chemical shifts. The author attempted a magic-angle flipping experiment, which would have given the CSA powder pattern of both species,[91] but the results were poor due to limited signal strength.

Finally, evacuation at 140°C was seen to remove species adsorbed in the supercage, but not those in the beta cage. Desorption in this temperature range and higher has been reported to result in the evolution of dimethyl ether as a primary decomposition product of methanol on several H-zeolites.[92]

The formation of dimethyl ether requires the combination of two methanol molecules:

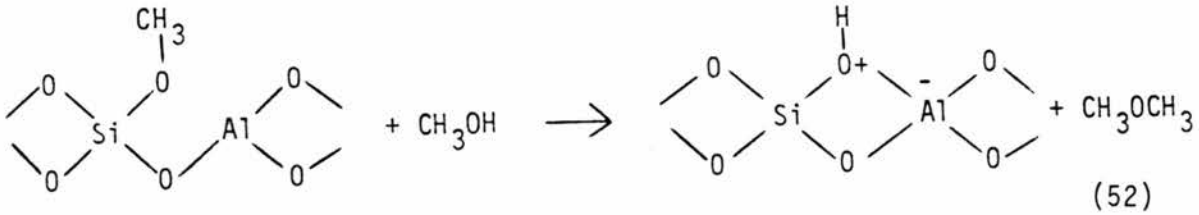

(52)

Methoxysilane groups located in beta cages are retained upon heating at 140°C, because free methanol is excluded from the beta cage and is thus unavailable for this reaction. On the basis of this observation, it is likely that the methoxysilane linkage observed via IR spectroscopy after heating is predominantly due to species in the beta cage.

CHAPTER 6

FINAL REMARKS

The work in this part has demonstrated the utility of solid-state ^{13}C NMR techniques for the study of species adsorbed onto activated catalysts. The dipolar coupling has in particular been found useful in the analysis of HY/MEOH. Finally, there is also great potential in the application of the Combined Rotation and Multiple-Pulse Spectroscopy (CRAMPS)[93] to zeolites and other acidic surfaces. With this technique one is able to obtain relatively high-resolution spectra of the protons in the zeolite,[94] which are the catalytically active species.

REFERENCES

1. D.W. Breck, "Zeolite Molecular Sieves: Structure Chemistry and Uses". John Wiley and Sons, New York, 1974.
2. D. Barthomeuf, ACS Symposium Series V40 p. 453, American Chemical Society, Wash., D.C. 1977.
4. a. D. Freude, T. Frolich, M. Hunger, H. Pfiefer and G. Scheler, Chem. Phys. Lett., 98, 263 (1983).

   b. H. Pfeifer and H. Schmiedel, J. Colloid Interface Sci., 85, 502 (1982).

   c. P.A. Jacobs and H.K. Beyer, J. Phys. Chem., 83, 1174 (1979).
5. See ref. 1.
6. "Intrazeolite Chemistry", G.D. Stuckey and F.G. Dwyer eds., ACS Symposium Series, v. 128, American Chemical Society, Washington, D.C., 1983.
7. "The Properties and Applications of Zeolites", Chemical Society Special Publications L33, The Chemical Society, Burlington House, London, 1980.
9. I.E. Maxwell, Adv. Catal., 31, 2 (1982).
10. M.L. Poutsma in "Zeolite Chemistry and Catalysis" A.C.S. Monograph 171, p. 437, American Chemical Society, Washington, D.C., 1980.
11. P. Dejaifev, J.C. Vedrine and E.G. Derouane, J. Catal., 63, 331.
12. S.M. Csicsery in "Zeolite Chemistry and Catalysis", A.C.S. Monograph 171, 180. American Chemical Society, Washington, D.C., 1980.

13. See ref. 1.

14. D.J. Barthomeuf and R. Beaumont, J. Catal., 26, 218 (1972).

15. C.V. McDaniel and P.K. Mather in "Zeolite Chemistry and Catalysis", A.C.S. Monograph 171, p. 285, American Chemical Society, Washington, D.C. 1975.

16. See ref. 1.

17. L.V.C. Rees and C.J. Williams, Trans. Faraday Soc., 61, 1481 (1965).

18. See ref. 2.

19. D.H. Olson and E. Dempsey, J. Catal., 13, 221 (1969).

20. R.L. Stevenson, J. Catal., 21, 113 (1971).

21. T.R. Hughes and H.M.J. White, J. Phys. Chem., 71, 2192 (1967).

22. J.W. Ward and R.C. Hansford, J. Catal., 13, 364 (1969).

23. See ref. 19.

24. A.P. Bolton and M.A. Lanewala, J. Catal., 18, 154 (1970).

25. G.T. Kerr, J. Phys. Chem., 71, 4155 (1967).

26. See ref. 1.

27. G.T. Kerr, J. Catal., 15, 200 (1969).

28. R. Beaumont and D.J. Varthomeuf, J. Catal., 27, 45 (1972).

29. H. Lechert, Catal. Rev. Sci. Eng., 14, 1 (1976).

30. H. Lechert and K.P. Wittern, Ber. Bunsenges. Phys. Chem., 82, 1054 (1978).

31. H. Pfeifer, Phys. Reports, 26, 1107 (1976).

32. H. Pfeifer, NMR: Basic Principles and Progress, v. 7, p. 53, Springer-Verlag, New York, 1972.

33. E.O. Stejskal and J.E. Tanner, J. Chem. Phys., 42, 288 (1965).

34. H. Lechert and P.K. Wittern, Ber. Bunseges. Phys. Chem., 82, 1054 (1978).

35. H.A. Resing, Advan. Mol. Relax. Proc., 3, 199 (1972).

36. D. Michel and H. Pfeifer, J. Magn. Reson., 45, 30 (1981).

37. J. Klinowski, Prog. NMR Spectroscopy, 16, 237 (1984).

38. G.E. Maciel, J.F. Haw, I-S. Chuang, B.L. Hawkins, T.A. Early, D.R. McKay and L. Petrakis, J. Am. Chem. Soc., 5529 (1983).

39. D. Freude, M. Hunger, H. Pfeifer, Chem. Phys. Lett., 91, 307 (1982).

40. R. Eckman and A.J. Vega, J. Am. Chem. Soc., 105, 4842 (1983).

41. J.F. Haw, I-Ssuer Chuang, B.L. Hawkins and G.E. Maciel, J. Am. Chem. Soc., 105, 7206 (1983).

42. W.P. Rothwell, W.X. Shen and J.H. Lunsford, J. Am. Chem. Soc., 106, 2452 (1984).

43. R.A. Wind, F.E. Anthonio, M.J. Duijvestijn, J. Smidt, J. Trommel and G.M.C. deVette, J. Magn. Reson., 52, 424 (1983).

44. A. Pines, M.G. Gibby and G.S. Waugh, J. Chem. Phys., 56, 1776 (1975).

45. E.O. Stejskal and J. Schaefer, J. Chem. Phys., 18, 560 (1975).

46. J. Schaefer, E.O. Stejskal and R. Buchdal, Macromolecules, 10, 384 (1977).

47. D. Torchia, J. Magn. Reson., 30, 613 (1978).

48. E. Dempsey, J. Catal., 33, 497 (1974).

49. M. Mehring, NMR: Basic Principle and Progress, VII, Springer-Verlag, N.Y. 1983.

50. J. Schaefer, E.O. Stejskal and R. Buchdal, Macromolecules, 10 384 (1977).

51. A.N. Garroway, J. Magn. Reson., 34, 283 (1979).

52. D.L. VanderHart and A.N. Garroway, J. Chem. Phys., 71, 2773 (1979).

53. S.J. Emid, J. Mag. Reson., 42, 187 (1981).

54. P. Salvador and J. Fripiat, J. Phys. Chem., 79, 1842 (1975).

55. See ref. 49.

56. See ref. 49.

57. H. Pfeifer, Phys. Reports, 26, 293 (1976).

58. A. Abragam, "The Principles of Nuclear Magnetism" Oxford University Press, Oxford 1961.

59. H.W. Speiss, NMR: Basic Principles and Progress, V. 15, Springer Verlag, New York, 1978.

60. C.H. Townes and A.C. Shawlow, "Microwave Spectroscopy", p. 110, McGraw-Hill, New York, 1955.

61. J.F. Haw and G.E. Maciel, Anal. Chem., 55, 1262 (1983).

62. D. Demco, J. Tegenfeldt and J.S. Waugh, Phys. Rev., B11, 4133 (1975).

63. A. Abragam, "The Principles of Nuclear Magnetism", Oxford University Press, Oxford 1961.

64. See ref. 62.

65. M.M. Maricq and J.S. Waugh, J. Chem. Phys., 70, 3300 (1979).

66. M.M. Maricq, Ph.D. thesis, M.I.T. 1979.

67. H.S. Gutowsky and G.E. Pake, J. Chem. Phys., 18, 162 (1950).

68. P.S. Allen and A. Cooking, J. Chem. Phys., 47, 4286 (1967).

69. G.T. Kerr, E. Dempsey and R.J. Mikovsky, J. Phys. Chem., 69, 4050 (1965).

70. L. Pauling, The Nature of the Chemical Bond", Cornell University Press, Ithaca, N.Y., 1960.

71. S.S. Khvoschev and S.P.Zhadnov, Dokl. Akad. Nauk SSR, 200, 1156 (1971).

72. C.A. Fyfe, G.J. Kennedy, C.T. DeSchutter and G.T. Kokotailo, J. Chem. Soc. Chem. Commun., 1984, 541.

73 a. See ref. 55.

73 b. P. Salvador and W. Klading, J. Chem. Soc. Faraday Trans., 1, 73, 1153 (1973).

74. D.W. Breck, W.G. Eversole, R.M. Milton, T.B. Reed and T.L. Thomas, J. Am. Chem. Soc., 78, 5693 (1956).

75. R. Aiello, R.M. Barrer, J. Arthur and I.S. Kerr, Trans Faraday Soc., 66, 1610 (1970).

76. See ref. 55.

77. H. Karge, Zeit. fur Physik. Chem. Neue Folge, 83, 100 (1973).

78. J. Karger, J. Phys. Chemie (Leipzig), 248, 27 (1971).

79. See ref. 29.

80. H.J. Raucher, D. Michhel, D. Deininger and D. Geschke, J. Mol. Catal., 9, 369 (1980).

81. H.W. Speiss, NMR: Basic Principles and Progress. V15 Springer-Verlag, New York, 1978.

82. See ref. 1.

83 a. V. Bosacek, D.Freude, T.Frolich, H. Pfeifer and H.Schmiedel, J. Colloid Interface Sci., **85**, 502 (1982).

b. D. Freude, M. Hunger, H. Pfeifer and G. Scheler, Chem. Phys. Lett. **98**, 263 (1983).

84. N.M. Szeverenyi, M.J. Sullivan and G.E. Maciel, J. Mag. Reson., 47, 462 (1982).

85. a. P.K. Mahrer, F.D. Hunter and J. Scherzer, Adv. Chem. Series, V101, p. 266, American Chemical Society, Washington, D.C. 1971.

86. A.P. Bolton and M.A. Lanewalla, J. Catal, 18, 154 (1970).

87. See ref. 74.

88. a. V. Bosacek and Z. Tvaruzkova, Coll. Czech. Chem. Commun., 36, 551 (1971).

b. H. Karge, Zeit. fur Physik. Chem. Neue Folge, 76, 133 (1971).

89. A. Bax, N.M. Szeverenyi and G.E. Maciel, J. Magn. Reson., 55, 494 (1983).

90. See ref.89.

91. R.G. Pembleton, L.M. Ryan and B.C. Gerstein, Rev. Sci. Instrum., 48, 1286 (1977).

92. D. Freude, T. Frolich, M. Hunger, H. Pfeifer and G. Scheler, Chem. Phys. Lett., 98, 263 (1983).